Master's thesis

NTNU
Norwegian University of Science and Technology
Faculty of Natural Sciences
Department of Physics

Sigrid Aunsmo

Supercurrent-Induced Proximity Effects at Spin-Orbit Coupled Interfaces

Master's thesis in MTFYMA
Supervisor: Jacob Linder
June 2023

NTNU
Norwegian University of Science and Technology

QuSpin

Sigrid Aunsmo

Supercurrent-Induced Proximity Effects at Spin-Orbit Coupled Interfaces

Master's thesis in MTFYMA
Supervisor: Jacob Linder
June 2023

Norwegian University of Science and Technology
Faculty of Natural Sciences
Department of Physics

NTNU
Norwegian University of
Science and Technology

Abstract

Proximity effects from interfacing superconductors with other materials is an active field of research. Quantum effects occurring in such interfaces are of interest both from a theoretical perspective of understanding fundamental physics and for application in the field of quantum information. In the last two decades, particular interest has been found in proximity effects from combining ferromagnets with superconductors. Whereas a conventional superconductor contains singlet Cooper pairs, the combination of conventional superconductors and ferromagnets also induces spin-triplet Cooper pairs. Since these triplets can carry spin polarization they are highly relevant for the field of spintronics.

In this thesis, quasiclassical theory was used to perform an analytical and numerical study of proximity effects caused by supercurrents in combination with a spin-orbit coupled interface. Singlet supercurrents, triplet supercurrents, and spin supercurrents were created using conventional singlet superconductors in combination with spin-active interfaces. A normal metal was attached to the current-carrying material, separated by a thin layer of spin-orbit coupled material. Induced magnetization in the normal metal was studied.

We have found that the angle between the spin-active interface magnetization and the attached normal metal affects the induced magnetization. Moreover, we found that the different currents depend differently on this angle. By this, we found induced magnetization that can be used to distinguish singlet, triplet, and spin currents.

Sammendrag

Proksimitetseffekt fra å sammenkoble superledere med andre materialer er et aktivt forskningsfelt. Kvanteeffekter som oppstår i slike grensesjikt er interessante både fra et rent teoretisk perspektiv for å forstå fundamental fysikk, og fra et praktisk perspektiv for anvendelser innen kvanteinformasjon. De siste to tiårene har proksimitetseffekter fra kombinasjoner av superledere og ferromagneter vakt stor interesse. I en vanlig superleder er Cooper-parene koblet sammen i singlet spinnpar, men i koblingene mellom superledere og ferromagneter kan også triplet Cooper-par oppstå. At disse triplettene er spin-polariserte gjør de relevante for spintronikkanvendelser.

I denne oppgaven er kvasiklassisk teori brukt til å studere proksimitetseffekter fra superstrømmer i kombinasjon med spinn-bane koblede grensesjikt. Dette er studert både numerisk og analytisk. Singlett-, triplett- og spinn-strøm settes opp ved bruk av konvensjonelle singlett superledere i kombinajson med spinn-aktive grensesjikt. Et normalt metall festes til det strømførende materialet, separert med et tynt lag med spinn-bane kobling materiale. Indusert magnetisering i det normale ble studert.

Det ble funnet at vinkelen mellom magnetiseringene i de spin-aktive grensesjiktene og det tilkoblede normale metallet påvirker magnetiseringen i det normale metallet. Videre kan den induserte magnetiseringen brukes til å skille mellom singlett-, triplett- og spinnstrøm.

Preface

This master's thesis amounts to 30 ECTS credits and concludes my integrated master's degree in Applied Physics and Mathematics at the Norwegian University of Science and Technology.

I want to thank my supervisor Jacob Linder for the guidance during the last year. I have truly enjoyed the project and appreciated the help and insight from our weekly meetings. Additionally, I want to thank my fellow master students for the enriching and supportive environment in our study hall. Lastly, I also thank my boyfriend Halvor for being a great support and for taking the time to read through my thesis.

Contents

Chapter 1

Introduction

When Heike Kamerlingh Onnes cooled down mercury to 4.2 K in 1911 [1–3], nobody had predicted that the resistivity would abruptly drop to zero. At that time, the theoretical framework required to understand this quantum mechanical phenomenon known as the superconducting phase had not yet been established. It was not until 1957, after significant progress had been made in the field of quantum mechanics, that the first microscopic theory of superconductivity was developed by J. Bardeen, L. Cooper, and J. R. Schrieffer [4]. In this theory, an attractive force between electrons is introduced, most commonly through a phonon-mediated interaction. At low enough temperatures, this interaction pairs electrons together in so-called Cooper pairs. These pairs are protected against scattering by an energy gap, allowing a current to flow without resistance.

The absence of electrical resistance is an intriguing property of the superconducting phase. A perhaps even more characteristic trait of the phase is the Meissner effect, which describes the expulsion of magnetic fields from the interior of a superconductor [5]. Furthermore, the proximity effect adds another fascinating aspect to superconductivity by describing how Cooper pairs from the superconductor can leak through to adjacent materials. Interfacing superconductors with other materials allows for the emergence of new quantum effects that arise from the combined interaction of both materials, rather than from either material alone.

Over the past two decades, proximity effects from combining ferromagnets (F) and superconductors (S) have captured the attention and interest of physicists. This might at first seem strange since ferromagnetism and superconductivity are thought of as competing phenomena that do not exist together. In a conventional superconductor, the electrons are paired in a spin-singlet state. The exchange field of the ferromagnet, which tries to align the spins, thus effectively splits up the electron pair and makes the singlet Cooper pair short-ranged in the ferromagnet. The reason these S/F interfaces were thought to be interesting was that several works predicted that these interfaces cause triplet Cooper pairs to arise [6–9]. The triplet that is spin-neutral in the exchange-field orientation is, for the same reason as for the singlet, short-ranged in a ferromagnet. However, the triplets with spins aligned in the exchange field direction are long-ranged as they are not subjected to the spin-splitting effect of the exchange field. In a ferromagnet with a constant exchange field in proximity to a conventional singlet superconductor, it is the spin-neutral short-ranged triplet Cooper pair that is induced. However, ferromagnetic multilayers with varying exchange fields can create a triplet in one thin region that is long-ranged in the next region where the exchange field is rotated [10–13]. The first experimental evidence of the triplet pairing from superconductor-ferromagnet proximity

effect was found in 2006 by R.S. Keizer et al. [14]. Since then several experimental works have found supporting results [15–18]. More theoretical work has also been done on ferromagnetic-superconductor proximity effects [18–22]. Bergeret et al. [6] showed that the triplet Cooper pairs they predicted at S/F interfaces are odd in frequency. Such odd-frequency states were first suggested by Berezinskii [23], and physicists have taken an interest in studying properties and signatures of such odd-frequency states [7, 11, 24, 25].

These triplet Cooper pairs can be spin-polarized which makes them an intriguing subject for spintronics. Spintronics, short for spin electronics, is a field of study that focuses on utilizing the intrinsic spin of electrons, in addition to their charge, for information processing and storage. As supercurrents are dissipationless, the field of superconducting spintronics is of great interest for creating energy-efficient spintronic devices [26].

One method of theoretically investigating proximity effects is using the quasiclassical theory [27, 28]. The key assumption in quasiclassical approximation is that the Fermi wavelength is the smallest length scale of the system, or equivalently that the Fermi energy is the largest energy. In the quasiclassical theory, it is assumed that the Green function, describing both particles, holes, and Cooper pairs, is sharply peaked at the Fermi momentum. Since the Fermi wavelength is small, the Green function will thereby be rapidly oscillating and therefore have large derivatives that are difficult to handle. By integrating out the Fermi momentum one manages to integrate out this rapidly oscillating part and is instead left with a slowly varying wavefunction that contains the information about the physical observables. Further simplification can be made by assuming that the system is diffusive, as done by Usadel [29]. Within the quasiclassical theory and the diffusive regime, transport equations and boundary conditions can be derived and used to study proximity effects. This is the method we use in this thesis and a brief discussion of the theory will be given before the proximity effects are investigated.

In 2022 J. Linder and M. Amundsen derived quasiclassical boundary conditions for interfaces where a thin layer of a spin-orbit coupling material has been added [30]. They predict that through such an interface, a singlet supercurrent can induce triplet Cooper pairs in the neighboring material, which results in an induced magnetization. In this thesis, we expand this study to involve the creation of the supercurrent. Spin-active interfaces can be used to facilitate the creation of triplet charge current and spin currents [31–33]. The aim of this study is to discover experimental signatures capable of distinguishing the above-mentioned currents, hoping that it one day could be utilized for spintronic devices.

1.1 Structure

The first part of the thesis establishes the theoretical framework needed to study proximity effects in the diffusive quasiclassical theory. This includes presenting the equations of motion, the bulk superconductor solution, the observables of interest, and boundary conditions. As this part was thoroughly discussed in the specialization project, the details of the derivations are left out and only the most important parts are presented here.

In the next part, the particular system we study is presented. Thereafter we include an analytical and numerical study of the supercurrent-induced proximity effects at spin-orbit coupled interfaces and present the results.

The final summarizes the main results and discusses potential further work.

1.2 Notation

To keep the notation and calculation simple we use natural units $\hbar = c = k_B = 1$.

In this thesis, we will use 2×2, 4×4, and 8×8 matrices. To be able to distinguish them we write

- $\underline{M}$ for 2×2 matrices,
- $\hat{M}$ for 4×4 matrices,
- $\check{M}$ for 8×8 matrices.

Sometimes matrices of different sizes are used in the same equation. In such cases, it should be understood that the matrix of smaller dimension is implicitly a tensor product with the identity matrix meaning that $\check{A}\hat{B} = \check{A}(\underline{\mathbb{1}} \otimes \hat{B})$.

The Pauli matrices are denoted with τ_x, τ_y and τ_z and since they are commonly used they will be written without underline

$$\tau_x = \begin{pmatrix} 0 & 1 \\ 1 & 0 \end{pmatrix}, \quad \tau_y = \begin{pmatrix} 0 & -i \\ i & 0 \end{pmatrix}, \quad \tau_z = \begin{pmatrix} 1 & 0 \\ 0 & -1 \end{pmatrix}. \tag{1.1}$$

We also write the vector of Pauli matrices $\boldsymbol{\tau} = (\tau_x, \tau_y, \tau_z)$. Further, we define the following 4×4 matrices

$$\hat{\tau}_i = \begin{pmatrix} \tau_i & 0 \\ 0 & \tau_i^* \end{pmatrix}, \tag{1.2}$$

and

$$\hat{\rho}_1 = \begin{pmatrix} 0 & 0 & 0 & 1 \\ 0 & 0 & 1 & 0 \\ 0 & 1 & 0 & 0 \\ 1 & 0 & 0 & 0 \end{pmatrix}, \quad \hat{\rho}_2 = \begin{pmatrix} 0 & 0 & 0 & -i \\ 0 & 0 & -i & 0 \\ 0 & i & 0 & 0 \\ i & 0 & 0 & 0 \end{pmatrix}, \quad \hat{\rho}_3 = \begin{pmatrix} 1 & 0 & 0 & 0 \\ 0 & 1 & 0 & 0 \\ 0 & 0 & -1 & 0 \\ 0 & 0 & 0 & -1 \end{pmatrix}. \tag{1.3}$$

The following notation will be used for commutators and anticommutators

$$[A, B] = AB - BA, \tag{1.4}$$
$$\{A, B\} = AB + BA. \tag{1.5}$$

For convenience, we define electron operators in Nambu $\otimes$ spin space

$$\psi = \begin{pmatrix} \psi_\uparrow \\ \psi_\downarrow \\ \psi_\uparrow^\dagger \\ \psi_\downarrow^\dagger \end{pmatrix}, \quad \psi^\dagger = \begin{pmatrix} \psi_\uparrow^\dagger & \psi_\downarrow^\dagger & \psi_\uparrow & \psi_\downarrow \end{pmatrix}, \tag{1.6}$$

where $\psi_\sigma, \psi_\sigma^\dagger$ are annihilation and creation operators for an electron with spin σ.

The operation which will be referred to as tilde-conjugation is defined as complex conjugating and inverting the energy $E \to -E$.

$$\tilde{F}(E) = F(-E)^*. \tag{1.7}$$

Chapter 2

Quasiclassical Theory

Quasiclassical theory is a much used method of studying multilayered systems of superconductors, normal metals, half metals, insulators and ferromagnets [28, 34]. The theory is developed by Eilenberger [27] and by Larkin and Ovchinnikov [35].

This chapter presents the kinetic equation, relevant boundary conditions, bulk superconductor solution and observables in the quasiclassical theory. Finally, the Riccati parameterization is presented, which is a practical parameterization for numerically solving the Usadel equation. Much of the theory up until the Riccati parametrization is based on the specialization project from the previous semester. Therefore, many of the details will be left out from the main part of this thesis. Some of the more detailed calculations can be found in the appendix, and much of the content can also be found in the master's thesis by Morten [36], Fyhn [37] and Amundsen [38] and in the works of Kamenev [39], Kita [40] Gor'kov [41] and Chandrasekhar [28].

2.1 System Hamiltonian

The very first step of finding an equation of motion is to set up the relevant Hamiltonian. Here this includes a kinetic term, H_0, a impurity scattering interaction H_{imp}, a BCS interaction term, H_{int}, and a ferromagnetic term H_{FM}. The BCS term is found by including an attractive force between electrons of opposite spin and performing a mean-field approximation. For a thorough explanation of the BCS theory we refer to chapters 8 and 9 in the book by T. Kita [40]. At first we allow the terms to be time-dependent and the total Hamiltonian can be written in terms of the second quantized electron annihilation and creation operators, ψ_σ and $\psi_\sigma^\dagger$, as

$$\begin{aligned}
H(t) =& H_0(t) + H_{\text{int}}(t) + H_{\text{imp}}(t) + H_{\text{FM}}(t), \\
H_0(t) =& \int \mathrm{d}\boldsymbol{r} \sum_\sigma \psi_\sigma^\dagger(\boldsymbol{r},t)\Big[-\frac{1}{2m}\Big(\nabla_{\boldsymbol{r}} - ie\boldsymbol{A}(\boldsymbol{r},t)\Big)^2 + e\varphi(\boldsymbol{r},t) - \mu\Big]\psi_\sigma(\boldsymbol{r},t), \\
H_{\text{int}}(t) =& -\lambda \int \mathrm{d}\boldsymbol{r} \left[\Delta^*(\boldsymbol{r},t)\psi_\downarrow(\boldsymbol{r},t)\psi_\uparrow(\boldsymbol{r},t) + \Delta(\boldsymbol{r},t)\psi_\uparrow^\dagger(\boldsymbol{r},t)\psi_\downarrow^\dagger(\boldsymbol{r},t)\right], \\
H_{\text{imp}}(t) =& \int \mathrm{d}\boldsymbol{r} \sum_\sigma \psi_\sigma^\dagger(\boldsymbol{r},t) V_{\text{imp}}(\boldsymbol{r},t)\psi_\sigma(\boldsymbol{r},t), \\
H_{\text{FM}}(t) =& -\int \mathrm{d}\boldsymbol{r} \sum_{\sigma\sigma'} \psi_\sigma^\dagger(\boldsymbol{r},t)\boldsymbol{h}\cdot\boldsymbol{\tau}_{\sigma\sigma'}\psi_{\sigma'}(\boldsymbol{r},t).
\end{aligned} \tag{2.1}$$

The subscript σ refers to the spin of the electron, m is the electron mass, $\boldsymbol{A}$ is the electromagnetic vector potential, φ is the electromagnetic scalar potential, μ is the chemical potential and $\boldsymbol{h}$ is the exchange field. V_{imp} is the impurity potential which plays a central role in allowing us to assume that the wavefunction is isotropic. The superconducting order parameter is defined as $\Delta(\boldsymbol{r}) = \langle\psi_\uparrow(\boldsymbol{r},t)\psi_\downarrow(\boldsymbol{r},t)\rangle$.

2.2 Equation of motion

The Heisenberg equation of motion for an operator a reads

$$i\partial_t a = [a, H]. \tag{2.2}$$

This can be used to find the equation of motion for the electron creation and annihilation operators

$$\begin{aligned} i\partial_t\psi_\sigma(\boldsymbol{r},t) = &-[\tfrac{1}{2m}(\nabla_{\boldsymbol{r}} - ie\boldsymbol{A})^2 + e\varphi - \mu]\psi_\sigma \\ &+ \Delta(\boldsymbol{r},t)(\delta_{\sigma\uparrow}\psi^\dagger_\downarrow(\boldsymbol{r},t) - \delta_{\sigma\downarrow}\psi^\dagger_\downarrow(\boldsymbol{r},t)) \\ &+ V_{\text{imp}}\psi_\sigma(\boldsymbol{r},t) - \sum_{\sigma'}[\boldsymbol{h}\cdot\boldsymbol{\tau}]\psi_{\sigma'}(\boldsymbol{r},t), \end{aligned} \tag{2.3}$$

where $\delta_{\sigma\sigma'}$ is the Kronecker delta. In Nambu $\otimes$ spin space, this can be written compactly in 4×4 matrix notation using the spinors $\psi = (\psi_\uparrow, \psi_\downarrow, \psi^\dagger_\uparrow, \psi^\dagger_\downarrow)$

$$i\partial_t\hat{\rho}_3\psi(\boldsymbol{r},t) = \hat{H}(\boldsymbol{r},t)\psi(\boldsymbol{r},t), \tag{2.4}$$

where $\hat{H}$ is defined as

$$\begin{aligned} \hat{H} &= \hat{\xi} + \hat{\Delta} + V_{\text{imp}}\hat{1} - \hat{M}, \\ \hat{\xi} &= -\tfrac{1}{2m}(\nabla - ie\boldsymbol{A}\hat{\rho}_3)^2 + e\varphi\hat{1} - \mu\hat{1}, \\ \hat{\Delta} &= \begin{pmatrix} 0 & 0 & 0 & \Delta \\ 0 & 0 & -\Delta & 0 \\ 0 & \Delta^* & 0 & 0 \\ -\Delta^* & 0 & 0 & 0 \end{pmatrix}, \\ \hat{M} &= \boldsymbol{h}\cdot\boldsymbol{\tau}. \end{aligned} \tag{2.5}$$

Green functions

Moving forward we introduce a powerful and much used tool in studying quantum mechanical systems, the Green function. Further, we introduce the Keldysh Green function [42], which is commonly used to study non-equilibrium systems. A more thorough discussion of the Keldysh formalism is found in the book by A. Kamenev chapters 2 and 9 [39].

First, the 2×2 retarded, $\underline{G}^R$, advanced, $\underline{G}^A$, and Keldysh, $\underline{G}^K$, Green functions are defined as well as the anomalous Green functions $\underline{F}$. For this, we use the 4-vector notation $x = (\boldsymbol{r}, t)$.

$$\underline{G}^R_{\sigma\sigma'}(x_1,x_2) = -i\Theta(t_1-t_2)\left\langle\{\psi_\sigma(x_1),\psi^\dagger_{\sigma'}(x_2)\}\right\rangle, \tag{2.6}$$
$$\underline{G}^A_{\sigma\sigma'}(x_1,x_2) = i\Theta(t_2-t_1)\left\langle\{\psi_\sigma(x_1),\psi^\dagger_{\sigma'}(x_2)\}\right\rangle, \tag{2.7}$$
$$\underline{G}^K_{\sigma\sigma'}(x_1,x_2) = -i\left\langle[\psi_\sigma(x_1),\psi^\dagger_{\sigma'}(x_2)]\right\rangle, \tag{2.8}$$
$$\underline{F}^R_{\sigma\sigma'}(x_1,x_2) = -i\Theta(t_1-t_2)\left\langle\{\psi_\sigma(x_1),\psi_{\sigma'}(x_2)\}\right\rangle, \tag{2.9}$$
$$\underline{F}^A_{\sigma\sigma'}(x_1,x_2) = i\Theta(t_2-t_1)\left\langle\{\psi_\sigma(x_1),\psi_{\sigma'}(x_2))\}\right\rangle, \tag{2.10}$$
$$\underline{F}^K_{\sigma\sigma'}(x_1,x_2) = -i\left\langle[\psi_\sigma(1),\psi_{\sigma'}(x_2)]\right\rangle, \tag{2.11}$$

where Θ is the unit step function. We can group these together and define the 4×4 Green functions

$$\hat{G}^{R/A}(x_1,x_2) = \begin{pmatrix} \underline{G}^{R/A}(x_1,x_2) & \underline{F}^{R/A}(x_1,x_2) \\ (\underline{F}^{R/A}(x_1,x_2))^* & (\underline{G}^{R/A}(x_1,x_2))^* \end{pmatrix}, \tag{2.12}$$
$$\hat{G}^{K}(x_1,x_2) = \begin{pmatrix} \underline{G}^{K}(x_1,x_2) & \underline{F}^{K}(x_1,x_2) \\ -(\underline{F}^{K}(x_1,x_2))^* & -(\underline{G}^{K}(x_1,x_2))^* \end{pmatrix}. \tag{2.13}$$

Finally, we also define the 8×8 Green function which contains all the above Green functions

$$\check{G} = \begin{pmatrix} \hat{G}^R & \hat{G}^K \\ 0 & \hat{G}^A \end{pmatrix}. \tag{2.14}$$

By using the equation of motion for the creation and annihilation operators the equation of motion for the 8×8 Green function can be found to be

$$i\partial_{t_1}\hat{\rho}_3\check{G}(x_1,x_2) = \delta(x_1-x_2) + \hat{\rho}_3\hat{H}(x_1)\hat{\rho}_3\check{G}(x_1,x_2), \tag{2.15}$$
$$-i\partial_{t_2}\check{G}(x_1,x_2)\hat{\rho}_3 = \delta(x_1-x_2) + \check{G}(x_1,x_2)\hat{H}^\dagger(x_2), \tag{2.16}$$

where $\delta(x)$ is the Dirac delta function. We subtract the left-handed Equation (2.15) from the right-handed Equation (2.16), which gets rid of the δ-function

$$\big(i\partial_{t_1}\hat{\rho}_3 - \hat{\rho}_3\hat{H}(x_1)\hat{\rho}_3\big)\check{G}(x_1,x_2) - \check{G}(x_1,x_2)\big(-i\partial_{t_2}\hat{\rho}_3 - \hat{H}^\dagger(x_2)\big) = 0. \tag{2.17}$$

The effect of the impurity potential can be regarded using a self-energy as shown in Appendix B.1. Equation (2.17) can then be written as

$$\begin{aligned}&\big(i\partial_{t_1}\hat{\rho}_3 - \hat{\rho}_3\hat{H}_0(x_1)\hat{\rho}_3\big)\check{G}(x_1,x_2) - \int \mathrm{d}x_3\hat{\Sigma}(x_1,x_3)\check{G}(x_3,x_2) \\ &- \check{G}(x_1,x_2)\big(-i\partial_{t_2}\hat{\rho}_3 - \hat{H}_0{}^\dagger(x_2)\big) + \int \mathrm{d}x_3\check{G}(x_1,x_3)\hat{\Sigma}(x_3,x_2) = 0,\end{aligned} \tag{2.18}$$

where H_0 is the Hamiltonian without the impurity potential, and Σ is the impurity self energy. Notice that

$$\hat{\rho}_3\hat{H}_0\hat{\rho}_3 = \hat{\xi} - \hat{\Delta} + \hat{S} - \hat{M}, \tag{2.19}$$

so the two $\hat{\rho}_3$ matrices only change the $\hat{\Delta}$ into $-\hat{\Delta}$ whereas the other block diagonal terms stay unchanged. Equation (2.18) can be written as

$$\begin{aligned} 0 = \; & i\partial_{t_1}\hat{\rho}_3\check{G}(x_1,x_2) + i\partial_{t_2}\check{G}(x_1,x_2)\hat{\rho}_3 \\ & - \hat{\xi}(x_1)\check{G}(x_1,x_2) + \check{G}(x_1,x_2)\hat{\xi}^*(x_2) \\ & - \hat{S}(x_1)\check{G}(x_1,x_2) + \check{G}(x_1,x_2)\hat{S}(x_2) \\ & + \hat{M}(x_1)\check{G}(x_1,x_2) + \check{G}(x_1,x_2)\hat{M}(x_2) \\ & + \hat{\Delta}(x_1)\check{G}(x_1,x_2) + \check{G}(x_1,x_2)\Delta(x_2) \\ & - \int \mathrm{d}x_3\hat{\Sigma}(x_1,x_3)\check{G}(x_3,x_2) - \int \mathrm{d}x_3\check{G}(x_1,x_3)\hat{\Sigma}(x_3,x_2). \end{aligned} \tag{2.20}$$

Wigner transformations

In the interest of being able to apply the quasiclassical approximation, the mixed representation is introduced and Wigner transformation is performed on Equation (2.20). The mixed representation refers to changing from the individual particle coordinates x_1 and x_2 to the center of mass coordinate $X = \frac{1}{2}(x_1 + x_2)$ and the relative coordinate $x = x_1 - x_2$. The Wigner transformation is defined as a Fourier transform over the relative coordinate such that the Wigner transform of a function $A(x_1, x_2)$ is

$$A(X,p) \equiv \int \mathrm{d}x \mathrm{e}^{-ipx} A(x_1,x_2). \tag{2.21}$$

We also define the Wigner transform of a convolution, which sometimes is referred to as a "star product" as

$$\begin{aligned} A \otimes B(X,p) &\equiv \int \mathrm{d}(x_1 - x_3)\mathrm{e}^{-ip(x_1-x_3)} \int \mathrm{d}x_2 A(x_1,x_2)B(x_2,x_3) \\ &= \mathrm{e}^{i(\partial_{X_A}\partial_{p_B} - \partial_{X_B}\partial_{p_A})/2} A(X,p)B(X,p). \end{aligned} \tag{2.22}$$

The second line in the expression above is a convenient way of writing the "star product". A derivation of the second line expression is included in Appendix A.1. Moreover, we define the commutator/anticommutator notation of star products

$$\begin{aligned} \left[A \overset{\otimes}{,} B\right] &= A \otimes B(X,p) - B \otimes A(X,p), \\ \left\{A \overset{\otimes}{,} B\right\} &= A \otimes B(X,p) + B \otimes A(X,p). \end{aligned} \tag{2.23}$$

The details of the transformation of Equation (2.20) can be found in Appendix A.3 The transformed equation, often referred to as the Gorkov equation [43] reads

$$-\tfrac{ie}{2m}\left\{\boldsymbol{A}\hat{\rho}_3 \overset{\otimes}{,} \nabla_{\boldsymbol{R}}\check{G}\right\} + \tfrac{\boldsymbol{p}}{m}\cdot\bar{\nabla}\check{G} + \left[E\hat{\rho}_3 - \tfrac{e^2}{2m}\boldsymbol{A}^2 - e\varphi + \hat{M} + \hat{\Delta} - \hat{\Sigma} \overset{\otimes}{,} \check{G}\right] = 0, \tag{2.24}$$

where $\bar{\nabla}\check{G} = \nabla_{\boldsymbol{R}}\check{G} - ie[\boldsymbol{A}\hat{\rho}_3, \check{G}]$.

2.3 Quasiclassical Approximation

As Equation (2.24) is expressed with the relative momentum p we can now apply the quasiclassical approximation. The central assumption in the quasiclassical approximation

is that the Fermi wavelength λ_F is the shortest length scale in our system and that every other length, l, in our system is much larger $\lambda_F \ll l$. This is equivalent to saying that the Fermi energy, E_F in our system is much larger than all other energies and energy fluctuations. We assume that both the length scales of derivatives and $e\boldsymbol{A}$ are large compared to λ_F. By this assumption we remove all ∇, and $\boldsymbol{A}$ terms from the Equation (2.24), except those who are accompanied by $\boldsymbol{p}$, which can be large.

In addition to removing gradients, we will in this study assume that the system is stationary and remove time derivatives. Removing the time derivatives and gradients gives

$$\left[A \overset{\otimes}{,} B\right] = [A, B], \tag{2.25}$$

$$\left\{A \overset{\otimes}{,} B\right\} = \{A, B\}. \tag{2.26}$$

By these approximations, Equation (2.24) simplifies to

$$\boldsymbol{p} \cdot \frac{e}{m}[\boldsymbol{A}\hat{\rho}_3, \check{G}] + \frac{\boldsymbol{p}}{m} \cdot \nabla_{\boldsymbol{R}}\check{G} + [E\hat{\rho}_3 - e\varphi + \hat{M} + \hat{\Delta} - \hat{\Sigma}, \check{G}] = 0. \tag{2.27}$$

In the quasiclassical approximation, we also assume that the Green function is strongly peaked around the Fermi level. The reason for this assumption is that inside the Fermi-sea the states are mostly filled at low temperatures. Because of the Pauli principle electrons cannot be scattered into an already occupied state, and hence they will not give considerable contributions to kinetics. Above the Fermi-level states are mostly unoccupied, so there are no electrons to be scattered, hence no contributions will come from such states either. By this reasoning, the quasiclassical Green function is defined as

$$\check{g}(\boldsymbol{p}_F, E) = \frac{i}{\pi}\int_{-\infty}^{\infty} \mathrm{d}\xi_{\boldsymbol{p}}\check{G}(\boldsymbol{p}, E), \tag{2.28}$$

where $\xi_{\boldsymbol{p}} = \frac{\boldsymbol{p}^2}{2m}$. This quasiclassical Green function keeps the angular dependency of $\boldsymbol{p}_F$ but the magnitude of $\boldsymbol{p}$ is integrated out. It should be commented that the integral is diverging, a problem that could be solved as done by Eilenberger by using a special integration contour, or by Serene and Rainer [44] by introducing a cut-off frequency.

We now integrate Equation (2.27) and we say that $\check{G}$ is so strongly peaked around p_F that we also can say that $\boldsymbol{p} = \boldsymbol{p}_F$ inside the integral and hence move the $\boldsymbol{p}_F$ outside the integral. This gives us the equation which in the literature often is referred to as the Eilenberger equation [27]

$$\frac{\boldsymbol{p}_F}{m} \cdot \bar{\nabla}\check{g} + [E\hat{\rho}_3 - e\varphi + \hat{M} + \hat{\Delta} - \hat{\Sigma}, \check{g}] = 0. \tag{2.29}$$

Further restrictions can be put on the quasiclassical Green function by introducing the normalization condition

$$\check{g}\check{g} = 1. \tag{2.30}$$

Although there are different ways to normalize the Green function, this is the most common normalization and is thoroughly discussed in [45].

2.4 Diffusive limit and Usadel Equation

The next and important step is assuming the system to be diffusive. This means that we are in the region where the Green function has been scattered enough to consider the

wavefunction to be isotropic. We expand the Green function in the spherical harmonics and keep only the s- and p-wave part [41]

$$\hat{g} \approx \hat{g}_s + \boldsymbol{e}_F \cdot \hat{\boldsymbol{g}}_p. \tag{2.31}$$

From impurity averaging it can also be shown that the quasiclassical self-energy in the self-consistent Born approximation can in the diffusive limit be written as

$$\sigma \approx -\frac{i}{2\tau}\check{g}_s, \tag{2.32}$$

where τ is the relaxation time. This is shown in appendix B.2.

By using this and the normalization condition it can be found that the quasiclassical equation of motion can, in the diffusive limit, be written as

$$D\bar{\nabla}(\check{g}_s\nabla\check{g}_s) + i[E\hat{\rho}_3 - e\varphi + \hat{M} + \Delta, \check{g}_s] = 0, \tag{2.33}$$

where $D = \frac{1}{3}\tau v_{\mathrm{F}}$ and v_{F} is the Fermi velocity. This is the commonly named Usadel equation [29]. Moving on we remove the s-subscript for simplicity of notation.

2.5 Bulk superconductor solution

Assuming that the system is in equilibrium we only need to find a solution for the retarded Green function, since it can be found from the definition that

$$\hat{g}^A = -\hat{\rho}_3\hat{g}^R\hat{\rho}_3, \tag{2.34}$$

and in equilibrium we have the fluctuation-dissipation relation [46]

$$\hat{g}^K = (\hat{g}^R(E) - \hat{g}^A(E))\tanh(E/2T). \tag{2.35}$$

It can be shown, as in [28] that the bulk superconductor solution to the Usadel equation is

$$\hat{g}^R = \left(\frac{\mathrm{sgn}(E)}{\sqrt{E^2 - |\Delta|^2}}\Theta(E^2 - |\Delta|^2) - \frac{i}{\sqrt{|\Delta|^2 - E^2}}\Theta(|\Delta|^2 - E^2)\right)(\hat{\rho}_3 E + \hat{\Delta}). \tag{2.36}$$

The solution has the shape

$$\hat{g} = \begin{pmatrix} g & 0 & 0 & f \\ 0 & g & -f & 0 \\ 0 & -\tilde{f} & -\tilde{g} & 0 \\ \tilde{f} & 0 & 0 & -\tilde{g} \end{pmatrix} = \begin{pmatrix} \underline{g} & \underline{f} \\ -\underline{\tilde{f}} & -\underline{\tilde{g}} \end{pmatrix}, \tag{2.37}$$

where the tilde-notation means $\tilde{g}(E) = g(-E)^*$.

This bulk conventional superconductor solution only contains singlet Cooper pairs. With triplet Cooper pairs present, $\underline{f}$ and $\underline{g}$ will change form, and can also include diagonal elements. In these cases, the structure of the last matrix in Equation (2.37) will remain intact. It should here also be mentioned that the superconductor can have a phase. A physical observable is never dependent on a phase, however, a phase difference can affect the physics. In case of a phase, ϕ, we would simply add a phase factor $\mathrm{e}^{i\phi}$ to $\underline{f}$ and $\mathrm{e}^{-i\phi}$ to $\underline{\tilde{f}}$. Notice that in a singlet superconductor, the tilde conjugated anomalous Green function satisfy $\tilde{f} = -f\mathrm{e}^{-2i\phi}$.

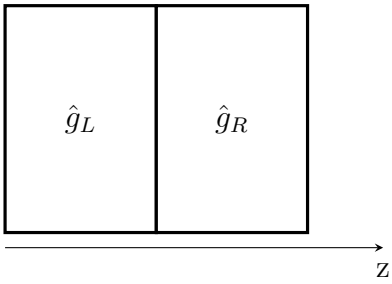

Figure 2.1: A illustration of interfaces between two materials. The z-axis is defined to be orthogonal to the interface.

2.6 Singlet-triplet decomposition

In this thesis, we study systems where not only the conventional singlet Cooper pairs are present but also triplet pairing. As it will later prove to be convenient, the $\boldsymbol{d}$-vector notation is introduced. This singlet-triplet decomposition looks like

$$\underline{f} = (f_s + \boldsymbol{d}\cdot\boldsymbol{\tau})i\tau_y = \begin{pmatrix} -d_x + id_y & f_s + d_z \\ -f_s + d_z & d_x + id_y \end{pmatrix}. \tag{2.38}$$

This decomposition is discussed in more detail in other works [47, 48]. The triplets are defined such that $d_z = (|\uparrow\downarrow\rangle + |\downarrow\uparrow\rangle)_z$ where the z-subscript indicates that $\uparrow$ is chosen to align with the positive z-direction. Similarly $d_x = (|\uparrow\downarrow\rangle + |\downarrow\uparrow\rangle)_x$ and $d_y = (|\uparrow\downarrow\rangle + |\downarrow\uparrow\rangle)_y$. So the d_i-component correspond to the spin-neutral triplet in the i-directions. As discussed in the paper by H. Giil and J. Linder [11] this $\boldsymbol{d}$-vector usually behaves oppositely from the singlet under tilde conjugation $\tilde{\boldsymbol{d}} = \boldsymbol{d}$, or with a phase involved, $\tilde{\boldsymbol{d}} = \boldsymbol{d}\mathrm{e}^{-2i\phi}$. How the components behave under tilde conjugation will be a central part of the discussion later in this thesis.

2.7 Boundary conditions

In the previous section we found the equation of motion. To solve the system, the differential equation needs to be accompanied by a set of boundary conditions. The system, which will be studied in this thesis, includes different types of interfaces. In the following section, we discuss the boundary conditions from each of the interface types. The simplest and most used boundary condition is the Kuprianov-Lukichev boundary conditions [49]. For the study later on, this will be used when we look at a singlet charge current created by a normal Josephson junction. Further, we will discuss the spin-active boundaries that we will be used to create triplet charge currents and spin currents. Lastly, we discuss the Rashba spin-orbit coupling boundaries which is a cornerstone of this thesis. These will be used between the current-carrying material and a normal metal to get experimental signatures in the normal metal induced by the supercurrents.

Figure 2.1 describes the general system for which the boundary conditions are set up. Presenting the boundary conditions here we assume that we have an interface normal in the z-direction. We call the material to the "left" L, and the material to the "right" R. We will mark the left and right Green functions by an R or L subscript that should not be confused with the superscript R used previously for the marking the retarded Green

functions. In general, the boundary conditions are written on the form

$$\hat{g}_L \partial_z \hat{g}_L = \hat{I}, \tag{2.39}$$

where $\hat{I}$ is the matrix current that takes into account both transmission and reflection at the interface [50]. All the boundary conditions presented below are presented for the derivative of the left side Green function $\partial_z \hat{g}_L$. Finding the boundary condition for the right side Green function can be done by simply interchanging L and R and changing sign on the right-hand side terms.

2.7.1 Kuprianov-Lukichev boundary conditions

The Kuprianov-Lukichev boundary condition [49] is the simplest quasiclassical boundary condition that considers only spin-independent tunneling between the materials. These boundary conditions read

$$\hat{g}_L \partial_z \hat{g}_L = \Omega_L[\hat{g}_L, \hat{g}_R], \tag{2.40}$$

where Ω_L is a material-specific constant that depends on the ratio between the bulk resistance of the two sides of the interface and the length of the left material.

2.7.2 Spin-active boundary conditions

For the purpose of creating triplet currents, spin-active interfaces will be used. Spin-active boundary conditions is a term used for boundary conditions where strongly spin-polarized magnetic materials are involved. These materials could be either strongly spin-polarized magnetic insulators or half-metallic ferromagnets. In this work we will consider interfaces where a half-metallic ferromagnet is introduced between two materials, one of which will be a superconductor and the other a ferromagnet or a normal metal. Triplets can then be induced from spin-mixing caused by reflective scattering of the wavefunction and by spin-dependent transmission probabilities.

The boundary conditions for spin-active tunneling interface to the first order of tunneling probabilities and spin-mixing angles, described in [31] will be used. In these boundary conditions, three more terms than the normal Kuprianov-Lukichev term are included. A derivation of these boundary conditions is found in [51] and the boundary conditions read

$$\hat{g}_L \partial_z \hat{g}_L = G_0[\hat{g}_L, \hat{g}_R] + G_1[\hat{g}_L, \hat{m}\hat{g}_R\hat{m}] + G_{MR} + [\hat{g}_L, \{\hat{g}_R, \hat{m}\}] - iG_\varphi[\hat{g}_L, \hat{m}]. \tag{2.41}$$

We recognize the G_0 term as the Kuprianov-Lukichev term. G_{MR} is a magnetoresistive term and G_1 is a de-pairing term which both originate from having spin-dependent tunneling probabilities. We define polarization as

$$P = \frac{T_\uparrow - T_\downarrow}{T_\uparrow + T_\downarrow}, \tag{2.42}$$

where $T_\uparrow, T_\downarrow$ is the transmission probability for spin up and spin down respectively. The expressions for G_1 and G_{MR} read

$$G_1/G_0 = \frac{1-\sqrt{1-P^2}}{1+\sqrt{1-P^2}}, \quad G_{\mathrm{MR}}/G_0 = \frac{P}{1+\sqrt{1-P^2}}. \tag{2.43}$$

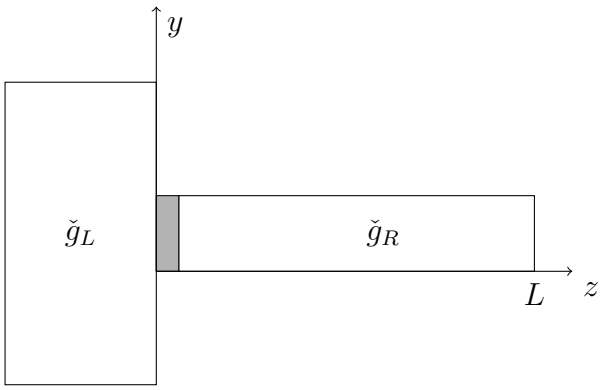

Figure 2.2: The general system for which the spin-orbit coupling boundary conditions are derived, the system is considered to be narrow in the x-direction such that the Green function has no x-dependency.

Further, the G_φ term takes into account spin-dependent scattering at the interface, and more about this spin-mixing scattering can be read in [52]. G_φ depends on the spin-mixing angles φ which is the spin-dependent scattering phase shift. It should here be noted that P and G_φ really are a sum over scattering channels, but here it is assumed that the scattering channels are equal such that the summation can be removed.

2.7.3 Spin-orbit coupling boundary conditions

Another type of interface can be made by including a thin region of a spin-orbit coupling material. In the paper by J. Linder and M. Amundsen [30], they derived quasiclassical boundary conditions for such interfaces where the gradient parallel to the interface is taken into account. The type of boundaries described by these boundary conditions is shown in Figure 2.2, where the left side Green functions are allowed to have a y-dependency. A Rashba spin-orbit coupling interaction was used in the interface and both tunneling and reflection terms were considered.

Since a couple of smaller errors, were found in the paper, the derivation of these boundary conditions is also included in Appendix C. If we assume that the right side Green function has no y-dependency the boundary conditions reads

$$\begin{aligned} D\check{g}_L\partial_z\check{g}_L =& T_0^2[\check{g}_L,\check{g}_R] + T_1^2 p_F^2[\check{g}_L,\hat{\boldsymbol{\tau}}_\parallel\check{g}_R\hat{\boldsymbol{\tau}}_\parallel] - mDT_1T_0[\check{g}_L,\{\hat{\tau}_{\parallel,x},\check{g}_R\partial_y\check{g}_R\}] \\ &- Dd\alpha^2[\hat{\rho}_x,\check{g}_L\hat{\rho}_x\check{g}_L] - Dd\alpha^2[\hat{\rho}_y,\check{g}_L\hat{\rho}_y\check{g}_L]. \end{aligned} \tag{2.44}$$

In the equation above T_0, T_1 are diagonal and off-diagonal elements of the tunneling matrix, α is the strength of the spin-orbit coupling interaction, and d is the thickness of the spin-orbit coupling material.

2.8 Observables

As mentioned we will be looking at how charge currents and spin currents affect the magnetization induced through the spin-orbit coupled interface. To do so we need to know what the expressions for magnetization and currents look like in the quasiclassical theory. Thus, in this section, the quasiclassical expressions for the magnetization, spin

and charge currents are presented. To simplify the analytical study later on we also take the time to present the observables expressed in the singlet-triplet decomposition in the weak proximity regime. Again, the detailed derivation of these expressions was presented in the specialization project and is left out, but the final expressions are presented.

2.8.1 Currents

The quasiclassical expression for current can be found by using the continuity equation $\partial_t \rho + \nabla \cdot \boldsymbol{J} = 0$, where $\boldsymbol{J}$ is the current of a quantity and ρ is the corresponding density.

For charge, we have that the charge density can be written as $\rho = e\langle \psi^\dagger \hat{\rho}_3 \psi \rangle$, and for spin the spin density can be written as $\langle \psi^\dagger \frac{1}{2} \hat{\rho}_3 \boldsymbol{\tau} \psi \rangle$. By using the equation of motion for the creation and annihilation operator and writing the expression in terms of the quasiclassical Green function we get the charge current expression

$$\boldsymbol{J} = \frac{eN_0 D}{4} \int \mathrm{d}E \mathrm{Tr}\big[\hat{\rho}_3 \check{g} \bar{\nabla} \check{g})^K\big]. \tag{2.45}$$

The spin current is similar, we just have to add the $\frac{1}{2}\boldsymbol{\tau}$ in front of the $\hat{\rho}_3$.

As mentioned we are interested in writing the expressions in terms of the singlet-triplet decomposition terms f_s and $\boldsymbol{d}$. By linearizing, assuming $\hat{g} = \hat{\rho}_3 + \hat{f}$ and only keeping the first order in $\hat{f}$, using the relation $\hat{g}^A = -\hat{\rho}_3 (\hat{g}^R)^\dagger \hat{\rho}_3$ and that we in equilibrium have $\hat{g}^K = (\hat{g}^R - \hat{g}^A)\tanh(\frac{\beta E}{2})$, we get the following expressions for the current $\boldsymbol{J}$ and spin current $\boldsymbol{J_s}$

$$\boldsymbol{J} = J_0 \int_0^\infty \frac{\mathrm{d}E}{\Delta_0} \tanh(\tfrac{\beta E}{2}) \mathrm{Re}\big([f_s \nabla \tilde{f}_s - d_z \nabla \tilde{d}_z - d_x \nabla \tilde{d}_x - d_y \nabla \tilde{d}_y] - [. \tilde{.} .]\big), \tag{2.46}$$

$$\boldsymbol{J}_{s_x} = J_{s0} \int_0^\infty \frac{\mathrm{d}E}{\Delta_0} \tanh(\tfrac{\beta E}{2}) \mathrm{Im}([d_y \nabla \tilde{d}_z - d_z \nabla \tilde{d}_y] + [. \tilde{.} .]), \tag{2.47}$$

$$\boldsymbol{J}_{s_y} = J_{s0} \int_0^\infty \frac{\mathrm{d}E}{\Delta_0} \tanh(\tfrac{\beta E}{2}) \mathrm{Im}([d_z \nabla \tilde{d}_x - d_x \nabla \tilde{d}_z] + [. \tilde{.} .]), \tag{2.48}$$

$$\boldsymbol{J}_{s_z} = J_{s0} \int_0^\infty \frac{\mathrm{d}E}{\Delta_0} \tanh(\tfrac{\beta E}{2}) \mathrm{Im}([d_x \nabla \tilde{d}_y - d_y \nabla \tilde{d}_x] + [. \tilde{.} .]), \tag{2.49}$$

where $J_0 = 2eN_0 D\Delta_0$ and $J_{s0} = N_0 D\Delta_0$. We have written the integral in terms of the dimensionless variable E/Δ_0, where $\Delta_0 = \Delta(T = 0)$ is the zero temperature energy gap. This means that J/J_0 is also a dimensionless variable which is practical for the numerical study. To arrive at these equations we have also used that

$$\int_{-\infty}^{\infty} \mathrm{d}E f(E)^* = -\int_{-\infty}^{\infty} \mathrm{d}E \tilde{f}(E). \tag{2.50}$$

In the following sections, we will separate the part of the charge current carried by the singlet and the triplet components. We define the current component carried by the different components as

$$\boldsymbol{J}_{f_s} = J_0 \int_0^\infty \frac{\mathrm{d}E}{\Delta_0} \tanh(\tfrac{\beta E}{2}) \mathrm{Re}\big([f_s \nabla \tilde{f}_s] - [. \tilde{.} .]\big), \tag{2.51}$$

$$\boldsymbol{J}_{d_i} = -J_0 \int_0^\infty \frac{\mathrm{d}E}{\Delta_0} \tanh(\tfrac{\beta E}{2}) \mathrm{Re}\big([d_i \nabla \tilde{d}_i] - [. \tilde{.} .]\big), \tag{2.52}$$

where $\boldsymbol{J}_{f_s}$ is the charge current carried by the singlet component and $\boldsymbol{J}_{d_i}$ is carried by the d_i component.

2.8.2 Magnetization

It can be shown that the quasiclassical expression for magnetization reads

$$\boldsymbol{M} = \frac{\mu_0}{8}\int \mathrm{d}E\mathrm{Tr}(\hat{\boldsymbol{\tau}}\hat{g}^K). \tag{2.53}$$

It should be mentioned that this expression does not take into account the contribution from the Fermi sea, such that a ferromagnetic exchange field will not be captured by this expression.

Once more we want to express the magnetization in terms of the singlet-triplet decomposed components. This can be done similarly to the current, by using the expression for $\hat{g}^A$ and the equilibrium expression for $\hat{g}^K$. This time there will be no first-order contribution so we have to take into account the normalization condition, $(\hat{g}^R)^2 = 1$, to find the normalized expression for $\underline{g}$ and $\underline{\tilde{g}}$. By this method, it can be found that the magnetization, to the second order in f, reads

$$M_x = M_0\int_0^\infty \frac{\mathrm{d}E}{\Delta_0}\tanh(\tfrac{\beta E}{2})\mathrm{Re}(\tilde{d}_x f_s - d_x\tilde{f}_s), \tag{2.54}$$

$$M_y = M_0\int_0^\infty \frac{\mathrm{d}E}{\Delta_0}\tanh(\tfrac{\beta E}{2})\mathrm{Re}(\tilde{d}_y f_s - d_y\tilde{f}_s), \tag{2.55}$$

$$M_z = M_0\int_0^\infty \frac{\mathrm{d}E}{\Delta_0}\tanh(\tfrac{\beta E}{2})\mathrm{Re}(\tilde{d}_z f_s - d_z\tilde{f}_s), \tag{2.56}$$

where $M_0 = \mu_0\Delta_0$.

2.9 Riccati parametrization

One way of parametrizing the Green function is the Riccati parametrization [53, 54]. The Riccati parametrization is advantageous for numerical computation because the parameters are bounded between 0 and 1. For the purpose of studying systems numerically we will here go through the derivation of the Riccati parametrized Usadel equation as well as the Riccati parametrized boundary equation.

First of all the parameters need to be defined. N and γ are defined as follows

$$\hat{g} = \begin{pmatrix} N(1+\gamma\tilde{\gamma}) & 2N\gamma \\ -\tilde{N}\tilde{\gamma} & -\tilde{N}(1+\tilde{\gamma}\gamma)\end{pmatrix}. \tag{2.57}$$

N and γ are 2×2 matrices, but for the purpose of keeping the expressions tidier, the underline notation is dropped for these matrices. By the normalization condition it is seen that $N = (1-\gamma\tilde{\gamma})^{-1}$ and $\tilde{N} = (1-\tilde{\gamma}\gamma)^{-1}$.

A couple of useful identities can be found

$$N\gamma = \gamma\tilde{N},\ \ \tilde{N}\tilde{\gamma} = \tilde{\gamma}N. \tag{2.58}$$

Notice also that this gives

$$\gamma\tilde{\gamma} = 1 - N^{-1}. \tag{2.59}$$

When writing the Usadel equation and the boundary conditions in this parametrization, we will have to consider derivatives. To simplify the notation we therefore introduce

$\gamma' = \partial_z \gamma$. The following way of writing derivatives will also be useful

$$\partial_z N = N(\gamma'\tilde{\gamma} + \gamma\tilde{\gamma}')N, \tag{2.60}$$
$$\partial_z \tilde{N} = \tilde{N}(\tilde{\gamma}'\gamma + \tilde{\gamma}\gamma')\tilde{N}, \tag{2.61}$$
$$\partial_z (N\gamma) = N(\gamma' + \gamma\tilde{\gamma}'\gamma)\tilde{N}, \tag{2.62}$$
$$\partial_z (\tilde{N}\tilde{\gamma}) = \tilde{N}(\tilde{\gamma}' + \tilde{\gamma}\gamma'\tilde{\gamma})N, \tag{2.63}$$
$$\tag{2.64}$$

all of which can be found by using the identities above.

The derivation of the Riccati parametrized Usadel equation and the Kuprianov-Lukichev boundary condition is thoroughly described in the paper by Jacobsen et al. [54]. To separate out the $\partial_z^2\gamma$ term from the Usadel equation, which is a 4×4 matrix equation, we take the upper-right 2×2 matrix minus the upper-left 2×2 matrix multiplied by γ. Thereafter we multily with $\frac{1}{2}N^{-1}$ from the left. This means writing

$$\tfrac{1}{2}N^{-1}([\dots]_{12} - [\dots]_{11}\gamma), \tag{2.65}$$

where $[\dots]$ is the full matrix equation and the subscript indicates block matrix. For the boundary condition, $\partial_z\gamma$ is found by the same procedure. The Riccati parameterized Usadel equation for a ferromagnet reads

$$\partial_z^2\gamma = -2iE\gamma - i\boldsymbol{h}\cdot(\tau\gamma - \gamma\tau^*) - 2\gamma'\tilde{N}\tilde{\gamma}\gamma', \tag{2.66}$$

where for a normal metal, the only adjustment needed is to set $\boldsymbol{h} = 0$. Further, it can be shown that the Riccati parameterized bulk superconductor solution is

$$\gamma_{\mathrm{BCS}} = \begin{pmatrix} 0 & b \\ -b & 0 \end{pmatrix}, \tag{2.67}$$

where

$$b = \begin{cases} \frac{\Delta}{E+i\sqrt{\Delta^2-E^2}} & \text{for} |E| > \Delta, \\ \frac{\Delta\,\mathrm{sgn}(E)}{|E|+\sqrt{E^2-\Delta^2}} & \text{for} |E| < \Delta. \end{cases} \tag{2.68}$$

2.9.1 Riccati parametrization of boundary conditions

Before starting on the Riccati parametrizing of the specific boundary conditions we note that many of the terms, both in the spin-orbit coupling and spin-active boundary conditions, have the same form. Here a practical method for Riccati parametrizing this type of term is presented in order to simplify the calculation in the two following sections.

Several of the terms take the form

$$[\hat{g}_L, \hat{U}], \tag{2.69}$$

where $\hat{U}$ is a matrix whose exact form depends on the specific boundary conditions. In general, we write $\hat{U}$ as

$$\hat{U} = \begin{pmatrix} \hat{U}_{11} & \hat{U}_{12} \\ \hat{U}_{21} & \hat{U}_{22} \end{pmatrix}. \tag{2.70}$$

It can be found that the procedure described by Equation (2.65) performed to the left side of the boundary conditions $g\partial_z g$ gives

$$\frac{1}{2}N_L^{-1}\big([\hat{g}_L\partial_z\hat{g}_L]_{12} - [\hat{g}_L\partial_z\hat{g}_L]_{11}\gamma_L\big) = \partial_z\gamma_L, \tag{2.71}$$

as seen in [54].

This is the left-hand side of the Riccati parameterized boundary conditions. For the complete boundary conditions, we also have to do the same on the right-hand side. This means we need to take $\frac{1}{2}N_L^{-1}([\dots]_{12} - [\dots]_{11}\gamma_L)$ of every term on the right-hand side of the boundary conditions. Thus we start by finding a procedure for all terms that come in the form of Equation (2.69).

$$\begin{aligned}&\frac{1}{2}N_L^{-1}\big([\hat{g}_L,\hat{U}]^{1,2} - [\hat{g}_L,\hat{U}]^{1,1}\gamma_L\big)\\&= \frac{1}{2}N_L^{-1}\big(\underline{g}_L\hat{U}_{12} + \underline{f}_L\hat{U}_{22} - \hat{U}_{11}\underline{f}_L + \hat{U}_{12}\tilde{\underline{g}}_L - (\underline{g}_L\hat{U}_{11} + \underline{f}_L\hat{U}_{21} - \hat{U}_{11}\underline{g}_L + \hat{U}_{12}\tilde{\underline{f}}_L)\gamma_L\big).\end{aligned} \tag{2.72}$$

As a next step, every term with the same 2×2 $\hat{U}_{ij}$ matrix is put together and we insert $\underline{f} = 2N\gamma$ and $\underline{g} = 2N - 1$. The $\hat{U}_{11}$ terms can be written as

$$\begin{aligned}&\tfrac{1}{2}N_L^{-1}(-\hat{U}_{11}\underline{f}_L - \underline{g}_L\hat{U}_{11}\gamma_L + \hat{U}_{11}\underline{g}_L\gamma_L)\\&= \tfrac{1}{2}N_L^{-1}(-\hat{U}_{11}2N_L\gamma_L - (2N_L-1)\hat{U}_{11}\gamma_L + \hat{U}_{11}(2N_L-1)\gamma_L)\\&= -\hat{U}_{11}\gamma_L.\end{aligned} \tag{2.73}$$

In the same manner the $\hat{U}_{12}$ terms become

$$\begin{aligned}&\tfrac{1}{2}N_L^{-1}\big(\underline{g}_L\hat{U}_{12} + \hat{U}_{12}\tilde{\underline{g}}_L - \hat{U}_{12}\tilde{\underline{f}}_L\gamma_L\big)\\&= \tfrac{1}{2}N_L^{-1}\big((2N_L-1)\hat{U}_{12} + \hat{U}_{12}(2\tilde{N}_L - 1) - \hat{U}_{12}2\tilde{N}_L\tilde{\gamma}_L\gamma_L\big)\\&= \hat{U}_{12}.\end{aligned} \tag{2.74}$$

The $\hat{U}_{21}$ term should also be written in terms of γ as

$$\begin{aligned}&\tfrac{1}{2}N_L^{-1}(-\underline{f}_L\hat{U}_{21}\gamma_L)\\&= -\gamma_L\hat{U}_{21}\gamma_L.\end{aligned} \tag{2.75}$$

And finally the $\hat{U}_{22}$ term can be written as

$$\begin{aligned}&\tfrac{1}{2}N_L^{-1}(\underline{f}_L\hat{U})\\&= \gamma_L\hat{U}_{22}.\end{aligned} \tag{2.76}$$

Putting everything together we get

$$\frac{1}{2}N_L^{-1}\big([\hat{g}_L,\hat{U}]^{1,2} - [\hat{g}_L,\hat{U}]^{1,1}\gamma_L\big) = -\hat{U}_{11}\gamma_L + \hat{U}_{12} - \gamma_L\hat{U}_{21}\gamma_L + \gamma_L\hat{U}_{22}. \tag{2.77}$$

We note that this also can be used for the Kuprianov-Lukichev boundary conditions, where we would use $\hat{U} = \Omega\hat{g}_R$. From this, and using the identities in Equation (2.58) and (2.59), the Kuprianov-Lukichev boundary conditions can be found to be

$$\partial_z\gamma_L = \Omega(1 - \gamma_L\tilde{\gamma}_R)N_R(\gamma_R - \gamma_L), \tag{2.78}$$

$$\partial_z\gamma_R = \Omega(1 - \gamma_R\tilde{\gamma}_L)N_L(\gamma_L - \gamma_R). \tag{2.79}$$

$$\tag{2.80}$$

In the following, both the spin-orbit coupled and spin-active boundary conditions will be written in the Riccati parameterized form using the method described here. In the following derivation, the underline notation of the 2×2 Greens function $\underline{g}$ and $\underline{f}$ is removed to keep the calculation tidier.

Riccati parametrization of the SOC boundary conditions

We now look into the Riccati parametrization of spin-orbit coupled boundary conditions given in Equation (2.44), where we do the same to every term on the right-hand side as we did to the left-hand side in Equation (2.71) The first term is simply the Kuprianov-Lukichev boundary term. The rest of the terms we go through one by one.

The first term is $\frac{2}{3}T_1^2p_F^2[\hat{g}_L, \hat{\boldsymbol{\tau}}_\parallel\hat{g}_R\hat{\boldsymbol{\tau}}_\parallel]$, for which we define the matrix

$$\hat{U}^{(1)} = \hat{\boldsymbol{\tau}}_\parallel\hat{g}_R\hat{\boldsymbol{\tau}}_\parallel = \begin{pmatrix} \tau_x g_L\tau_x & -\tau_x f_L\tau_x^* \\ \tau_x^*\tilde{f}_L\tau_x & -\tau_x^*\tilde{g}_L\tau_x^* \end{pmatrix} + \begin{pmatrix} \tau_y g_L\tau_y & -\tau_y f_L\tau_y^* \\ \tau_y^*\tilde{f}_L\tau_y & -\tau_y^*\tilde{g}_L\tau_y^* \end{pmatrix}, \tag{2.81}$$

where we leave out the prefactor $\frac{2}{3}T_1^2p_F^2$. Thus the contribution from this term will according to Equation (2.77) be

$$\begin{aligned} &\frac{1}{2}N_L^{-1}\big([\hat{g}_L, \frac{2}{3}T_1^2p_F^2[\hat{g}_L, \hat{\boldsymbol{\tau}}_\parallel\hat{g}_R\hat{\boldsymbol{\tau}}_\parallel]]^{1,2} - [\hat{g}_L, \frac{2}{3}T_1^2p_F^2[\hat{g}_L, \hat{\boldsymbol{\tau}}_\parallel\hat{g}_R\hat{\boldsymbol{\tau}}_\parallel]]^{1,1}\gamma_L\big) \\ =&\big[-(\tau_x g_L\tau_x + \tau_y g_L\tau_y)\gamma_L - \tau_x f_L\tau_x^* - \tau_y f_L\tau_y^* - \gamma_L(\tau_x^*\tilde{f}_L\tau_x + \tau_y^*\tilde{f}_L\tau_y)\gamma_L \\ &+\gamma_L(-\tau_x^*\tilde{g}_L\tau_x^* - \tau_y^*\tilde{g}_L\tau_y^*)\big]. \end{aligned} \tag{2.82}$$

We insert $f = 2N\gamma$ and $g = (2N-1)$ get

$$\begin{aligned} &[-\tau_x N_L\tau_x\gamma_L + \gamma_L - \tau_x N_L\gamma_L\tau_x^* - \gamma_L\tau_x^*\tilde{N}_L\tilde{\gamma}_L\tau_x\gamma_L - \gamma_L\tau_x^*\tilde{N}_L\tau_x^* \\ &-\tau_y N_L\tau_y\gamma_L + \gamma_L - \tau_y N_L\gamma_L\tau_y^* - \gamma_L\tau_y^*\tilde{N}_L\tilde{\gamma}_L\tau_y\gamma_L - \gamma_L\tau_y^*\tilde{N}_L\tau_y^*]. \end{aligned} \tag{2.83}$$

From the second term we define

$$\begin{aligned} \hat{U}^{(2)} =&\{\hat{\tau}_{\parallel,x}, \hat{g}_R\partial_y\hat{g}_R\} \\ =&\begin{pmatrix} \tau_x[g_Rg_R' - f_R\tilde{f}_R'] & \tau_x[g_Rf_R' - f_R\tilde{g}_R'] \\ -\tau_x^*[\tilde{f}_Rg_R' + \tilde{g}_R\tilde{f}_R'] & -\tau_x[-\tilde{f}_Rf_R' + \tilde{g}_R\tilde{g}_R'] \end{pmatrix} \\ &+\begin{pmatrix} [g_Rg_R' - f_R\tilde{f}_R']\tau_x & -[g_Rf_R' - f_R\tilde{g}_R']\tau_x^* \\ [\tilde{f}_Rg_R' + \tilde{g}_R\tilde{f}_R']\tau_x & -[-\tilde{f}_Rf_R' + \tilde{g}_R\tilde{g}_R']\tau_x^* \end{pmatrix}, \end{aligned} \tag{2.84}$$

which gives us the contribution to the right-hand side

$$\begin{aligned} &\big[-(\tau_x[g_Rg_R' - f_R\tilde{f}_R'] + [g_Rg_R' - f_R\tilde{f}_R']\tau_x)\gamma_R \\ &+\tau_x[g_Rf_R' - f_R\tilde{g}_R'] - [g_Rf_R' - f_R\tilde{g}_R']\tau_x^* \\ &-\gamma_R(-\tau_x^*[\tilde{f}_Rg_R' + \tilde{g}_R\tilde{f}_R'] + [\tilde{f}_Rg_R' + \tilde{g}_R\tilde{f}_R']\tau_x)\gamma_R \\ &\gamma_R(-\tau_x[-\tilde{f}_Rf_R' + \tilde{g}_R\tilde{g}_R'] - [-\tilde{f}_Rf_R' + \tilde{g}_R\tilde{g}_R']\tau_x^*)\big]. \end{aligned} \tag{2.85}$$

Using Equation (2.63) and (2.64) we see that we may write the following

$$\begin{aligned} [g_Rg_R' - f_R\tilde{f}_R'] &= N_R[\gamma_R'\tilde{\gamma}_R - \gamma_R\tilde{\gamma}_R']N_R, \\ [g_Rf_R' - f_R\tilde{g}_R'] &= N_R[\gamma_R' - \gamma_R\tilde{\gamma}_R'\gamma_R]\tilde{N}_R. \end{aligned} \tag{2.86}$$

Thus the contribution to the right-hand side of the Riccati parametrized boundary conditions can be written as

$$\begin{aligned} &\tau_x 2N_R[\gamma_R' - \gamma_R\tilde{\gamma}_R'\gamma_R]\tilde{N}_R - 2N_R[\gamma_R' - \gamma_R\tilde{\gamma}_R'\gamma_R] \\ &-\gamma_L\tau_x^*2\tilde{N}_R[\tilde{\gamma}_R'\gamma_R - \tilde{\gamma}_R\gamma_R'] - \gamma_L 2\tilde{N}_R[\tilde{\gamma}_R'\gamma_R - \tilde{\gamma}_R\gamma_R']\tilde{N}_R\tau_x^* \\ &-\tau_x 2N_R[\gamma_R'\tilde{\gamma}_R - \gamma_R\tilde{\gamma}_R]N_R\gamma_L - 2N_R[\gamma_R'\tilde{\gamma}_R - \gamma_R\tilde{\gamma}_R]N_R\tau_x\gamma_L \\ &+\gamma_L\tau_x^*2\tilde{N}_R[\tilde{\gamma}_R' - \tilde{\gamma}_R\gamma_R'\tilde{\gamma}_R]N_R\gamma_L - \gamma_L 2\tilde{N}_R[\tilde{\gamma}_R' - \tilde{\gamma}_R\gamma_R'\tilde{\gamma}_R]N_R\tau_x\gamma_L. \end{aligned} \tag{2.87}$$

The third and fourth terms in Equation (2.44) do not have the shape as in Equation (2.77), so we have to treat them differently. The two terms do, however, have the same shape as each other. Therefore we only have to do the calculation once by performing the parametrization procedure on

$$[\hat{\rho}_i, \hat{g}_L\hat{\rho}_i\hat{g}_L]. \tag{2.88}$$

First, we write out $g_L\hat{\rho}_i g_L$

$$g_L\hat{\rho}_i g_L = \begin{pmatrix} g_L\tau_i g_L + f_L\tau_i^*\tilde{f}_L & g_L\tau_i f_L + f_L\tau_i^*\tilde{g}_L \\ -\tilde{f}_L\tau_i g_L - \tilde{g}_L\tau_i^*\tilde{f}_L & -\tilde{f}_L\tau_i f_L - \tilde{g}_L\tau_i^*\tilde{g}_L \end{pmatrix}. \tag{2.89}$$

The upper left component of the whole expression then reads

$$[\hat{\rho}_i, \hat{g}_L\hat{\rho}_i\hat{g}_L]^{(1,1)} = \tau_i g_L\tau_i g_L + \tau_i f_L\tau_i^*\tilde{f}_L - g_L\tau_i g_L\tau_i - f_L\tau_i^*\tilde{f}_L\tau_i, \tag{2.90}$$

and the upper right part reads

$$[\hat{\rho}_i, \hat{g}_L\hat{\rho}_i\hat{g}_L]^{(1,2)} = \tau_i g_L\tau_i f_L + \tau_i f_L\tau_i^*\tilde{g}_L + g_L\tau_i f_L\tau_i^* + f_L\tau_i^*\tilde{g}_L\tau_i^*. \tag{2.91}$$

We write g and f in terms of the Riccati parametrized expressions and get that the contribution from these terms to the right-hand side is

$$\begin{aligned} &\tfrac{1}{2}N_L^{-1}\big[\tau_i(2N_L-1)\tau_i 2N_L\gamma_L + \tau_i 2N_L\gamma_L\tau_i^*(2\tilde{N}_L-1) + (2N_L-1)\tau_i 2N_L\gamma_L\tau_i^* \\ &+ 2N_L\gamma_L\tau_i^*(2\tilde{N}_L-1)\tau_i^* - [\tau_i(2N_L-1)\tau_i(2N_L-1) + \tau_i 2N_L\gamma_L\tau_i^* 2\tilde{N}_L\tilde{\gamma}_L \\ &- (2N_L-1)\tau_i(2N_L-1)\sigma 9 - 2N_L\gamma_L\tau_i^* 2\tilde{N}_L\tilde{\gamma}_L]\gamma_L\big] \\ &= -2\gamma_L + 2\tau_i N_L\gamma_L\tau_i^* + 2\gamma_L\tau_i^*\tilde{N}_L\tau_i^* + 2\tau_i N_L\tau_i\gamma_L + 2\gamma_L\tau_i^*\tilde{N}_L\tilde{\gamma}_L\tau_i\gamma_L. \end{aligned} \tag{2.92}$$

Putting all of the terms together we get the complete Riccati parametrized spin-orbit coupled boundary conditions

$$\begin{aligned} \partial_z\gamma_L =& 2T_0(1-\gamma_L\tilde{\gamma}_R)N_R(\gamma_R-\gamma_L) \\ &+ 2\tfrac{2}{3}T_1^2p_F^2\big(-\tau_x N_L\tau_x\gamma_L + \gamma_L - \tau_x N_L\gamma_L\tau_x^* - \gamma_L\tau_x^*\tilde{N}_L\tilde{\gamma}_L\tau_x\gamma_L - \gamma_L\tau_x^*\tilde{N}_L\tau_x^* \\ &- \tau_y N_L\tau_y\gamma_L + \gamma_L - \tau_y N_L\gamma_L\tau_y^* - \gamma_L\tau_y^*\tilde{N}_L\tilde{\gamma}_L\tau_y\gamma_L - \gamma_L\tau_y^*\tilde{N}_L\tau_y^*\big) \\ &- mDT_1T_0\big(+\tau_x 2N_R[\gamma_R'-\gamma_R\tilde{\gamma}_R'\gamma_R]\tilde{N}_R - 2N_R[\gamma_R'-\gamma_R\tilde{\gamma}_R'\gamma_R] \\ &- \gamma_L\tau_x^*2\tilde{N}_R[\tilde{\gamma}_R'\gamma_R - \tilde{\gamma}_R\gamma_R'] - \gamma_L 2\tilde{N}_R[\tilde{\gamma}_R'\gamma_R - \tilde{\gamma}_R\gamma_R']\tilde{N}_R\tau_x^* \\ &- \tau_x 2N_R[\gamma_R'\tilde{\gamma}_R - \gamma_R\tilde{\gamma}_R]N_R\gamma_L - 2N_R[\gamma_R'\tilde{\gamma}_R - \gamma_R\tilde{\gamma}_R]N_R\tau_x\gamma_L \\ &+ \gamma_L\tau_x^*2\tilde{N}_R[\tilde{\gamma}_R' - \tilde{\gamma}_R\gamma_R'\tilde{\gamma}_R]N_R\gamma_L - \gamma_L 2\tilde{N}_R[\tilde{\gamma}_R' - \tilde{\gamma}_R\gamma_R'\tilde{\gamma}_R]N_R\tau_x\gamma_L\big) \\ &- Dd\alpha^2\big(-2\gamma_L + 2\tau_x N_L\gamma_L\tau_x^* + 2\gamma_L\tau_x^*\tilde{N}_L\tau_x^* + 2\tau_x N_L\tau_x\gamma_L + 2\gamma_L\tau_x^*\tilde{N}_L\tilde{\gamma}_L\tau_x\gamma_L\big) \\ &- Dd\alpha^2\big(-2\gamma_L + 2\tau_y N_L\gamma_L\tau_y^* + 2\gamma_L\tau_y^*\tilde{N}_L\tau_y^* + 2\tau_y N_L\tau_y\gamma_L + 2\gamma_L\tau_y^*\tilde{N}_L\tilde{\gamma}_L\tau_y\gamma_L\big). \end{aligned} \tag{2.93}$$

Riccati parametrization of the spin active boundary conditions

Now we find the Riccati parameterized boundary conditions for the spin-active interfaces given in Equation (2.41). All the terms in this boundary condition are on form as in Equation (2.69). As for the spin-orbit coupling boundary conditions the first term is

simply the Kuprianov-Lukichev term. The rest we go through one term at a time starting with the G_1 term. Here we define

$$U_1 = \hat{m}\hat{g}_R\hat{m} = \begin{pmatrix} \boldsymbol{m}\cdot\boldsymbol{\tau} g_R \boldsymbol{m}\cdot\boldsymbol{\tau} & \boldsymbol{m}\cdot\boldsymbol{\tau} f_R \boldsymbol{m}\cdot\boldsymbol{\tau}^* \\ -\boldsymbol{m}\cdot\boldsymbol{\tau}^* \tilde{f}_R \boldsymbol{m}\cdot\boldsymbol{\tau} & -\boldsymbol{m}\cdot\boldsymbol{\tau}^* \tilde{g}_R \boldsymbol{m}\cdot\boldsymbol{\tau}^* \end{pmatrix}, \tag{2.94}$$

which gives the contribution to the right-hand side

$$-\boldsymbol{m}\cdot\boldsymbol{\tau} g_R \boldsymbol{m}\boldsymbol{\tau}\gamma_L + \boldsymbol{m}\boldsymbol{\tau} f_R \boldsymbol{m}\boldsymbol{\tau}^* + \gamma_L \boldsymbol{m}\boldsymbol{\tau}^* \tilde{f}_R \boldsymbol{m}\boldsymbol{\tau}\gamma_L - \gamma_L \boldsymbol{m}\boldsymbol{\tau}^* \tilde{g}_R \boldsymbol{m}\boldsymbol{\tau}^*. \tag{2.95}$$

By inserting the $f = 2N\gamma$ and $g = 2N - 1$ and using the useful identities this can be written as

$$\begin{aligned} &\boldsymbol{m}\cdot\boldsymbol{\tau} N_R \gamma_R \boldsymbol{m}\cdot\boldsymbol{\tau}^* - \gamma_L \boldsymbol{m}\cdot\boldsymbol{\tau}^* \tilde{N}_R \tilde{\gamma}_R \boldsymbol{m}\boldsymbol{\tau}^* + m^2\gamma_L \\ &- \boldsymbol{m}\cdot\boldsymbol{\tau} \tilde{N}_R \boldsymbol{m}\cdot\boldsymbol{\tau}\gamma_L + \gamma_L \boldsymbol{m}\cdot\boldsymbol{\tau}^* \tilde{N}_R \tilde{\gamma} \boldsymbol{m}\cdot\boldsymbol{\tau}\gamma_L. \end{aligned} \tag{2.96}$$

For the second term, we define the U-matrix

$$U_{\mathrm{MR}} = \{\hat{g}_R, \hat{m}\} = \begin{pmatrix} g_R \boldsymbol{m}\cdot\boldsymbol{\tau} + \boldsymbol{m}\cdot\boldsymbol{\tau} g_R & f_R \boldsymbol{m}\cdot\boldsymbol{\tau}^* + \boldsymbol{m}\cdot\boldsymbol{\tau} f_R \\ -\tilde{f}_R \boldsymbol{m}\cdot\boldsymbol{\tau} - \boldsymbol{m}\cdot\boldsymbol{\tau}^* \tilde{f}_R & -\tilde{g}_R \boldsymbol{m}\cdot\boldsymbol{\tau}^* - \boldsymbol{m}\cdot\boldsymbol{\tau}^* \tilde{g}_R \end{pmatrix}, \tag{2.97}$$

which gives the contribution to the right-hand side

$$\begin{aligned} &-(g_R \boldsymbol{m}\cdot\boldsymbol{\tau} + \boldsymbol{m}\cdot\boldsymbol{\tau} g_R)\gamma_L \\ &+ f_R \boldsymbol{m}\cdot\boldsymbol{\tau}^* + \boldsymbol{m}\cdot\boldsymbol{\tau} f_R \\ &- \gamma_L(-\tilde{f}_R \boldsymbol{m}\cdot\boldsymbol{\tau} - \boldsymbol{m}\cdot\boldsymbol{\tau}^* \tilde{f}_R)\gamma_L \\ &+ \gamma_L(-\tilde{g}_R \boldsymbol{m}\cdot\boldsymbol{\tau}^* - \boldsymbol{m}\cdot\boldsymbol{\tau}^* \tilde{g}_R). \end{aligned} \tag{2.98}$$

Written only in terms of the Riccati parameters this reads

$$\begin{aligned} &N_R\gamma_R \boldsymbol{m}\boldsymbol{\tau}^* + \boldsymbol{m}\cdot\boldsymbol{\tau} N_R\gamma_R - \gamma_L[\tilde{N}_R \boldsymbol{m}\cdot\boldsymbol{\tau}^* + \boldsymbol{m}\cdot\boldsymbol{\tau}^* \tilde{N}_R - \boldsymbol{m}\cdot\boldsymbol{\tau}^*] \\ &- [N_R \boldsymbol{m}\cdot\boldsymbol{\tau} - \boldsymbol{m}\cdot\boldsymbol{\tau} + \boldsymbol{m}\cdot\boldsymbol{\tau} N_R]\gamma_L - \gamma_L[\tilde{N}_R \tilde{\gamma}_R \boldsymbol{m}\cdot\boldsymbol{\tau} + \boldsymbol{m}\boldsymbol{\tau}^* \tilde{N}_R \tilde{\gamma}_R]\gamma_L \end{aligned} \tag{2.99}$$

For the third term, the U-matrix is simply

$$U_\phi = \hat{m}, \tag{2.100}$$

which gives the contribution

$$-\boldsymbol{m}\cdot\boldsymbol{\tau}\gamma_L + \gamma_L \boldsymbol{m}\cdot\boldsymbol{\tau}^*. \tag{2.101}$$

The total Riccati parameterized spin-active boundary conditions thus read

$$\begin{aligned} \partial_z\gamma_L =& G_0(1 - \gamma_L\tilde{\gamma}_R)N_R(\gamma_R - \gamma_L) \\ &+ G_1\big(\boldsymbol{m}\cdot\boldsymbol{\tau} N_R\gamma_R \boldsymbol{m}\cdot\boldsymbol{\tau}^* - \gamma_L \boldsymbol{m}\cdot\boldsymbol{\tau}^* \tilde{N}_R \tilde{\gamma}_R \boldsymbol{m}\boldsymbol{\tau}^* + m^2\gamma_L \\ &- \boldsymbol{m}\cdot\boldsymbol{\tau} \tilde{N}_R \boldsymbol{m}\cdot\boldsymbol{\tau}\gamma_L + \gamma_L \boldsymbol{m}\cdot\boldsymbol{\tau}^* \tilde{N}_R \tilde{\gamma} \boldsymbol{m}\cdot\boldsymbol{\tau}\gamma_L\big) \\ &+ G_{\mathrm{MR}}\big(N_R\gamma_R \boldsymbol{m}\boldsymbol{\tau}^* + \boldsymbol{m}\cdot\boldsymbol{\tau} N_R\gamma_R - \gamma_L[\tilde{N}_R \boldsymbol{m}\cdot\boldsymbol{\tau}^* + \boldsymbol{m}\cdot\boldsymbol{\tau}^* \tilde{N}_R - \boldsymbol{m}\cdot\boldsymbol{\tau}^*] \\ &- [N_R \boldsymbol{m}\cdot\boldsymbol{\tau} - \boldsymbol{m}\cdot\boldsymbol{\tau} + \boldsymbol{m}\cdot\boldsymbol{\tau} N_R]\gamma_L - \gamma_L[\tilde{N}_R \tilde{\gamma}_R \boldsymbol{m}\cdot\boldsymbol{\tau} + \boldsymbol{m}\boldsymbol{\tau}^* \tilde{N}_R \tilde{\gamma}_R]\gamma_L\big) \\ &+ iG_\phi\big(-\boldsymbol{m}\cdot\boldsymbol{\tau}\gamma_L + \gamma_L \boldsymbol{m}\cdot\boldsymbol{\tau}^*\big). \end{aligned} \tag{2.102}$$

Chapter 3

Supercurrents and Induced Magnetization

In this chapter, we will investigate how we can use spin-active boundaries to create spin and charge currents and how they in turn can induce a magnetization in a normal metal through a spin-orbit coupling interface. The three different cases, singlet current, triplet charge current, and spin current are considered. First, the setup and numerical methods are discussed. Next, an analytical study of the system is presented, where the linearized boundary conditions are used to make predictions of what should be expected in the numerical study. Finally, the numerical results are presented.

3.1 Setup

The system we are studying is illustrated in Figure 3.1. The region in which the supercurrents will flow is drawn to the left and will therefore be referred to as (L). Similarly, the region where induced magnetization will be studied is drawn to the right and is called (R). In this study we let the region (R) be a normal metal, and (L) will either be a normal metal or a ferromagnet depending on the situation. The z position at which (R) is connected to (L) is called z_0. In most situations, we use $z_0 = l/2$, and it will be specified when other values are used. The grey region between (L) and (R) is the spin-orbit coupled material, for which the spin-orbit coupled boundary conditions will be used. At $z = 0$ and $z = l$, conventional BCS superconductors, S1 and S2, are attached to the (L) material. These superconductors are the sources for Cooper pairs in the rest of the system. Between (L) and the superconductor spin-active interfaces are introduced and are marked as grey regions in the figure. The interface magnetizations in the spin-active interfaces are called $\boldsymbol{m}_1$ and $\boldsymbol{m}_2$.

To create the singlet charge current, the interface magnetizations are switched off $\boldsymbol{m}_1 = \boldsymbol{m}_2 = 0$, which is equivalent to using the regular Kuprianov-Lukichev boundary conditions. Furthermore, (L) is a normal metal in the singlet current case. As the superconductors S1 and S2 only contain singlet Cooper pairs, no triplets will be induced in (L) in this scenario. We want a supercurrent to flow through the (L) region. This is achieved by applying a phase difference, ϕ, between S1 and S2.

To create the triplet charge currents and the spin current, the interface magnetizations are switched on. The triplet charge current is created in the same way as in the singlet case, by applying a phase difference. As we will see later, a spin current can be created without applying a phase difference.

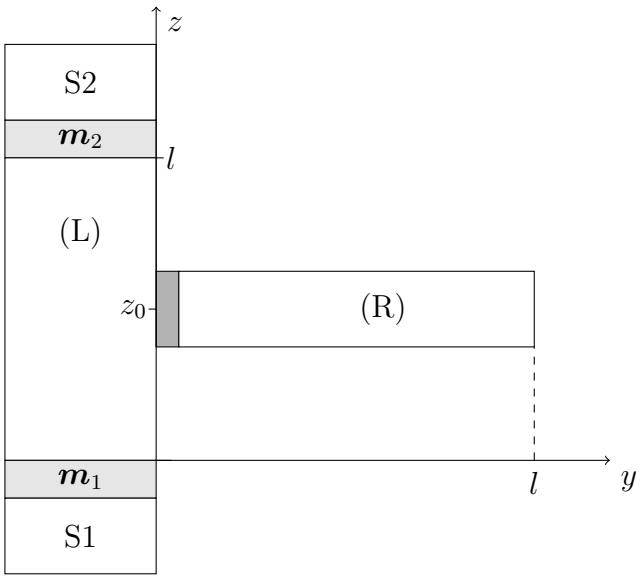

Figure 3.1: The system in which supercurrents and induced magnetization are investigated. The material to the left, (L), is the material in which the supercurrent will flow. This material will be either a ferromagnet or a normal metal. To get the currents flowing, two conventional superconductors are connected to (L), and a phase difference between them is applied. In between the superconductors and (L) spin active interfaces are included in the purpose of creating triplet Cooper pairs and thereby also triplet supercurrents. A normal metal, (R), is connected to (L) through a spin-orbit coupling interface. This material borders to vacuum at $y = l$.

For the purpose of discovering effects caused solely by triplets, a ferromagnetic exchange field is included in the material (L). Because of the exchange field, the singlet becomes short-ranged and dies out rapidly in the (L) region. In an experimental setup, it would be of importance to separate the magnetization from an exchange field and the magnetization induced by supercurrents. Therefore the exchange field is modeled to be spatially varying in (L) such that it is zero in the middle region, but large at the sides. In practice, this can be realized by attaching thin ferromagnetic regions with a strong exchange field right next to the superconductors and then having a long normal metal region separating the ferromagnets. In this way, the singlets and short-range triplets are filtered out by the thin, strongly polarized ferromagnetic regions, whereas the long-range triplets remain and can propagate through the normal metal. More specifically, it is the triplet component that is spin-neutral in the exchange field orientation $\boldsymbol{d}||\boldsymbol{h}$ that is short-ranged, and the others are long-ranged.

As we will discuss in the following analytical study, the difference between the d_z and d_y component is quite insignificant in the spin-orbit coupled interface, it is the d_x component that is by far the most relevant. Therefore, we focus most of the discussion on the case where the interface magnetizations lie in the xy-plane, and the exchange field points in the z-direction, $\boldsymbol{h} = (0, 0, h(z))$. We do, however, include rotation of both $\boldsymbol{m}_1$ and $\boldsymbol{m}_2$ with an angle α around the z-axis, and the angle between $\boldsymbol{m}_1$ and $\boldsymbol{m}_2$ which we call θ. These angles are illustrated in Figure 3.2. We also note here that the directions chosen are advantageous for an experimental setup, as rotating the interface magnetizations in plane is a simpler task than driving them out of the xy-plane.

We also remark that rotating both interface magnetizations, $\boldsymbol{m}_1$ and $\boldsymbol{m}_2$, by an angle

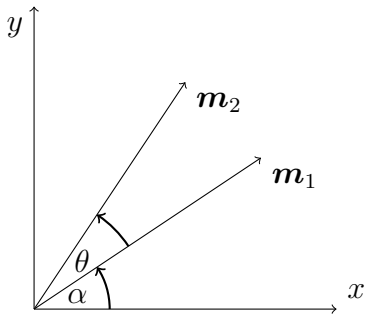

Figure 3.2: The figure shows the definition of the angles α and θ. α is defined as the angle between the x-axis and the interface magnetization of in the first interface $\boldsymbol{m}_1$. θ is the angle between the two interface magnetizations.

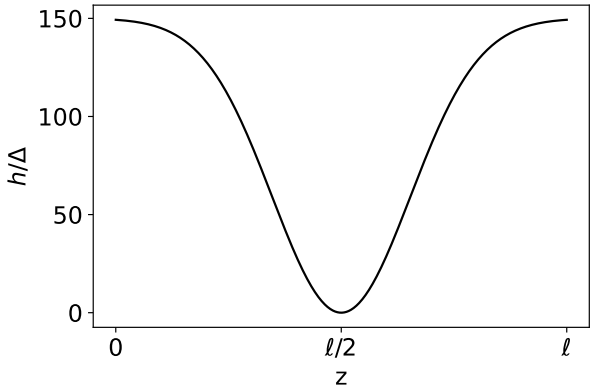

Figure 3.3: The figure shows the exchange field function $h(z)$ which is applied to the left material (L) in the triplet current cases.

α is equivalent to rotating material (L) around the z-axis. If we consider (L) to be an unknown material, α dependent signatures can thus be utilized to determine the current in the unknown material, given that measurements in different attachment angles are possible.

We note that we have mainly focused on discovering in which situations induced magnetization occurs, not on the strength of a realistic magnetization, which would require using physically realistic parameters. As we can not guarantee that all parameters are realistic, we do also not draw conclusions about the strength of the induced magnetization, only about the possible existence of the magnetizations. In the numerical study, we have used the following spin-orbit coupled interface parameters $T_0^2 = 0.2, \frac{2}{3}T_1^2 p_F^2 = mDT_1T_2 = Dd\alpha = 0.1$. As in the paper by Ouasso et al. [32], we set $P = 0.12$ and $G_\phi = 0.3G_0$ whenever the interface is described by non-zero values for these parameters. However, to be able to create pure charge currents we also use $P = 0$ or $G_\phi = 0$. The interface magnetization strength we use is $m = |\boldsymbol{m}_1| = |\boldsymbol{m}_2| = 10$, and the spin-independent tunneling $G_0 = 1$. Furthermore, a combination of the length of material (L), l, that is short enough to preserve some of the triplets, and strength of $\boldsymbol{h}$ that is strong enough to remove the singlet, had to be found. Setting the length of material l to eight times the bulk superconducting coherence length $l = 8\xi_s = 8\sqrt{D/\Delta_0}$, and $h(z)$ as in Figure 3.3 was found to work well. Note here that in the setup in Figure 3.1, the axes are defined differently than in section 2.7.3, however, the only difference is changing the $\boldsymbol{\tau}_\parallel$.

3.1.1 Numerical method

Both sides of the interface are affected by each other. However, here it is assumed that the proximity effect is weak and that it is sufficient to consider the proximity effect to go one way. This means that the effect (L) has on S1 and S2 is neglected, and only the effect from the superconductor on the material (L) is considered. The superconductors are thus assumed to be the bulk superconductors all the way to the spin-active interfaces. The bulk superconductor Green function can by this assumption be used directly in the boundary conditions used to solve system (L). Similarly, the effect from (R) on (L) is neglected, and the solution for system (L) at $z = z_0$ is used directly into the spin-orbit coupled boundary conditions for (R). Furthermore, the materials are individually modeled as one-dimensional, meaning that material (L) is extended in the z-direction and (R) in the y-direction.

The system which has to be solved is now a one-dimensional Usadel equation. This is a second-order differential equation for two variables γ and $\tilde{\gamma}$, and to solve it numerically we rewrite it as four first-order differential equations writing

$$\begin{pmatrix} \gamma' \\ \gamma'' \\ \tilde{\gamma}' \\ \tilde{\gamma}'' \end{pmatrix} = f \begin{pmatrix} \gamma \\ \gamma' \\ \tilde{\gamma} \\ \tilde{\gamma}' \end{pmatrix}, \tag{3.1}$$

where $f()$ is a function that returns the derivative of the input. The function will thus return γ' as the derivative for γ and use the Riccati parameterized Usadel equation to find the derivative of γ', and similarly for $\tilde{\gamma}$. Thus we have a system of 16 complex differential equations, four elements in each of the matrices $\gamma, \gamma', \tilde{\gamma}$, and $\tilde{\gamma}'$. The boundary conditions give restrictions to γ' and $\tilde{\gamma}'$ on each side of the material.

To solve the system we have used the boundary value problem solver from SciPy [55]. To stabilize the solver, the real and imaginary parts are split such that the 16 complex equations become 32 real ones. To increase numerical stability an inelastic scattering is also included by adding a small imaginary component to the energy, which here is set to $\delta = 0.01$ as used in [32]. This imaginary component is often referred to as the Dynes parameter and has also been found to exist experimentally [56]. Shortly explained, it has the effect of broadening the peaks of the Green functions that occur at $E = 0$ and $E = \Delta$.

As mentioned, the interface magnetizations are rotated in the xy-plane in the triplet cases. To save computation time, the Usadel equation only has to be solved once in material (L) for one given θ and one given set of interface parameters. The angle α can simply be taken into account by rotating the triplet components $d_{x,L}$ and $d_{y,L}$, such that

$$\begin{aligned} d_{x,L}(\alpha) &= d_{x,L}(0)\cos(\alpha) + d_{y,L}(0)\sin(\alpha), \\ d_{y,L}(\alpha) &= -d_{x,L}(0)\sin(\alpha) + d_{y,L}(0)\cos(\alpha). \end{aligned} \tag{3.2}$$

This means that instead of solving the system in (L) for every α, we solve it once and then rotate the solution to proceed to study the material (R). For the material (R), however, the Usadel equation needs to be solved separately for every value of α.

To verify our numerical method we have tested it on some known cases. We notice that the singlet current behaves as expected in a Josephson junction [57, 58]. We also see that our conclusion for the induced magnetization from a singlet charge current is the same as in the paper by J. Linder and M. Amundsen [30]. Also for the rest of the cases,

the numerical results seem to be supported by the analytical study. Another sanity check is to see that the physical observables are not dependent on the value of the individual phases in S1 and S2, only the phase difference between them. It was therefore tested and seen that currents and magnetization were unchanged under addition of the same phase to both of the superconductors. Additionally, it was seen that the current in material (L) was conserved throughout the material both in the singlet and the triplet case as should be expected in an equilibrium system.

The code used for the numerical study can be found on GitHub [59].

3.2 A brief analytical study

To get an idea of what to expect from the numerical study, we start by analyzing the system using the linearized boundary conditions, as well as the magnetization and current expressions. We will see that there is a clear relation between singlet charge current, J_{f_s}, and induced magnetization in the x-direction, M_x. A similar relation also exists between a triplet charge current carried by the d_x triplet, J_{d_x}, and M_x.

In the weak proximity regime, we assume that the quasiclassical Green function is close to the normal metal solution, $\hat{g}_N = \hat{\rho}_3$, but with a small superconducting part, $\hat{f}$, induced by the proximity superconductors. We thereby assume that we can use the weak proximity solution $\hat{g} \approx \hat{\rho}_3 + \hat{f}$. Using the singlet-triplet decomposition, the spin-orbit coupled boundary conditions can be written as follows keeping only the terms of the first order in $\hat{f}$.

$$\partial_y f_{s,R} = -mDT_1T_2(\partial_z d_{x,L}) - 2(T_0^2 - 2\tfrac{2}{3}T_1^2p_F^2)(f_{s,L} - f_{s,R}) \tag{3.3}$$
$$\partial_y d_{z,R} = -(8Dd\alpha - 2T_0^2 + 4\tfrac{2}{3}T_1^2p_F^2)d_{z,R} - 2d_{z,L}(T_0^2 + 2\tfrac{2}{3}T_1^2p_F^2) \tag{3.4}$$
$$\partial_y d_{x,R} = -4(\partial_z f_{s,L})mDT_1T_2 - (4\tfrac{2}{3}T_1^2p_F^2 + 4Dd\alpha - 2T_0^2)d_{x,R} - 2d_{x,L}T_0^2 \tag{3.5}$$
$$\partial_y d_{y,R} = -(4\tfrac{2}{3}T_1^2p_F^2 + 4Dd\alpha - 2T_0^2)d_{y,R} - 2T_0^2 d_{y,L} \tag{3.6}$$

From this, we see that there is a link between $f_{s,R}$ and $\partial_z d_{x,L}$ and the other way around between $d_{x,R}$ and $\partial_z f_{s,L}$. Whereas, to the first order, $d_{y,R}$ can only be induced by $d_{y,L}$ and $d_{z,R}$ only by $d_{z,L}$.

Furthermore, we can use the solution to the linearized Usadel equation in a normal metal

$$\begin{aligned} f_s &= A_s e^{-ky} + B_s e^{ky}, \\ d_x &= A_x e^{-ky} + B_x e^{ky}, \end{aligned} \tag{3.7}$$

where $k = \sqrt{-2iE/D}$ and A_s, A_x, B_s, and B_s are constants that have to be determined using the boundary conditions. If we assume that $l = \infty$, the B factors have to be zero in order to avoid blowing up the function. This gives $f_{s,R} \propto \partial_y f_{s,R}$ and $\boldsymbol{d}_R \propto \partial_y \boldsymbol{d}_R$. In the following, we will use these proportionalities to investigate the connection between the different currents and the induced magnetization.

3.2.1 Singlet current

We start by discussing the singlet charge current case. In this scenario, there are no triplet components present in (L). Thus there is no induced d_y or d_z on the right side of

the interface. Furthermore, there is no d_x and thus no $\partial_z d_x$ on the left side. Thus from Equation (3.3) and Equation (3.5) we see that

$$f_{s,R} \propto f_{s,L}, \tag{3.8}$$
$$d_{x,R} \propto \partial_z f_{s,L}. \tag{3.9}$$

Note that the tilde-conjugated components have the same proportionality between the left and right sides. Thus we can see that

$$f_{s,L}\partial_z \tilde{f}_{s,L} - \tilde{f}_{s,L}\partial_z f_s \propto f_{s,R}\tilde{d}_{x,R} - \tilde{f}_{s,R}d_{x,R}. \tag{3.10}$$

From Equation (2.51) and Equation (2.54) we see that the real part of the left side in the expression above is exactly what occurs in the expression for a singlet current in material (L), J_{f_s}. We also see that the real part of the right side in the expression is exactly what occurs in the induced magnetization expression M_x.

Thus from the analytical expression, we conclude that there is a clear connection between induced magnetization and the singlet charge current. We note, however, that $f_{s,L}\partial_z \tilde{f}_{s,L} - \tilde{f}_{s,L}\partial_z f_{s,L}$ and $f_{s,R}\tilde{d}_{x,R} - \tilde{f}_{s,R}d_{x,R}$ might not have the same phase, such that the real part of these expressions might not be directly proportional.

3.2.2 Triplet charge current

Next, considering triplet charge currents we see that J_{d_y} and J_{d_z}, which contain varying d_y and d_z components in (L), do not induce a singlet in (R), at least to the first order in f. We can thus conclude that J_{d_y} and J_{d_z} induce no magnetization in (R). For the last type of triplet charge current, J_{d_x} the same argumentation as for the singlet charge current applies. The difference is that in this case we have

$$d_{x,R} \propto d_{x,L}, \tag{3.11}$$
$$f_{s,R} \propto \partial_z d_{x,L}. \tag{3.12}$$

This gives

$$d_{x,L}\partial_z \tilde{d}_{x,L} - \tilde{d}_{x,L}\partial_z d_x \propto f_{s,R}\tilde{d}_{x,R} - \tilde{f}_{s,R}d_{x,R}. \tag{3.13}$$

The left side of this expression occurs in J_{d_x} and the right side in M_x. So seemingly J_{d_x} and J_{f_s} induces the same magnetization.

A triplet charge current does, however, not have to be carried by a pure d_x, d_y, or d_z. In general, we can have an arbitrary $\boldsymbol{d}$-vector carrying the pure charge current. Keeping to the situation where the triplet vector $\boldsymbol{d}$ points in the xy-plane, we would get a current carried partially by d_x and partially by d_y. In this case, the part carried by d_x seems to induce a singlet component in (R), whereas the d_y part induces a d_y in (R) as well. By this, a magnetization in the y-direction would also be induced. Thus we see that with a triplet charge current, magnetization can also be induced in more than one direction. This is contrary to the singlet charge current. Because of the similarities of the d_z and d_y boundary conditions, we also note that we expect also a magnetization in the z-direction from a current carried partially by d_z, partially by d_x.

3.2.3 Spin current

As mentioned, magnetization induced by a spin current will also be explored. From section 2.8 we see that there is no d_x component involved in the x-polarized current J_{s_x}. From this spin current, no singlet can be induced in (R), and thus also no magnetization. Both for the y-polarized spin current, J_{s_y}, and the z-polarized spin current J_{s_z}, a d_x component is involved. Since the d_y and d_z components are treated similarly by the spin-orbit coupled interface, we settle for only studying J_{s_z}. Assumingly, J_{s_y} would induce a rotated, but similar magnetization.

The z-polarized spin current, J_{s_z} is seen in Equation (2.49) to be dependent on the imaginary part of the following expression

$$d_{x,L}\partial_z\tilde{d}_{y,L} - d_{y,L}\partial_z\tilde{d}_{x,L} + \tilde{d}_{x,L}\partial_y d_{y,L} - \tilde{d}_{y,L}\partial_z d_{x,L}. \tag{3.14}$$

Notice that from the linearized spin-orbit coupled boundary conditions, it can be found that

$$d_{y,L}\partial_z\tilde{d}_{x,L} \propto d_{y,R}\tilde{f}_{s,R}. \tag{3.15}$$

Notice that the real part of the right side also occurs in the M_y expression. The relation here is much less direct than in the charge current and M_x case. In the expression for M_y, the term and the tilde-conjugated of the term are subtracted from each other, but in the $J_{s,z}$ expression they are added together. Furthermore, M_y depends on the real part of the expression whereas J_{s_z} depends on the imaginary part. It does therefore seem like a spin current does not have to induce a magnetization, although we do not rule out that there can be some connection.

3.2.4 Linearized spin-active boundary conditions

Before the numerical study, we also look at the linearized spin-active boundary conditions in order to understand how the currents are created. We linearize Equation (2.41) and separate the parts for the singlet and triplets components. This gives the following equations for the interface between (L) and S2

$$\begin{aligned}
\partial_z f_{s,L} =& -2\boldsymbol{m}^2(f_{s,L} + f_{s,\mathrm{S2}})G_1 + 2G_0 f_{s,\mathrm{S2}} - 2G_0 f_{s,L} && (3.16)\\
&- 2G_\phi(d_{x,L}m_x + d_{y,L}m_y + d_{z,L}m_z).\\
\partial_z d_{x,L} =& (-2\boldsymbol{m}^2 G_1 - 2G_0)d_{x,L} + (4id_{y,L}m_z - 4id_{z,L}m_y)G_{\mathrm{MR}} - (2G_\phi)f_{s,L}m_x, && (3.17)\\
\partial_z d_{y,L} =& (-2\boldsymbol{m}^2 G_1 - 2G_0)d_{y,L} + (4id_{z,L}m_x - 4im_z d_{x,L})G_{\mathrm{MR}} - (2G_\phi)f_{s,L}m_y, && (3.18)\\
\partial_z d_{z,L} =& (-2\boldsymbol{m}^2 G_1 - 2G_0)d_{z,L} + (4id_{x,L}m_y - 4id_{y,L}m_x)G_{\mathrm{MR}} - (2G_\phi)f_{s,L}m_z, && (3.19)
\end{aligned}$$

where only the singlet component of the S2 is included since we regard this as a conventional singlet superconductor. The boundary condition for the S1 and (L) interface can be found as described in section 2.8 with exchanging subscript and changing signs.

For studying the triplet scenarios, material (L) will be a ferromagnet. In the most cases we study, the exchange field will be oriented in the z-direction which induces a d_z component in (L). As mentioned, this d_z triplet will then be short-ranged, and thus we focus this discussion on the d_x and d_y components induced by the spin-active boundary.

The terms that create the d_x and d_y triplets are the G_φ- and G_{MR}-terms. If we only have the G_ϕ term, we see that the induced $\boldsymbol{d}$ is parallel to the interface magnetization.

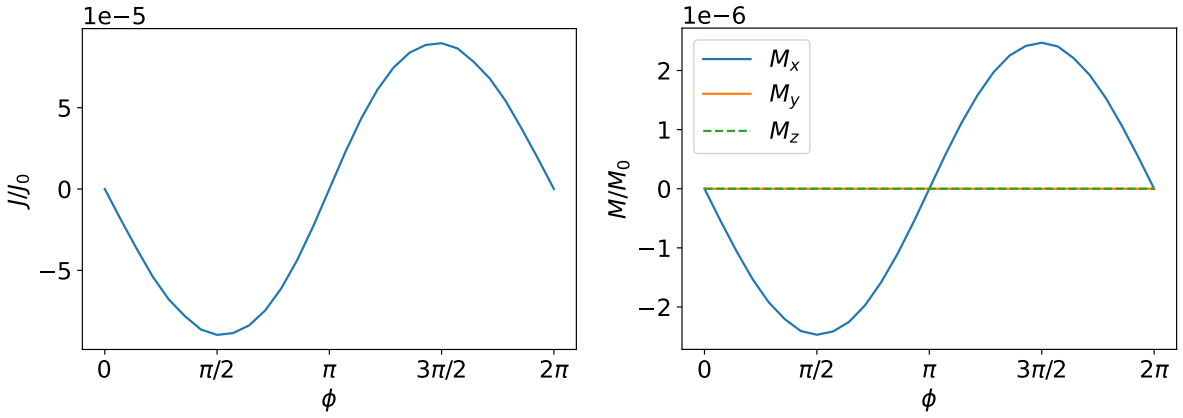

(a) (b)

Figure 3.4: Figure (a) shows the current induced in material (L) as a function of the phase difference between S1 and S2, ϕ. (b) shows the induced magnetization in (R), right next to the interface spin-orbit coupled interface at $y = 0$.

If we however, turn off G_ϕ but turn on G_{MR} we see that $\boldsymbol{d}$ is orthogonal to the interface magnetization, since d_z will already be present because of the exchange field in (L).

If we thus let the interface magnetization be parallel and only include one of the terms such that we have either $G_\phi = 0$ or $P = 0$, it closely resembles a conventional Josephson junction [57], except that it is only the triplet and not the singlet that is long-ranged. Applying a phase difference of the BCS superconductors S1 and S2, it is reasonable to expect that in this case, we can create a pure triplet charge current in (L). In that case, we are able to create only one long-ranged triplet component we know there can not be any spin currents. When both G_ϕ and G_{MR} are present, or $\theta \neq 0$, we see that both d_x and d_y will be created, and we might also find a spin current.

3.3 Numerical results

Having established some expectations from the analytical study, we proceed to the numerical study. In the following, we study the singlet current, triplet charge current, and spin current separately. We focus on the induced magnetization, and how it differs in the three cases.

3.3.1 Singlet current

The proximity effects of the singlet supercurrent are explored by removing the interface magnetizations and the exchange field in (L).

The current and magnetization as a function of ϕ is shown in Figure 3.4. The magnetization is evaluated at $y = 0$. As expected from the analytical study, no magnetization was induced in the y- or z-direction. Furthermore, it is seen from the figure that the induced M_x in (R) is proportional to the singlet current in (L). We remark that this supports the finding in the paper by J. Linder and M. Amundsen [30], who found that $M_x \propto J$ by using an effective model for the Green function in (L). In the effective model in their paper, the absolute value of the singlet component is constant, but with a phase e^{iJz}, where J is the current. In their model, the derivative of the singlet component thus

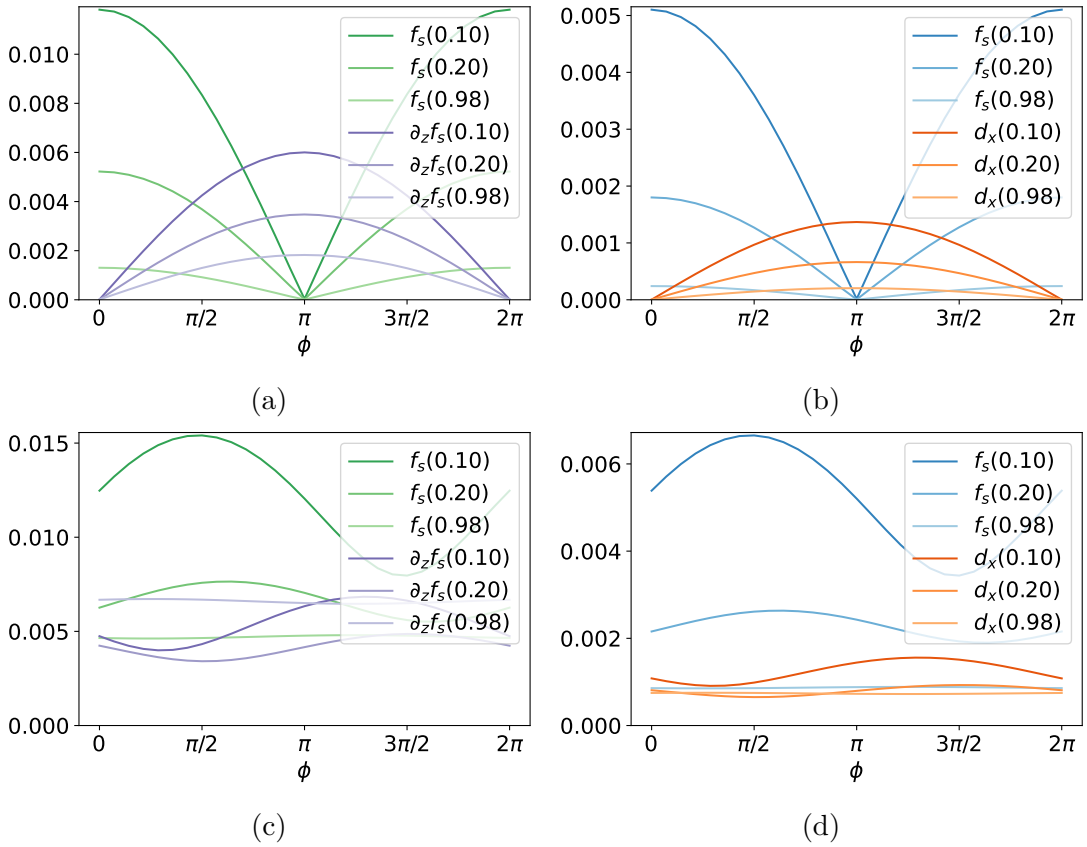

Figure 3.5: The figures (a) and (c) show the absolute value of the singlet component and its derivative in material (L). Figures (b) and (d) show the absolute value of the components $f_s(E/\Delta)$ and $d_x(E/\Delta)$ in material (R) as a function of ϕ for different energies, E/Δ. Figures (a) and (b) are found by using $z_0 = l/2$, whereas (c) and (d) are from using $z_0 = l/4$.

vanishes if $J = 0$. As we also include the creation of the current in our model, we can investigate this further. Inside a normal metal, we expect the Cooper pair wavefunction to decay when moving away from the superconductor. Therefore we expect a finite derivative also when there is no current.

We ask the question, of whether the disappearance of the magnetization at $J = 0$ is caused by the disappearance of the $f_{s,R}$ and $d_{x,R}$ components at $\phi = 0, \pi$ or by the tilde properties of the triplet and singlet component. To investigate this the plots in Figure 3.5 was made. The first situation explored is when material (R) is connected to the middle of material (L), $z_0 = l/2$. It is seen from the figure that the singlet component, $f_{s,L}$, is zero at $\phi = \pi$ and the derivative, $\partial_z f_{s,L}$, is zero at $\phi = 0$. The figure shows that this also causes $d_{x,R}$ to vanish at $\phi = 0$ and $f_{s,R}$ at $\phi = \pi$. From this, it cannot be concluded whether the tilde property itself could make the magnetization vanish.

Thus a new situation was explored, where $z_0 = l/4$ so that the material (R) is no longer connected to the middle of (L). From this the plots in Figure 3.5c and 3.5d were made. It is seen that neither $f_{s,L}$, nor $\partial_z f_{s,L}$ vanishes at any ϕ. Therefore also $d_{x,R}$ and $f_{s,R}$ is finite at every ϕ. It was checked and confirmed that the magnetization looks exactly like Figure 3.4b, also for $z_0 = l/4$. Thus we can conclude that it is the tilde properties that cause the magnetization to vanish at $\phi = 0, \pi$. The absence of induced magnetization does not necessarily imply the absence of a triplet in (R).

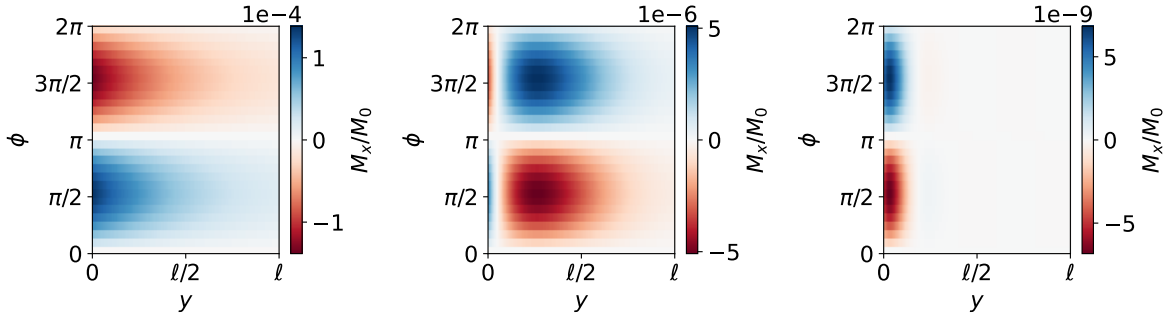

(a) (b) (c)

Figure 3.6: Contributions to the magnetization integral for different energies as a function of phase difference ϕ and position in material (R), y. The energies that are evaluated are $E\Delta = 0.01$ in (a), $E/\Delta = 0.05$ in (b) and $E/\Delta = 0.9$ in (c).

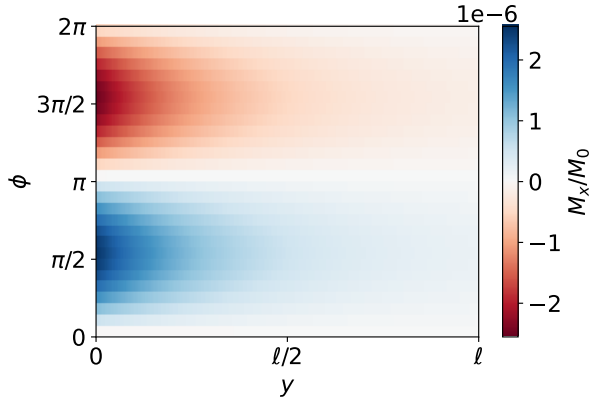

Figure 3.7: The magnetization as a function of phase difference ϕ and position y in the zero temperature case.

It was observed that the contribution to the magnetization, which is proportional to

$$\mathrm{Re}\{f_s(E)\tilde{d}_x(E) - \tilde{f}_s(E)d_x(E)\}, \tag{3.20}$$

oscillates as a function of y for some energies. This is contrary to the integrand of the current, which does not vary with z. Figure 3.6 shows what the expression in Equation (3.20) looks like for three different energies. Here it is seen that not only the size of the integrand but also the shape depends on E. To understand why the magnetization integrand is shifting sign as a function of y we explore how the f_s and d_x components behave in a normal metal.

Again we turn to the linearized equation to gain insight, and we start with the solution to the linearized Usadel equation in normal metal, given in Equation (3.7). As before we assume $l = \infty$, such that the factors B_s and B_x have to be zero. Thus, the real part of k damp out the Cooper pair wavefunctions in the normal metal. The imaginary part of k will make the wavefunctions rotate in the complex plane as a function of y. Also notice that k is invariant under tilde-conjugation $\tilde{k} = k$. The tilde-conjugated components have the same damping and the same rotation in the complex plane.

We now explore what happens to the expression in the magnetization, $f_s\tilde{d}_x - \tilde{f}_s d_x$. Using the solution from Equation 3.7 we find that

$$f_s\tilde{d}_x - \tilde{f}_s d_x = (A_s\tilde{A}_x - \tilde{A}_s A_x)\mathrm{e}^{-2ky}. \tag{3.21}$$

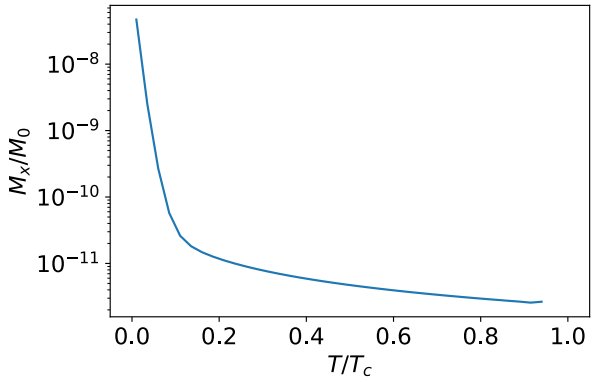

Figure 3.8: The magnetization from using a phase difference $\phi = \pi/4$ evaluated at $y = l$ as a function of temperature.

This expression rotates twice as fast in the complex plane as f_s and d_x. This rotation in the complex plane means that the real part of this expression, which the magnetization depends on, will oscillate. This explains why the magnetization integrand oscillates in y and also why this oscillation is different for different energies as the wave number k depends on the energy.

Performing the integral, however, shows that the magnetization does not change direction with y, at least not on these length scales used here for $T = 0$. This is shown in Figure 3.7.

The magnetization in Equation (2.54) has a factor $\tanh(\beta E/2)$ in the integrand. Varying the temperature changes how

$$\mathrm{Re}(f_s(E)\tilde{d}_x(E) - \tilde{f}_s(E)d_x(E)) \tag{3.22}$$

are weighted with respect to energy. A relevant question to ask is therefore how the temperature affects the magnetization. A quick temperature analysis was performed. To do so a couple of remarks about temperature have to be made. Firstly, it has to be taken into account that the energy gap changes with temperature. We chose the interpolation formula used in [60, 61],

$$\Delta(T) = \Delta(0)\tanh\left(1.74\sqrt{\tfrac{T_c}{T} - 1}\right), \tag{3.23}$$

where T_c is the critical temperature. This formula should be valid for $T \in (0, T_c)$. We also use the relation between the zero temperature gap and the critical temperature, $\frac{\Delta_0}{T_c} = 1.76$, as described in [62].

Figure 3.8 shows the magnetization evaluated at $y = l$ as a function of temperature. Even though the integrand has different signs at $y = l$, this graph shows that the sign of M_x at $y = l$ does not change.

3.3.2 Triplet charge current

In the following, the case with triplet charge current is explored and compared to the case with singlet charge current. To reduce the number of parameters, this discussion only considers zero temperature. A pure triplet charge current is created by having the interface magnetizations to be parallel, as discussed in section 3.2. Moreover, we have to

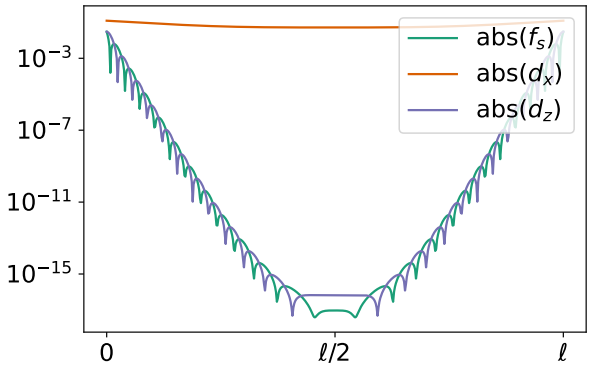

Figure 3.9: The absolute value of the triplet components evaluated for $E/\Delta = 0.14$. The figure shows that f_s and d_z are many orders of magnitude smaller than the d_x component.

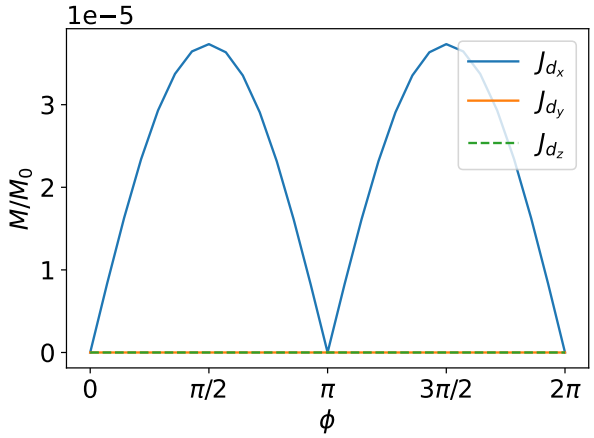

Figure 3.10: The absolute value of the magnetization in material (R) induced by d_x, d_y, and d_z carried charge current. It is seen that it is only the d_x carried charge current that induces a magnetization.

set either the polarization or the spin-mixing angles to zero. We explore both of these situations.

The first case explored is the zero polarization case, $P = 0$, but with finite spin-mixing angles $G_\phi \neq 0$. This is also explored by I. Gomperud and J. Linder [33], who show that a pure finite charge current occurs for parallel interface magnetizations, whereas spin-polarized currents are created for non-parallel interface magnetizations.

As discussed, we are interested in a situation where the singlet component is negligible compared to the triplets in (L). Figure 3.9 shows that both f_s and d_z die out on a short range into the material (L) when $\boldsymbol{m}_1 = \boldsymbol{m}_2 = (m, 0, 0)$ and $\boldsymbol{h}(z) = (0, 0, h(z))$. The singlet and the d_z triplet oscillate rapidly and decay quickly as should be expeccted [12, 13]. In the middle region, d_z and f_s are many orders of magnitude smaller than d_x and we conclude that the results from this section can be thought of as pure triplet effects.

The triplet charge current can be divided into the three components, J_{d_x}, J_{d_y} and J_{d_z}, which from section 3.2 are expected to give different results. The J_{d_x} current is created by using $\boldsymbol{m}_1 = \boldsymbol{m}_2 = (m, 0, 0)$ and $\boldsymbol{h} = (0, 0, h(z))$. In the same manner the J_{d_y} current is created by using $\boldsymbol{m}_1 = \boldsymbol{m}_2 = (0, m, 0)$ and $\boldsymbol{h} = (0, 0, h(z))$, and the J_{d_z} current is created with $\boldsymbol{m}_1 = \boldsymbol{m}_2 = (0, 0, m)$ and $\boldsymbol{h} = (h(z), 0, 0)$. The absolute value of the induced magnetization in (R), $|\boldsymbol{M}|$, is plotted for the three different triplet cases as

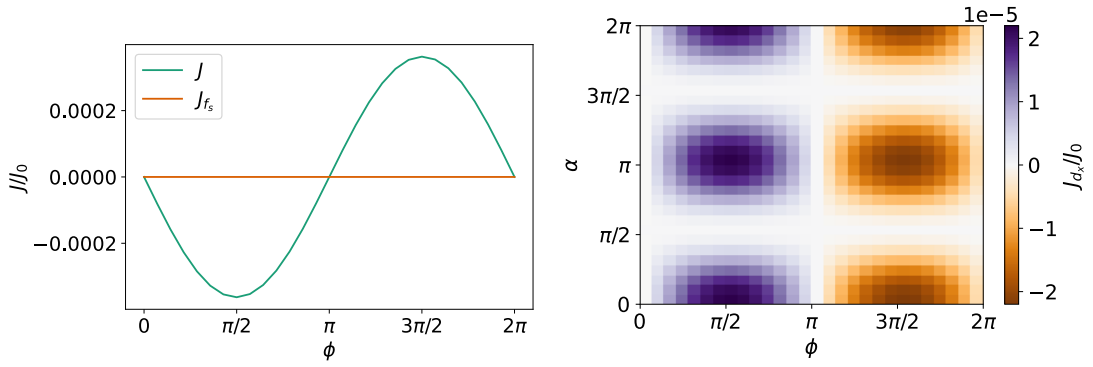

(a) (b)

Figure 3.11: Charge current as a function of ϕ in material (L). The green line in (a) shows the total current and the orange shows the singlet current. It is clear that the singlet current is negligible compared to the triplet current. Figure (b) shows only the d_x carried component of the current as both the phase difference ϕ and interface angles in the xy-plane, α are varied.

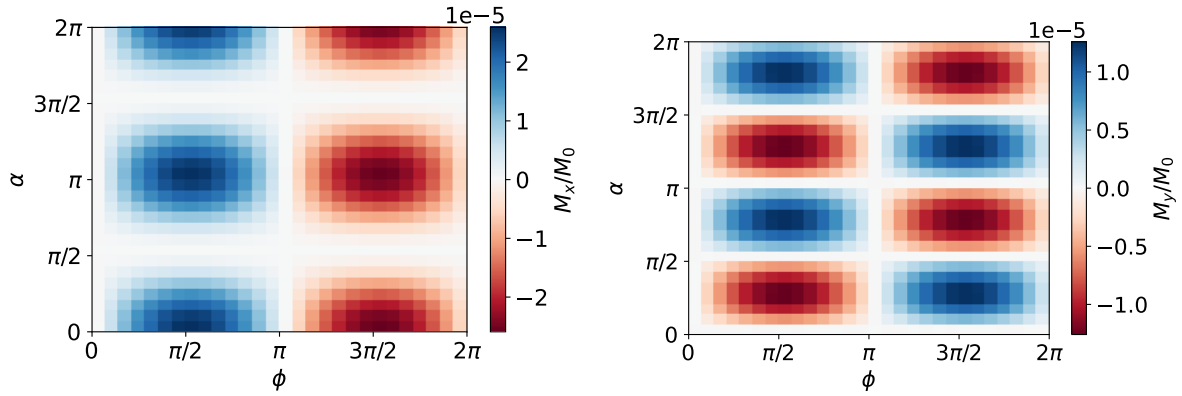

(a) (b)

Figure 3.12: The figure shows the induced magnetization in (L) in the triplet current case where $G_\phi = 0, P \neq 0$. Plot (a) is the induced m_x, and (b) is the induced m_y.

a function of ϕ in Figure 3.10. In agreement with our prediction in section 3.2 we find that only J_{d_x} induces a magnetization in (R). The induced magnetization can thereby be utilized to distinguish J_{d_x} from the other triplet currents.

As mentioned, a triplet current does however not have to be carried by a pure d_x, d_y or d_z, but could just as well be carried by any $\boldsymbol{d}$-triplet. Therefore, rotation of the interface magnetization in xy-plane is investigated. We will look at the induced magnetization, but first we consider the current. The current in material (L) is shown in Figure 3.11 as a function of the phase difference ϕ. The current has the same form as the singlet current, but this time it is carried by a triplet component.

As seen in section 3.2, the G_ϕ-term creates a $\boldsymbol{d}$-vector proportional to the interface magnetization. At $\alpha = 0$, the interface magnetizations are $\boldsymbol{m}_1 = \boldsymbol{m}_2 = (m, 0, 0)$, so it is natural that the charge current will only be carried by the d_x triplet. As $\boldsymbol{m}_1$ and $\boldsymbol{m}_2$ are rotated by an angle α in the xy-plane, so is the triplet vector $\boldsymbol{d}$. The proportion of the current carried by d_x, as a function of α, is shown in Figure 3.11b.

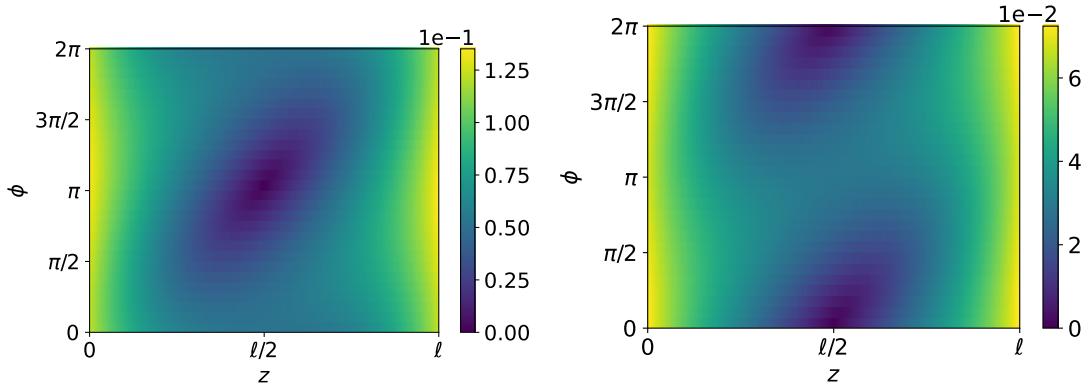

(a) (b)

Figure 3.13: Plot of the absolute value of $d_{x,L}$ in subfigure (a) and $\partial_z d_{x,L}$ in subfigure (b). The absolute values are plotted as a function of z and ϕ and are evaluated at $E/\Delta = 0.14$.

The induced magnetization in material (R) by the triplet current is plotted in Figure 3.12. As we have discussed in section 3.2 there should be a clear relation between J_{d_x} and M_x. Figure 3.12a confirms this resemblance, as the induced M_x has the same form as J_{d_x} in Figure 3.11.

The magnetization induced by the triplet current is clearly different from the singlet case. First of all, the induced magnetization varies with α. What this means is that in the singlet case, one would measure the same induced magnetization (in axes relative to (R)), no matter in what direction (R) was connected to (L). However, in the triplet case, the angle, at which (R) is connected to (L), makes a difference.

Other than the α-dependency, a new and significant signature arises in the triplet case, namely a magnetization component in the y-direction, as seen in Figure 3.12b. In the singlet case, only a M_x was induced. The induced M_y could therefore contribute to distinguish singlet and triplet currents. From Figure 3.12 we also notice that M_y has a different α-dependency than M_x. This can be explained by realizing that we expect $d_{x,L}$, and thus $\partial_z d_{x,L}$, to have a $\cos(\alpha)$ dependency. This would, according to the linearized spin-orbit coupled boundary conditions, give both $d_{x,R}$ and $f_{s,R}$ a $\cos(\alpha)$-dependency. Thus, M_x, a product of $d_{x,R}$ and $f_{s,R}$, naturally gets a $\cos^2(\alpha)$ dependency. Furthermore, $d_{y,L}$, and thus also $d_{y,R}$, should be expected to have a $\sin(\alpha)$ dependency. The magnetization in the y-direction, a product of $f_{s,R}$ and $d_{y,R}$ should therefore have a $\sin(\alpha)\cos(\alpha)$ dependency.

Similarly as in the singlet case, we investigate whether the disappearance of the magnetization at $\phi = 0$ and at $\phi = \pi$ can be explained by the tilde properties of the components. The absolute value of $d_{x,L}$ and $\partial_z d_{x,L}$ is shown as a function of z and ϕ in Figure 3.13. In the middle of the material, at $z = l/2$ we observe the same as in the singlet case, $d_{x,L} = 0$ for $\phi = \pi$ and $\partial_z d_{x,L} = 0$ for $\phi = 0$. When adjusting z_0 to $l/4$ in a similar manner as in the singlet current case, a bit more caution has to be taken, since f_s and d_z become larger towards the edges of (L). From Figure 3.9 we still see that there is a big difference between the triplet of interest and the singlet. It is therefore clear that the potential effects are caused by triplets and not the singlet. In our model, the exchange field is finite at $z = l/4$ and is not really suitable for measuring magnetization at $z_0 = l/4$, since the exchange field itself would induce a magnetization in (R). However, the quasiclassical model does not capture this magnetization induced by the exchange field, and thus our

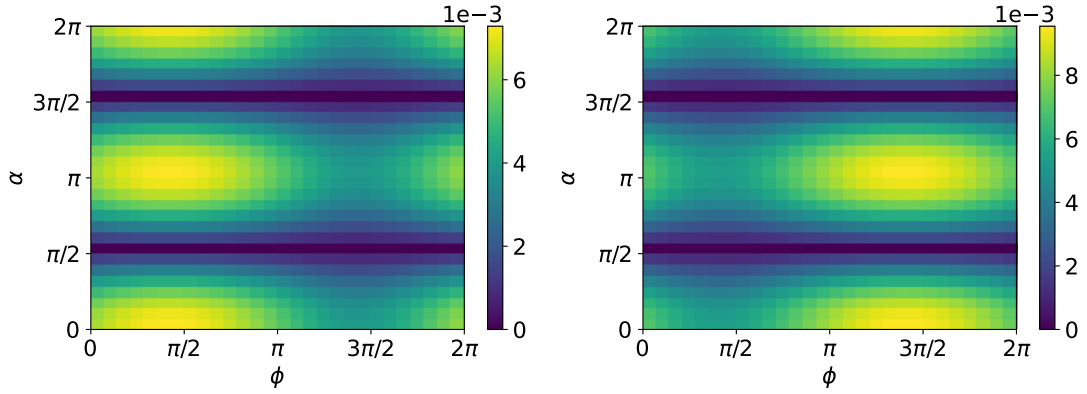

(a) (b)

Figure 3.14: (a) is the absolute value of the f_s component in (R) at $y = 0$ as a function of α and ϕ. (b) is the absolute value of the d_x component. This is from the case where $z_0 = l/4$ at $E/\Delta = 0.14$.

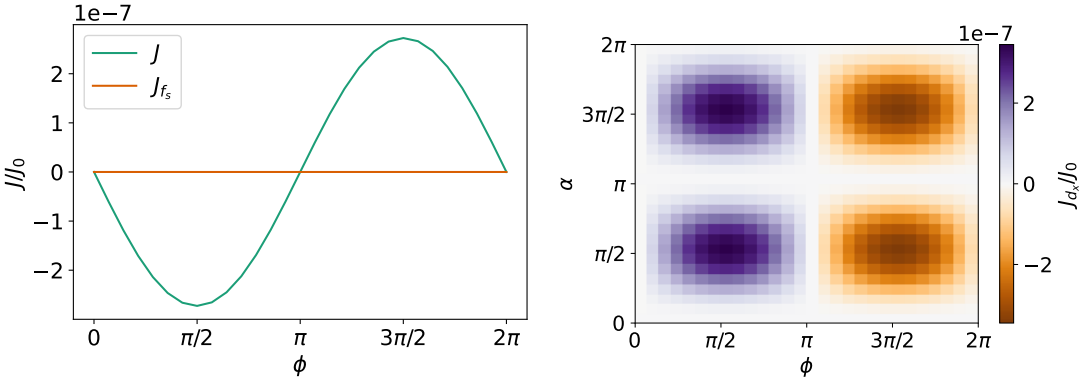

(a) (b)

Figure 3.15: Figure (a) shows the current as a function of ϕ in material (L) in the case of $G_\phi = 0, P \neq 0$. The singlet current is zero, which means that the current is carried by triplet components. Figure (b) shows how the d_x carried current as a function of ϕ and α.

model should hold for investigating the role of the tilde properties.

The d_x and f_s in (R) is plotted in Figure 3.14 for $z_0 = l/4$. It was also observed that at this value of z_0 both the induced M_x and M_y look exactly the same as for $z_0 = l/2$. This leads to the same conclusion as in the singlet case, the magnetization at $\phi = 0, \pi$ disappears because of the tilde properties of the component, not because of vanishing f_s and $\boldsymbol{d}$.

To check the robustness of the results another parameter set is also investigated. The interface magnetizations are kept parallel, however, the polarization is turned on, adding the magnetoresistive and the depairing term. Instead, the spin-mixing is turned off. From section 3.2 we see that the G_{MR} term creates a triplet $\boldsymbol{d}$ orthogonal to the interface magnetization and to $\boldsymbol{h}$. The current is shown in Figure 3.15 and the induced magnetization in Figure 3.16 There is a $\pi/2$ shift in α compared to the $P = 0$ situation because the induced triplet is orthogonal to the interface magnetization, instead of parallel. Other than that, the form of the magnetization is similar and the conclusions from the $P = 0$

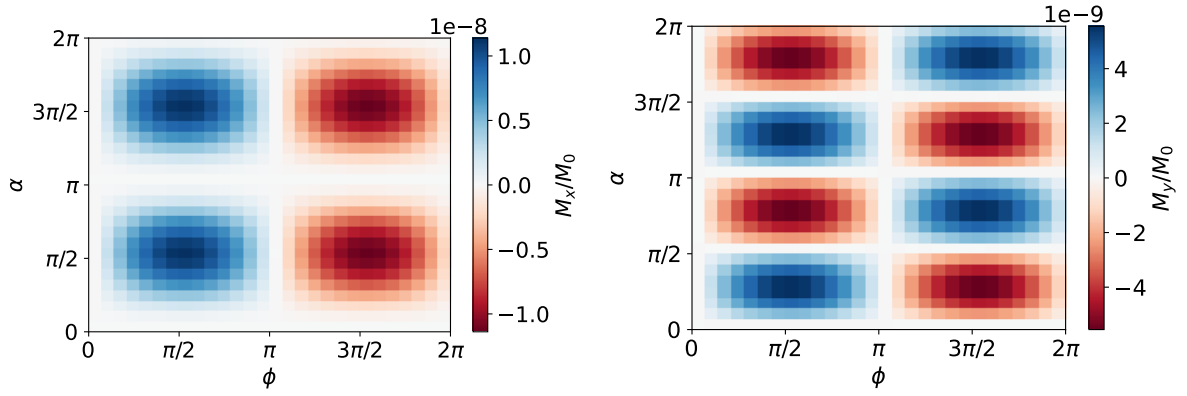

(a) (b)

Figure 3.16: The figure shows the induced magnetization in (L) in the triplet current case where $G_\phi = 0, P \neq 0$. Plot (a) is the induced M_x, and (b) is the induced M_y.

case hold.

The main results from the triplet case are that a pure J_{d_x} can be distinguished from a pure J_{d_y} or J_{d_z}, as the J_{d_x} is the only one that induces magnetization. When a current is carried partially by d_x and partially by d_y, as we got by varying α, we observed an induced magnetization also in the y-direction. We note that, because of the similarities in the boundary conditions for d_y and d_z, we expect a current carried partially by d_z to induce a magnetization in the z-direction. In the singlet case, only M_x can be induced, and magnetization induced in other directions is thus a signature of triplet current.

3.3.3 Spin current

Using the parameters $P = 0, G_\phi = 0.3$ and orthogonal interface magnetizations, $\theta = \frac{\pi}{2}$, induces a spin current in material (L). We will look at how the magnetization differs from the charge current cases and discuss why the results are reasonable.

Firstly we explain the currents. The charge current shown in Figure 3.17 oscillates as a function of ϕ with a period of π. This oscillation is twice as rapid as what we observed in the previous cases. It is known that the second-order contribution of the Josephson current is proportional to $\sin(2\phi)$ [58]. In addition to the periodicity, the order of magnitude of the total current J, which is much smaller than the maximum of the individual components J_{d_x} and J_{d_y} in Figure 3.17b, also suggest that this charge current is a second order effect.

We study Figure 3.17b further and notice that J_{d_x} is small for $\alpha = 0$. This can be understood from the linearized spin-active boundary conditions in section 3.2. When $\boldsymbol{m}_1 = (m, 0, 0)$ and $\boldsymbol{m}_2 = (0, m, 0)$ there is no d_y induced at the $z = 0$ interface, and no d_x at the $z = l$ interface (to the first order). Therefore the tilde symmetry, which is attributed to d_x at the $z = 0$ interface, stays unchanged through the material (L), even though a phase difference is present between S1 and S2. The same argumentation applies for d_y and explains why there is no first-order contribution to neither J_{d_x} nor J_{d_y} at $\alpha = 0$. At $\alpha = \pi/4$, however, both interface magnetizations contain both a x and a y component so that both d_x and d_y are induced at both interfaces. Adding a phase difference does therefore induce both J_{d_x} and J_{d_y}. An additional plot of J_{d_y} is redundant since it is the same as J_{d_x} only shifted with $\alpha = \pi/2$. We see from Figure 3.17b that J_{d_y} and J_{d_x} have

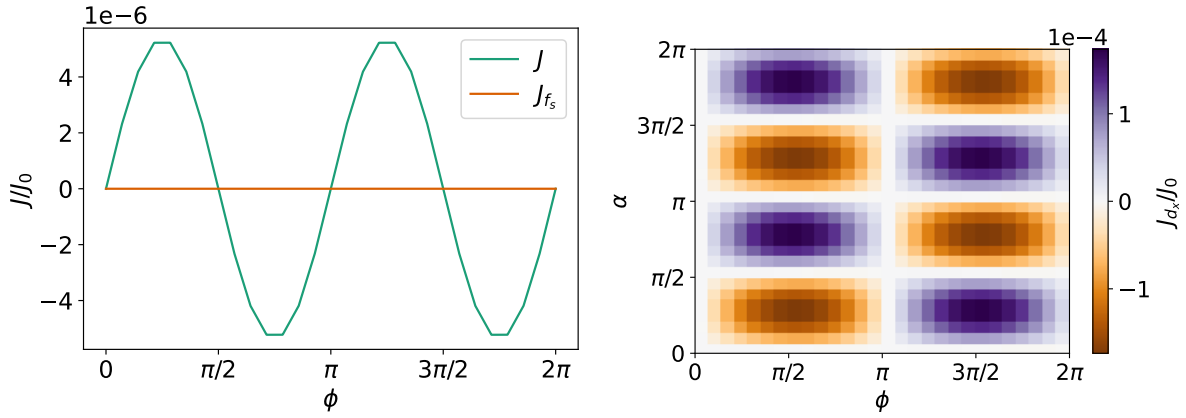

(a) (b)

Figure 3.17: Charge currents from the spin current case. Figure (a) shows that the charge current is small and oscillates as a function of ϕ with the period π. Figure (b) shows only the d_x component of the charge current plotted as a function of ϕ and α.

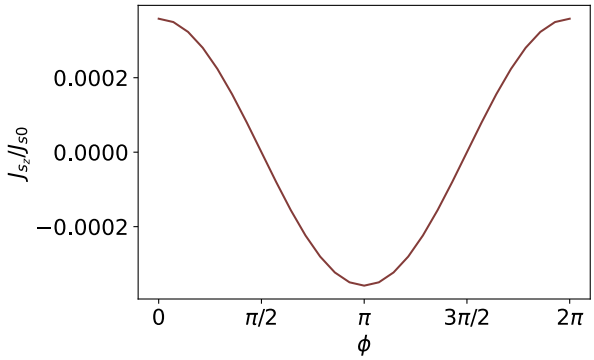

Figure 3.18: Spin current as a function ϕ.

the opposite sign and approximately cancel each other out, such that the total current indeed should be the current in Figure 3.17a. The reason J_{d_y} has the opposite sign from J_{d_x} is simply that when the x-components of the two interface magnetizations point in the same direction, the y-components point in the opposite direction, which causes the d_y current to flow in the opposite direction.

Having explained the charge current, we move on to the spin current which is shown in Figure 3.18. Notice that this current is shifted with $\phi = \pi/2$ compared to the charge currents in the charge current cases. To understand this we study the integrand of J_{s_z} from Equation (2.49)

$$d_{x,L}\partial_z\tilde{d}_{y,L} - d_{y,L}\partial_z\tilde{d}_{x,L} + \tilde{d}_{x,L}\partial_y d_{y,L} - \tilde{d}_{y,L}\partial_z d_{x,L}. \tag{3.24}$$

For $\phi = 0$, both triplets transform equally under tilde conjugation. Furthermore, we expect the d_x triplet to decay away from the $z = 0$ interface where it is induced, and similarly, d_y to decay away from the $z = l$ interface. By this, we expect the derivatives, $\partial_z d_{x,L}$ and $\partial_z d_{y,L}$, to have opposite signs. It follows that all the terms in Equation (3.24) get the same sign. Thus it seems reasonable that the spin current we found numerically in Figure 3.18 is finite at $\phi = 0$. For $\phi = \pi/2$, however, we expect d_y and d_x to have the opposite tilde symmetry, such that we, for example, could have $\tilde{d}_y = -d_y$ and

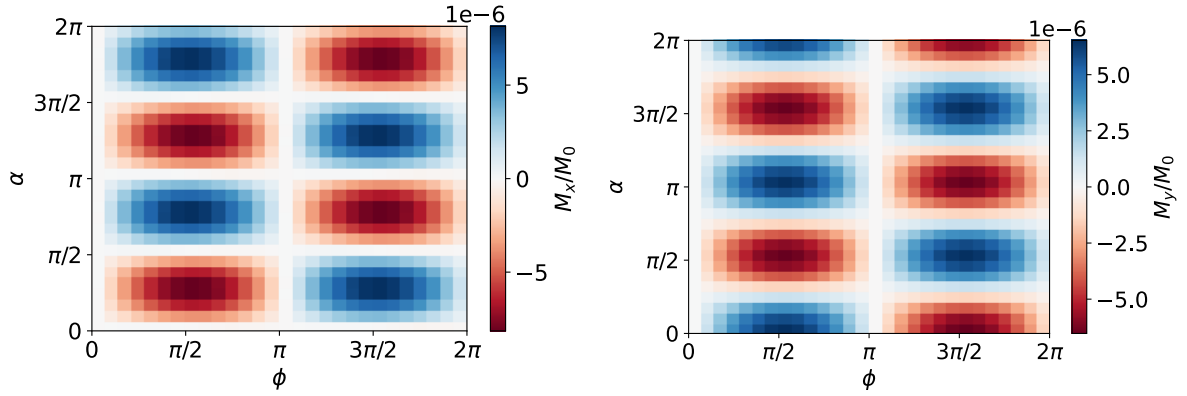

(a) (b)

Figure 3.19: Magnetization induced in the spin current scenario. Figure (a) shows the x-component of the magnetization and (b) the y-component as a function of α and ϕ.

$\tilde{d}_x = d_x$. The same tilde properties will apply to the derivatives so that $\partial_z \tilde{d}_y = -\partial_z d_y$ and $\partial_z \tilde{d}_x = \partial_z d_x$. With these tilde properties, we see that the terms in the J_{s_z} integrand cancel, and we get zero spin current for $\phi = \pi/2$.

In the previous cases, we have observed that the magnetization has the same ϕ-dependency as the current. However, in this case, the magnetization shown in Figure 3.19 is shifted by $\phi = \pi/2$ compared to the spin current. We see, however, that the proportionality between M_x and J_{d_x} still holds. In this case, however, M_x and J_{d_x} are different in the way that they change sign as α is varied. The induced magnetization in the y-direction, M_y, also differs from the charge current case. Here M_y is shifted by $\alpha = \pi/4$ compared to the triplet charge current case. The explanation for this shift can again be found in the tilde properties of the d_x and d_y components. At $\phi = \pi/2$ the d_y triplet should have the opposite tilde symmetry as the d_x triplet and thus also $\partial_z d_x$. Since f_s inherits the tilde property from $\partial_z d_x$, this means that $f_{s,R}$ and $d_{y,R}$ will have the opposite tilde symmetry as well, which is exactly what is needed to get an induced M_y. This explains why we do get an induced M_y at $\phi = 0$, even though there is no M_x. Because M_y is shifted in α, no value of α gives zero induced magnetization, unlike in the triplet charge current case.

We comment here, that due to time limitations, this set of spin current parameters is the only tested thoroughly. We see that the spin current we got is symmetric with respect to the phase difference ϕ, which makes it an exchange spin current. In the article by Ouassou et al. [32] the difference between this exchange spin current and a spin current which is antisymmetric with respect to ϕ, the polarization spin current, is discussed. The polarization spin current is the polarized part of the charge current and it would also be of interest to investigate magnetization induced by this type of spin current.

Chapter 4

Summary and Outlook

Our findings suggest that induced magnetization in a normal metal, facilitated by a spin-orbit coupled interface, can serve as a signature of the spin-polarization of a supercurrent in a neighboring material. The results are supported both by our analytical reasoning and numerical study. In the case of a singlet supercurrent, we confirmed the emergence of a magnetization in the x-direction, with the directions defined in Figure 3.1. A short study of the temperature dependency shows that in the singlet case, the magnetization simply seems to be decaying with increasing temperature.

Furthermore, we discovered that also a triplet charge current can induce magnetization if it is carried, at least partially, by the d_x triplet. The d_x charge current alone induces a M_x. However, together with another triplet, a magnetization can also be induced in other directions. A triplet charge current only carried by d_y or d_z does not induce a magnetization in the normal metal. With a rotation of the interface magnetizations in the xy-plane, we were able to investigate the combination of a current carried by d_x and d_y, which was seen to induce a magnetization in both x- and y-direction.

Also in the spin current scenario, we discovered induced magnetization. The spin current we investigated was an exchange spin current, and we saw that it was a $\phi = \pi/2$ offset between this spin current and the induced magnetization. The induced magnetization in the spin current case differs from the charge current case. In particular, we saw that M_x also changed sign with variation of α, which was not the case for the charge currents. Furthermore, for $\phi = \pi/2$ a magnetization either in the x-direction or in the y-direction was present for all values of α.

We conclude that, when taking into account the α-dependency of induced magnetization, the currents investigated have distinct signatures. This could provide a measurement protocol to directly use the spin-polarization of the triplet Cooper pairs in supercurrents to create a measurable spin signal in a dissipationless manner.

The study of the tilde properties shows that it is not only the presence of Cooper pairs in the normal metal that is needed to create the magnetization. To induce a magnetization the singlet and triplet also need to transform differently under tilde conjugation. For the charge current cases, it follows that the magnetization is directly proportional to the current, and not to the absolute value of the individual components.

In this thesis, we limited ourselves to studying induced magnetization. Further research could also consider the density of states, to look for new signatures to distinguish the different types of currents. We also note that in several cases we have triplet Cooper pairs that do not contribute to the magnetization because they have the same tilde symmetry as the singlet. A deeper investigation of the tilde symmetries that occur in the

spin-orbit coupled interfaces could possibly provide new insight into fundamental physics. We have only considered an exchange spin current, and for further studies, it would also be interesting to investigate a polarization spin current.

Finally, we emphasize the importance of experimental validation of the results, as it is highly desired to validate and strengthen the findings. We note that in order to make quantitative predictions it is required an evaluation of what would be realistic values for the parameters involved.

Appendix A

Wigner Transformations

*These derivations are taken from the specialization project with only a few changes. It is quite inspired by the master thesis by J. P. Morten [36], however, some part of that calculation were found to be slightly incorrect and should be corrected here.

The Wigner transformation of the Gor'kov equation is presented, but first it is seen how the Wigner transfromation of a convolution and a convolution with a gradient is presented.

A.1 Wigner transform of a convolution

Here we show that

$$\begin{aligned} A \otimes B(X,p) &\equiv \int \mathrm{d}x \mathrm{e}^{-ipx} \int \mathrm{d}x_3 A(x_1,x_3)B(x_3,x_2) \\ &= e^{\frac{i}{2}(\partial_{X_A}\partial_{p_B} - \partial_{X_B}\partial_{p_A})} A(X,p)B(X,p), \end{aligned} \tag{A.1}$$

where $x = x_1 - x_2$ and $X = \frac{1}{2}(X_1 + x_2)$. We start off with the expression

$$\int \mathrm{d}x \int \mathrm{d}x_3 \mathrm{e}^{-ipx} A(X + \tfrac{1}{2}x, x_3)B(x_3, X - \tfrac{1}{2}x), \tag{A.2}$$

and we shift the integration variable x_3 by an amount of X which gives us

$$\int \mathrm{d}x \int \mathrm{d}x_3 \mathrm{e}^{-ipx} A(X + \tfrac{1}{2}x, X + x_3)B(X + x_3, X - \tfrac{1}{2}x). \tag{A.3}$$

Further, we change integration variables to $u = x_3 + \frac{1}{2}x$, and $v = x_3 - \frac{1}{2}x$ and note that this transformation of variables has a Jacobi determinant equal to 1. We can thus write our expression as

$$\int \mathrm{d}u \int \mathrm{d}v \mathrm{e}^{-ip(u+v)} A(X + \tfrac{1}{2}(u+v), X + \tfrac{1}{2}(u-v))B(X + \tfrac{1}{2}(u-v), X - \tfrac{1}{2}(u-v)). \tag{A.4}$$

Next, we Taylor expand the function A with respect to u and B with respect to v,

and can, by following the steps below, arrive at the desired expression.

$$
\begin{aligned}
&\int \mathrm{d}u \int \mathrm{d}v \mathrm{e}^{-ip(u+v)} \sum_{n=0} \Big[\frac{u^n \partial_u^n}{n!} A(X+\frac{1}{2}(u+v), X+\frac{1}{2}(u-v))\Big]\Big|_{u=0} \\
&\quad \times \sum_{m=0} \Big[\frac{v^m \partial_v^m}{m!} B(X+\frac{1}{2}(u-v), X-\frac{1}{2}(u-v))\Big]\Big|_{v=0} \\
&= \int \mathrm{d}u \int \mathrm{d}v \mathrm{e}^{-ip(u+v)} \sum_{n=0} \Big[\frac{u^n \partial_X^n}{2^n n!} A(X+\frac{1}{2}v, X+-\frac{1}{2}v)\Big] \\
&\quad \times \sum_{m=0} \Big[\frac{v^m \partial_X^m}{(-2)^m m!} B(X+\frac{1}{2}u, X-\frac{1}{2}u)\Big] \\
&= \sum_{n=0}\sum_{m=0} \Big[\frac{\partial_X^n}{2^n n!} \int \mathrm{d}v v^m \mathrm{e}^{-ipv} A(X+\frac{1}{2}v, X+-\frac{1}{2}v)\Big] \\
&\quad \times \Big[\frac{\partial_X^m}{(-2)^m m!} \int \mathrm{d}u u^n \mathrm{e}^{-ipu} B(X+\frac{1}{2}u, X-\frac{1}{2}u)\Big] \\
&= \sum_{n=0}\sum_{m=0} \Big[\frac{\partial_X^n}{2^n n!} \int \mathrm{d}v (i\partial_p)^m \mathrm{e}^{-ipv} A(X+\frac{1}{2}v, X+-\frac{1}{2}v)\Big] \\
&\quad \times \Big[\frac{\partial_X^m}{(-2)^m m!} \int \mathrm{d}u (i\partial_p)^n \mathrm{e}^{-ipu} B(X+\frac{1}{2}u, X-\frac{1}{2}u)\Big] \\
&= \sum_{n=0}\sum_{m=0} \Big[\frac{\partial_X^n}{2^n n!} (i\partial_p)^m A(X,p)\Big]\Big[\frac{\partial_X^m}{(-2)^m m!} (i\partial_p)^n B(X,p)\Big] \\
&= e^{\frac{i}{2}(\partial_{X_A}\partial_{p_B} - \partial_{X_B}\partial_{p_A})} A(X,p)B(X,p).
\end{aligned}
\tag{A.5}
$$

A.2 Wigner transform of convolution with derivatives

Here we calculate the Wigner transform of terms of the form

$$
\boldsymbol{A}(x_1) \cdot \nabla_{\boldsymbol{r}_1} B(x_1, x_2). \tag{A.6}
$$

Note that $\nabla_{\boldsymbol{r}_1} = (\nabla_{\boldsymbol{r}_1}\boldsymbol{R})\nabla_{\boldsymbol{R}} + (\nabla_{\boldsymbol{r}_1}\boldsymbol{r})\nabla_{\boldsymbol{r}} = \frac{1}{2}\nabla_{\boldsymbol{R}} + \nabla_{\boldsymbol{r}}$, so the Wigner transform of Equation (A.6) can be written as

$$
\int \mathrm{d}x \boldsymbol{A}(X+\tfrac{1}{2}x) \cdot (\tfrac{1}{2}\nabla_{\boldsymbol{R}} + \nabla_{\boldsymbol{r}}) B(X+\tfrac{1}{2}x, X-\tfrac{1}{2}x). \tag{A.7}
$$

The $\nabla_{\boldsymbol{R}}$ term is trivial and by using the same procedure as for the non-derivative convolution case we get

$$
\tfrac{1}{2}\int \mathrm{d}x \boldsymbol{A}(X+\tfrac{1}{2}x) \cdot \nabla_{\boldsymbol{R}} B(X+\tfrac{1}{2}x, X-\tfrac{1}{2}x) = \tfrac{1}{2}\boldsymbol{A} \otimes \nabla_{\boldsymbol{R}} B(X,p). \tag{A.8}
$$

The $\nabla_{\boldsymbol{r}}$ term, however, demands some more work, so we continue focusing on this term

$$\begin{aligned}
&\int \mathrm{d}x \mathrm{e}^{-ipx} \boldsymbol{A}(X + \tfrac{1}{2}x) \cdot \tfrac{1}{2}\nabla_{\boldsymbol{r}} B(X + \tfrac{1}{2}x, X - \tfrac{1}{2}x) \\
&\quad = \tfrac{1}{2} \int \mathrm{d}x \mathrm{e}^{-ipx} \sum_{n=0} \Big[\frac{x^n \partial_X^n}{2^n n!} \boldsymbol{A}(X) \Big] \cdot \nabla_{\boldsymbol{r}} B(X + \tfrac{1}{2}x, X - \tfrac{1}{2}x) \\
&\quad = \sum_{n=0} \frac{1}{2^n n!} [\partial_X^n \boldsymbol{A}(X)] \int \mathrm{d}x x^n \mathrm{e}^{-ipx} \nabla_{\boldsymbol{r}} \int \frac{\mathrm{d}p'}{(2\pi)^4} \mathrm{e}^{ip'x} G(X, p') \\
&\quad = \sum_{n=0} \frac{i^n}{2^n n!} [\partial_X^n \boldsymbol{A}(X)] \partial_p^n \int \mathrm{d}x \mathrm{e}^{-ipx} (i\boldsymbol{p}') \int \frac{\mathrm{d}p'}{(2\pi)^4} \mathrm{e}^{ip'x} G(X, p') \\
&\quad = \sum_{n=0} \frac{i^n i}{2^n n!} [\partial_X^n \boldsymbol{A}(X)] \partial_p^n (\boldsymbol{p} G(X, p)) \\
&\quad = \sum_{n=0} \frac{i^n i}{2^n n!} [\partial_X^n \boldsymbol{A}(X)] \Big[n \nabla_{\boldsymbol{p}}^{n-1} (\partial_t)^n G(X, p) + \boldsymbol{p}\, \partial_p^n G(X, p) \Big].
\end{aligned} \tag{A.9}$$

The second term on the last line we can recognize as $\boldsymbol{p}\,(\boldsymbol{A} \otimes G(X, p))$. However, we need to look a bit closer at the first term.

At this point, we should remind ourselves that the Wigner transformation is really performed for one coordinate at a time so that the Taylor expansion is really an expansion in every one of the coordinates $\sum_n = \sum_{n_x, n_y, n_z, n_t}$. This means that in the second line below we are only changing the summation over the n for the spatial derivatives

$$\begin{aligned}
&\sum_{n=0} \frac{i^n i}{2^n n!} n \nabla_{\boldsymbol{p}}^{n-1} (\partial_t)^n G(X, p) \partial_X^n A(X) \\
&\quad = -\tfrac{1}{2} \sum_{n=0} \frac{i^n}{2^n n!} \nabla_{\boldsymbol{p}}^n G(X, p) \partial_X^n \nabla_{\boldsymbol{R}} \cdot A(X) \\
&\quad = -\tfrac{1}{2} \nabla_{\boldsymbol{R}} \cdot \boldsymbol{A} \otimes G(X, p).
\end{aligned} \tag{A.10}$$

Thus the total expression reads

$$\begin{aligned}
\int \mathrm{d}x \boldsymbol{A}(x_1) \cdot \nabla_{\boldsymbol{r}_1} B(x_1, x_2) = \tfrac{1}{2} \boldsymbol{A} \otimes \nabla_{\boldsymbol{R}} B(X, p) + i\boldsymbol{p}(\boldsymbol{A} \otimes B(X, p)) \\
- \tfrac{1}{2} (\nabla_{\boldsymbol{R}} \cdot \boldsymbol{A}) \otimes B(X, p).
\end{aligned} \tag{A.11}$$

For the similar right-handed expression we keep in mind that $\nabla_{\boldsymbol{r}_2} = -\nabla_{\boldsymbol{r}} + \frac{1}{2}\nabla_{\boldsymbol{R}}$ and that we also we get an extra $(-1)^n$ from the Taylor expansion so that we in total get

$$\begin{aligned}
\int \mathrm{d}x \nabla_{\boldsymbol{r}_2} B(x_1, x_2) \cdot \boldsymbol{A}(x_2) = \tfrac{1}{2} (\nabla_{\boldsymbol{R}} B(X, p)) \otimes \boldsymbol{A} - i\boldsymbol{p}(B(X, p) \otimes \boldsymbol{A}) \\
- \tfrac{1}{2} (\nabla_{\boldsymbol{R}} \boldsymbol{A}) \otimes B(X, p).
\end{aligned} \tag{A.12}$$

A.3 Wigner transforming the Gor'kov equation

We start with the equation

$$
\begin{aligned}
0 = {} & i\partial_{t_1}\hat{\rho}_3\check{G}(x_1,x_2) + i\partial_{t_2}\check{G}(x_1,x_2)\hat{\rho}_3 && \text{(A.13a)}\\
& - \hat{\xi}(x_1)\check{G}(x_1,x_2) + \check{G}(x_1,x_2)\hat{\xi}^*(x_2) && \text{(A.13b)}\\
& - \hat{S}(x_1)\check{G}(x_1,x_2) + \check{G}(x_1,x_2)\hat{S}(x_2) && \text{(A.13c)}\\
& + \hat{M}(x_1)\check{G}(x_1,x_2) + \check{G}(x_1,x_2)\hat{M}(x_2) && \text{(A.13d)}\\
& + \hat{\Delta}(x_1)\check{G}(x_1,x_2) + \check{G}(x_1,x_2)\Delta(x_2) && \text{(A.13e)}\\
& - \int \mathrm{d}x_3 \hat{\Sigma}(x_1,x_3)\check{G}(x_3,x_2) && \text{(A.13f)}\\
& - \int \mathrm{d}x_3 \check{G}(x_1,x_3)\hat{\Sigma}(x_3,x_2). && \text{(A.13g)}
\end{aligned}
$$

In the following, this equation is Wigner transformed term by term, starting with the first term in Equation (A.13a)

$$
\begin{aligned}
& i\int \mathrm{d}x\, \mathrm{e}^{-ipx}\partial_{t_1}\hat{\rho}_3\check{G}(x_1,x_2)\\
&= i\int \mathrm{d}x\, \mathrm{e}^{-ipx}\partial_{t_1}\hat{\rho}_3 \int \frac{\mathrm{d}p'}{(2\pi)^4}\mathrm{e}^{ip'x}\check{G}(X,p')\\
&= i\int \mathrm{d}x\, \mathrm{e}^{-ipx}\hat{\rho}_3 \int \frac{\mathrm{d}p'}{(2\pi)^4}\left[(\partial_{t_1}\mathrm{e}^{ip'x})\check{G}(X,p') - \mathrm{e}^{ip'x}\partial_{t_1}\check{G}(X,p')\right]\\
&= i\int \mathrm{d}x\, \mathrm{e}^{-ipx}\hat{\rho}_3 \int \frac{\mathrm{d}p'}{(2\pi)^4}\left[(-iE)\mathrm{e}^{ip'x}\check{G}(X,p') - \tfrac{1}{2}\mathrm{e}^{ip'x}\partial_T\check{G}(X,p')\right]\\
&= i\hat{\rho}_3 \int \frac{\mathrm{d}p'}{(2\pi)^4}(2\pi)^4\delta^4(p-p')\left[(-iE)\mathrm{e}^{ip'x}\check{G}(X,p') - \tfrac{1}{2}\mathrm{e}^{ip'x}\partial_T\check{G}(X,p')\right]\\
&= \hat{\rho}_3 E\check{G}(X,p) + i\hat{\rho}_3\partial_T\check{G}(X,p).
\end{aligned}
\tag{A.14}
$$

Going to the fourth line we use that $\partial_{t_1}\check{G}(X,p') = \frac{1}{2}\partial_T\check{G}(X,p')$, and that $\partial_{t_1}\mathrm{e}^{ipx} = \partial_t\mathrm{e}^{ipx}$. For the first term to the second term in (A.13a) the difference is that the second includes ∂_{t_2} instead of ∂_{t_1} which can be written as $\partial_{t_2}\mathrm{e}^{ipx} = -\partial_t\mathrm{e}^{ipx}$. The Wigner transform of (A.13a) thus reads

$$
\begin{aligned}
& i\Big[\frac{1}{2}\hat{\rho}_3\partial_T\check{G}(X,p) + (-iE)\hat{\rho}_3\check{G}(X,p) + \frac{1}{2}\partial_T\check{G}(x_1,x_2)\hat{\rho}_3 - (-iE)\check{G}(x_1,x_2)\hat{\rho}_3\Big]\\
&\quad = \left[E\hat{\rho}_3 \overset{\otimes}{,} G\right].
\end{aligned}
\tag{A.15}
$$

Next, we perform the Wigner transformation on (A.13b). We start by writing out the

term

$$\begin{aligned}
&-\hat{\xi}(x_1)\check{G}(x_1,x_2)+\check{G}(x_1,x_2)\hat{\xi}(x_2)\\
&\quad=\frac{1}{2m}(\nabla_{\boldsymbol{r}_1}-ie\hat{\rho}_3\boldsymbol{A}(x_1))^2\check{G}(x_1,x_2)-(e\varphi(x_1)-\mu)\check{G}\\
&\qquad-\frac{1}{2m}\check{G}(x_1,x_2)(\nabla_{\boldsymbol{r}_2}+ie\hat{\rho}_3\boldsymbol{A}(x_2))^2+\check{G}(x_1,x_2)(e\varphi(x_2)-\mu)\\
&\quad=\frac{1}{2m}\Big(\nabla^2_{\boldsymbol{r}_1}-\nabla^2_{\boldsymbol{r}_2}\Big)\check{G}(x_1,x_2)\\
&\qquad-\frac{ie}{2m}\Big[(\nabla_{\boldsymbol{r}_1}\cdot\boldsymbol{A}(x_1)\hat{\rho}_3)\check{G}(x_1,x_2)+\check{G}(x_1,x_2)(\nabla_{\boldsymbol{r}_2}\cdot\boldsymbol{A}(x_2)\hat{\rho}_3)\Big]\\
&\qquad-\frac{ie}{m}\Big[\boldsymbol{A}(x_1)\hat{\rho}_3(\nabla_{\boldsymbol{r}_1}\check{G}(x_1,x_2))+(\nabla_{\boldsymbol{r}_2}\check{G}(x_1,x_2))\boldsymbol{A}(x_2)\hat{\rho}_3\Big]\\
&\qquad-e^2\boldsymbol{A}^2(x_1)\check{G}(x_1,x_2)+e^2\boldsymbol{A}^2(x_2)\check{G}(x_1,x_2)\\
&\qquad-e\varphi(x_1)\check{G}(x_1,x_2)+e\check{G}(x_1,x_2)\varphi(x_2).
\end{aligned}\tag{A.16}$$

We Wigner transform each of the terms separately and start with the term

$$\begin{aligned}
&\int \mathrm{d}x\,\mathrm{e}^{-ipx}(\nabla^2_{\boldsymbol{r}_1}-\nabla^2_{\boldsymbol{r}_2})\check{G}(x_1,x_2)\\
&\qquad=\int \mathrm{d}x\,\mathrm{e}^{-ipx}2\nabla_{\boldsymbol{r}}\nabla_{\boldsymbol{R}}\int\frac{\mathrm{d}p'}{(2\pi)^4}\mathrm{e}^{ip'x}\check{G}(X,p')\\
&\qquad=2\int \mathrm{d}x\,\mathrm{e}^{-ipx}\int\frac{dp'}{(2\pi)^4}\mathrm{e}^{ip'x}\boldsymbol{p}'\cdot\nabla_{\boldsymbol{R}}\check{G}(X,p')\\
&\qquad=2\boldsymbol{p}\cdot\nabla_{\boldsymbol{R}}\check{G}(X,p).
\end{aligned}\tag{A.17}$$

For the term including $\nabla_{\boldsymbol{r}_1}\cdot\boldsymbol{A}$ we argue as follows

$$\begin{aligned}
\nabla_{\boldsymbol{r}_1}\cdot\boldsymbol{A}(x_1)&=((\nabla_{\boldsymbol{r}_1}\cdot\boldsymbol{r})\nabla_{\boldsymbol{r}}+(\nabla_{\boldsymbol{r}_1}\cdot\boldsymbol{R})\nabla_{\boldsymbol{r}})\cdot\boldsymbol{A}(X+x/2)\\
&=\nabla_{\boldsymbol{r}}\cdot\boldsymbol{A}(X+x/2)+\tfrac{1}{2}\nabla_{\boldsymbol{R}}\cdot\boldsymbol{A}(X+x/2)\\
&=\nabla_{\boldsymbol{R}}\cdot\boldsymbol{A}(X+x/2),
\end{aligned}\tag{A.18}$$

where we, in going to the last line, use that $\partial_y f(x+y/2)=\frac{1}{2}\partial_x f(x+y/2)$ which is seen from the way the arguments occur in f. Now, we can also do the same for $\nabla_{\boldsymbol{r}_2}\cdot\boldsymbol{A}(x_2)$

$$\begin{aligned}
\nabla_{\boldsymbol{r}_2}\cdot\boldsymbol{A}(x_2)&=((\nabla_{\boldsymbol{r}_2}\cdot\boldsymbol{r})\nabla_{\boldsymbol{r}}+(\nabla_{\boldsymbol{r}_2}\cdot\boldsymbol{R})\nabla_{\boldsymbol{r}})\ \cdot Avec(X-x/2)\\
&=-\nabla_{\boldsymbol{r}}\cdot\boldsymbol{A}(X-x/2)+\tfrac{1}{2}\nabla_{\boldsymbol{R}}\cdot\boldsymbol{A}(X-x/2)\\
&=\nabla_{\boldsymbol{R}}\cdot\boldsymbol{A}(X-x/2).
\end{aligned}\tag{A.19}$$

By this, we can see that the Wigner transform of the $\nabla\cdot\boldsymbol{A}$ terms can be written as follows

$$\begin{aligned}
&\frac{-ie}{2m}\int \mathrm{d}x\,\left[(\nabla_{\boldsymbol{r}_1}\cdot\boldsymbol{A}(x_1)\hat{\rho}_3)\check{G}(x_1,x_2)+\check{G}(x_1,x_2)\nabla_{\boldsymbol{r}_2}\cdot\boldsymbol{A}(x_2)\hat{\rho}_3\right]\\
&\qquad=\frac{-ie}{2m}\left\{\nabla_{\boldsymbol{R}}\cdot\boldsymbol{A}\hat{\rho}_3\ \overset{\otimes}{,}\check{G}\right\}.
\end{aligned}\tag{A.20}$$

For the transform of the $\nabla\check{G}$ terms, Appendix A.2 is used and it can be seen that the Wigner transform of the $\nabla\check{G}$-terms becomes

$$\begin{aligned}
&-\frac{ie}{m}\int \mathrm{d}x\,\mathrm{e}^{-ipx}[\boldsymbol{A}(x_1)\hat{\rho}_3\cdot\nabla_{\boldsymbol{r}_1}\check{G}(x_1,x_2)+(\nabla_{\boldsymbol{r}_2}\check{G}(x_1,x_2))\cdot\boldsymbol{A}(x_2)\hat{\rho}_3]\\
&\qquad=-\frac{ie}{2m}\left\{\boldsymbol{A}\hat{\rho}_3\ \overset{\otimes}{,}\nabla_{\boldsymbol{R}}\check{G}\right\}+\frac{e}{m}\boldsymbol{p}\left[\boldsymbol{A}\hat{\rho}_3\ \overset{\otimes}{,}\check{G}\right]+\frac{ie}{2m}\left\{\nabla_{\boldsymbol{R}}\cdot\boldsymbol{A}\hat{\rho}_3\ \overset{\otimes}{,}\check{G}\right\}.
\end{aligned}\tag{A.21}$$

The transformation of the rest of the terms in Equation (A.16), the φ-term and the μ-term, are straightforward, the same goes for the terms in (A.13c), (A.13d) and (A.13e). Using $\bar{\nabla}$ such that $\bar{\nabla}\check{g} = \nabla_{\boldsymbol{R}}\check{g} - ie[\boldsymbol{A}\hat{\rho}_3, \check{g}]$, we can now write the whole Wigner transform of Equation (2.18) as follows

$$\begin{aligned} &-\frac{ie}{2m}\left\{\boldsymbol{A}\hat{\rho}_3 \overset{\otimes}{,} \nabla_{\boldsymbol{R}}\check{G}\right\} + \frac{\boldsymbol{p}}{m}\cdot\bar{\nabla}\check{G} \\ &\qquad + \left[E\hat{\rho}_3 - \frac{\mathrm{e}^2}{2m}\boldsymbol{A}^2 - e\varphi - \hat{S} + \hat{M} + \hat{\Delta} - \hat{\Sigma} \overset{\otimes}{,} \check{G}\right] \\ &\qquad = 0. \end{aligned} \tag{A.22}$$

Appendix B

Self-Energy

*This appendix is taken from sections in the specialization project, and only a few changes have been made.

B.1 Introducing self-energy

To see how the self-energy can replace the potential in the equation of motion we start by splitting the Hamiltonian into a non-impurity part and an impurity part. In this section we will use $\hat{H}_0$ for the Hamiltonian including all other terms than the impurity potential, it should not be confused with the H_0 definition used earlier. The Hamiltonian is divided into the two parts

$$\begin{aligned} \hat{H} &= \hat{H}_0 + \hat{H}_{\text{imp}}, \\ \hat{H}_0 &= \hat{\xi} + \hat{\Delta} + \hat{S} - \hat{M}, \\ \hat{H}_{\text{imp}} &= V_{\text{imp}}. \end{aligned} \tag{B.1}$$

Now we can define G_0 to be the Green function for a system without H_{imp} so that we have

$$\Big(i\partial_t\hat{\rho}_3 - \hat{\rho}_3\hat{H}_0(\boldsymbol{r}_1)\hat{\rho}_3\Big)\check{G}_0(x_1,x_2) = \delta(x_1,x_2). \tag{B.2}$$

From the Dyson equation we get

$$G(x_1,x_2) = G_0(x_1,x_2) + \int \mathrm{d}x_3 \int \mathrm{d}x_4 G_0(x_1,x_3)\Sigma(x_3,x_4)G(x_4,x_2), \tag{B.3}$$

where Σ is the one-particle irreducible self-energy. Now, we act on Equation (B.3) with the operator $(i\partial_{t_1}\hat{\rho}_3 - \hat{\rho}_3 H_0(x_1)\hat{\rho}_3)$, which gives

$$\begin{aligned} &(i\partial_{t_1}\hat{\rho}_3 - \hat{\rho}_3 H_0(1x_)\hat{\rho}_3)G(x_1,x_2) \\ &\quad = (i\partial_{t_1}\hat{\rho}_3 - \hat{\rho}_3 H_0(x_1)\hat{\rho}_3)G_0(x_1,x_2) \\ &\qquad + \int \mathrm{d}x_3 \int \mathrm{d}x_4 (i\partial_{t_1}\hat{\rho}_3 - \hat{\rho}_3 H_0(x_1)\hat{\rho}_3)G_0(x_1,x_3)\Sigma(x_3,x_4)G(x_4,x_2) \\ &\implies (i\partial_{t_1}\hat{\rho}_3 - \hat{\rho}_3 H_0(x_1)\hat{\rho}_3)G(x_1,x_2) = \delta(x_1,x_2) + \int \mathrm{d}x_4 \Sigma(x_1,x_4)G(x_4,x_2). \end{aligned} \tag{B.4}$$

The same can be done for the left-handed equation. First, notice that the Dyson equation also can be written as

$$\check{G}(x_1,x_2) = G_0(x_1,x_2) + \int \mathrm{d}x_3 \int \mathrm{d}x_4 \check{G}(x_1,x_3)\hat{\Sigma}(x_3,x_4)\check{G}_0. \tag{B.5}$$

Acting from the right with the operator $(i\partial_{t_2} - \hat{H}_0(2))$ and using the left-handed equation of motion for G_0, $G_0(x_1, x_2)(i\partial_{t_2} - \hat{H}(x_2)) = \delta(x_1, x_2)$ then gives

$$\check{G}(x_1, x_2)(i\partial_{t_2} - \hat{H}_0(x_2)) = \delta(x_1, x_2) \int \mathrm{d}x_3 \check{G}(x_1, x_3)\hat{\Sigma}(x_3, x_2). \tag{B.6}$$

In effect, we see that the V_{imp} is removed from the H operator and instead a convolution between the Green function and the self-energy has been added to the equation of motion.

B.2 Diffusive quasiclassical self-energy

Impurity averaging

Before reaching the Usadel equation, approximations need to be applied to the self-energy Σ. The self-consistent Born approximation will be used, and to do so impurity averaging has to be discussed. The starting point is assuming that the impurity potential comes from identical impurities spread around in the material. If we have a system with N impurities located at positions $\boldsymbol{R}_1, \boldsymbol{R}_2, ...\boldsymbol{R}_N$, the impurity potential reads

$$V_{\mathrm{imp}}(\boldsymbol{r}) = \sum_{i=1}^{N} U(\boldsymbol{r} - \boldsymbol{R}_i), \tag{B.7}$$

where $U(\boldsymbol{r} - \boldsymbol{R}_1)$ is the potential at position $\boldsymbol{r}$ from one impurity located at position $\boldsymbol{R}$. The position of the impurities will vary in different realizations of the system, and for the calculation it is most meaningful to calculate the average over all possible realizations, namely all possible positions of $\boldsymbol{R}_1, ...\boldsymbol{R}_N$. We define the impurity average over a quantity X as follows

$$\langle X \rangle_{\mathrm{av}} \equiv \int \mathrm{d}\boldsymbol{R}_1 \int \mathrm{d}\boldsymbol{R}_2 \cdots \int \mathrm{d}\boldsymbol{R}_N X. \tag{B.8}$$

To see how the self-energy can be approximated the first step is writing the Dyson equation for G expanded in powers of V and G_0

$$\begin{aligned} G(x, x') = G_0(x, x') &+ \int \mathrm{d}1 G_0(x, 1)V(1)G_0(1, x') \\ &+ \int \mathrm{d}1 \int \mathrm{d}2 G_0(x, 1)V(1)G_0(1, 2)V(2)G_0(2, x') + \cdots . \end{aligned} \tag{B.9}$$

The impurity average of this equation reads

$$\begin{aligned} \langle G(x, x') \rangle = G_0(x, x') &+ \int \mathrm{d}1 G_0(x, 1) \langle V(1) \rangle G_0(1, x') \\ &+ \int \mathrm{d}1 \int \mathrm{d}2 G_0(x, 1) \langle V(1)G_0(1, 2)V(2) \rangle G_0(2, x') + \cdots . \end{aligned} \tag{B.10}$$

If we assume a uniform random distribution of impurities, the average over one impurity potential is a constant, and we can freely define what to call zero energy by adjusting the chemical potential, therefore we can set this average over one impurity to be zero

$$\int \mathrm{d}\boldsymbol{R}\, U(\boldsymbol{r} - \boldsymbol{R}) = \mathrm{const} = 0. \tag{B.11}$$

The average over the entire impurity potential is thus also zero

$$\langle V \rangle_{\text{av}} = \int \mathrm{d}\boldsymbol{R}_1 ... \int \mathrm{d}\boldsymbol{R}_N \sum_{i=1}^{N} U(\boldsymbol{r} - \boldsymbol{R}_i) = 0. \tag{B.12}$$

From this, it is seen that the first term in Equation (B.10) disappear. Looking further at the third term in Equation (B.10), we see that the sum can be split into one part where $i = j$ and one where $i \neq j$. Rewriting by splitting the sum we get

$$\begin{aligned}
&\langle V(1)G_0(1,2)V(2)\rangle \\
&\quad = \sum_i \int \mathrm{d}R_1 ... \int \mathrm{d}R_N U(\boldsymbol{r}_1 - \boldsymbol{R}_i) G_0(1,2) U(\boldsymbol{r}_2 - \boldsymbol{R}_i) \\
&\qquad + \sum_{i \neq j} \int \mathrm{d}R_1 ... \int \mathrm{d}R_N U(\boldsymbol{r}_1 - \boldsymbol{R}_i) G_0(1,2) U(\boldsymbol{r}_2 - \boldsymbol{R}_j) \\
&\quad = \sum_i \int \mathrm{d}R_i U(\boldsymbol{r}_1 - \boldsymbol{R}_i) G_0(1,2) U(\boldsymbol{r}_2 - \boldsymbol{R}_i) \int \mathrm{d}R_1 ... \int \mathrm{d}R_{i-1} \int \mathrm{d}R_{i+1} ... \int \mathrm{d}R_N \\
&\qquad + \sum_{i \neq j} \Big(\int \mathrm{d}R_i U(\boldsymbol{r}_1 - \boldsymbol{R}_i) \Big) G_0(1,2) \Big(\int \mathrm{d}R_j U(\boldsymbol{r}_2 - \boldsymbol{R}_j) \Big) \\
&\qquad\quad \times \int \mathrm{d}R_1 ... \int \mathrm{d}R_{i-1} \int \mathrm{d}R_{i+1} ... \int \mathrm{d}R_{j-1} \int \mathrm{d}R_{j+1} ... \int \mathrm{d}R_N \\
&\quad = \sum_i \int \mathrm{d}R_i U(\boldsymbol{r}_1 - \boldsymbol{R}_i) G_0(1,2) U(\boldsymbol{r}_2 - \boldsymbol{R}_j) \int \mathrm{d}R_1 ... \int \mathrm{d}R_{i-1} \int \mathrm{d}R_{i+1} ... \int \mathrm{d}R_N.
\end{aligned} \tag{B.13}$$

We can write the integrals that are contributing to the Green function diagrammatically, by attributing one dotted line to every $U(\boldsymbol{r} - \boldsymbol{R}_i)$, and when the i is equal j from another factor $U(\boldsymbol{r} - \boldsymbol{R}_j)$ the dotted lines are connected. If a line is not connected, the term vanishes. This is seen in the equation above, when $i \neq j$ for all other j the term becomes zero. We can now express the contributing terms in Equation (B.10) up to the fourth order of V with diagrams as in Figure B.1.

Self-consistent Born approximation

In the Born-approximation one only includes the term of second order of V, which is only the first diagram in Figure B.1,

$$\begin{aligned}
\langle G(x,x') \rangle_{\text{B}} = G_0(x,x') &\\
+ \int \mathrm{d}1 \int \mathrm{d}2 G_0(x,1) \int \mathrm{d}\boldsymbol{R}_1 ... \int \mathrm{d}\boldsymbol{R}_N &\\
\times \sum_{i,j=1}^{N} U(\boldsymbol{r}_1 - \boldsymbol{R}_i) G_0(1,2) U(\boldsymbol{r}_2 - \boldsymbol{R}_j) G_0(2,x'), &
\end{aligned} \tag{B.14}$$

where the subscript "B" stands for Born approximation. From Equation (B.14), it can be seen that the self-energy is

$$\Sigma_{\text{B}}(1,2) = \int \mathrm{d}\boldsymbol{R}_1 ... \int \mathrm{d}\boldsymbol{R}_N \sum_{i,j=1}^{N} U(\boldsymbol{r}_1 - \boldsymbol{R}_i) G_0(1,2) U(\boldsymbol{r}_2 - \boldsymbol{R}_j), \tag{B.15}$$

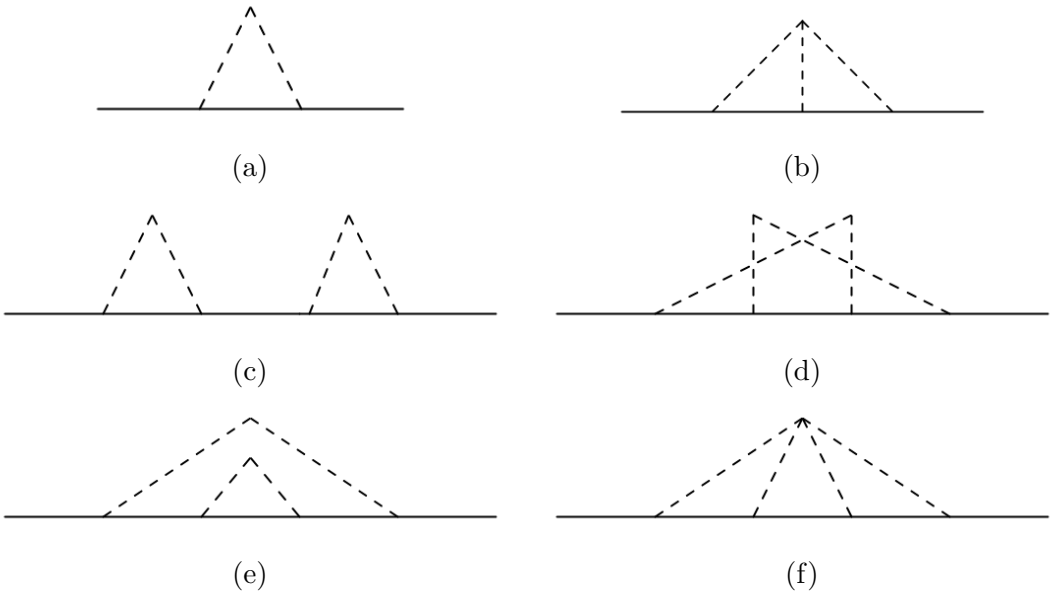

Figure B.1: Impurity scattering diagrams up to fourth order in V.

so that the impurity averaged Green's function now can be written as

$$\langle G(x,x')\rangle_{\mathrm{B}} = G_0(x,x') + \int \mathrm{d}1 \int \mathrm{d}2 G_0(x,1)\Sigma_{\mathrm{B}}(1,2)G_0(2,x'). \tag{B.16}$$

An improvement can be made by introducing the self-consistent Born approximation, for which the equation for the approximated Green function, G_{SCB} reads

$$\langle G(x,x')\rangle_{\mathrm{SCB}} = G_0(x,x') + \int \mathrm{d}1 \int \mathrm{d}2 G_0(x,1) \left\langle V(1) \left\langle G(1,2)\right\rangle_{\mathrm{SCB}} V(2)\right\rangle \left\langle G(2,x')\right\rangle_{\mathrm{SCB}}. \tag{B.17}$$

In this case, the self-energy reads

$$\Sigma_{\mathrm{SCB}}(1,2) = \left\langle V(1) \left\langle G(1,2)\right\rangle_{\mathrm{SCB}} V(2)\right\rangle. \tag{B.18}$$

Writing out G_{SCB} it can be seen that the diagrams (a), (c) and (e) from Figure B.1 are included.

Quasiclassical self-energy

The quasiclassical approximation should also be applied to the self-energy. We use the self-energy in the self-consistent Born approximation from Equation (B.18). We also use that we can write the impurity potential in terms of the Fourier transformed potential

$$V(\boldsymbol{r}) = \sum_{\boldsymbol{R}_i} U(\boldsymbol{r}-\boldsymbol{R}_i) = \sum_{\boldsymbol{R}_i}\sum_{\boldsymbol{q}} v(\boldsymbol{q}) \mathrm{e}^{i\boldsymbol{q}\cdot(\boldsymbol{r}-\boldsymbol{R}_i)}, \tag{B.19}$$

where $v(\boldsymbol{q})$ is the Fourier transform of the real space potential $U(\boldsymbol{r})$. We can then write the self-energy as follows

$$\begin{aligned}\Sigma(x_1,x_2) &= \sum_{\boldsymbol{R}_i}\sum_{\boldsymbol{q}} \mathrm{e}^{i\boldsymbol{q}\cdot(\boldsymbol{r}_1-\boldsymbol{R}_i)} G(x_1,x_2) \sum_{\boldsymbol{R}_j}\sum_{\boldsymbol{q}'} \mathrm{e}^{i\boldsymbol{q}'\cdot(\boldsymbol{r}_2-\boldsymbol{R}_j)} \\ &= N_i \sum_{\boldsymbol{R}_i}\sum_{\boldsymbol{q},\boldsymbol{q}'} G(x_1,x_2) v(\boldsymbol{q}) \mathrm{e}^{-i(\boldsymbol{q}+\boldsymbol{q}')\cdot\boldsymbol{R}_i} v(\boldsymbol{q}') \mathrm{e}^{i\boldsymbol{q}\cdot\boldsymbol{r}_1+i\boldsymbol{q}'\cdot\boldsymbol{r}_2} \\ &= N_i \sum_{\boldsymbol{q}} v(\boldsymbol{q}) G(x_1,x_2) v(-\boldsymbol{q}) \mathrm{e}^{i\boldsymbol{q}\cdot\boldsymbol{r}_1-i\boldsymbol{q}\cdot\boldsymbol{r}_2} \\ &= n_i \int \frac{\mathrm{d}\boldsymbol{q}}{(2\pi)^3} \mathrm{e}^{i\boldsymbol{q}\cdot\boldsymbol{r}_1-i\boldsymbol{q}\cdot\boldsymbol{r}_2} G(x_1,x_2) |v(\boldsymbol{q})|^2,\end{aligned} \tag{B.20}$$

where N_i is the number of impurities and n_i is the impurity density. In going from the first to the second line, we use that there is no contribution unless $i=j$. Assuming that $V(\boldsymbol{r})$ is real we conclude that $v(-\boldsymbol{q}) = v(\boldsymbol{q})^*$. The next step is Wigner transforming Σ

$$\begin{aligned}\Sigma(X,p) &= \int \mathrm{d}\boldsymbol{r} \int \mathrm{d}t\, \mathrm{e}^{-i\boldsymbol{p}\cdot\boldsymbol{r}} \mathrm{e}^{iEt} n_i \int \frac{d\boldsymbol{q}}{(2\pi)^3} |v(\boldsymbol{q})|^2 \mathrm{e}^{i\boldsymbol{q}\cdot\boldsymbol{r}} G(x_1,x_2) \\ &= n_i \int \frac{\mathrm{d}\boldsymbol{q}}{(2\pi)^3} |v(\boldsymbol{q})|^2 G(X,E,\boldsymbol{p}-\boldsymbol{q}) \\ &= n_i \int \frac{d\boldsymbol{q}}{(2\pi)^3} |v(\boldsymbol{p}-\boldsymbol{q})|^2 G(X,q).\end{aligned} \tag{B.21}$$

We use the approximation

$$\int \frac{\mathrm{d}\boldsymbol{p}}{(2\pi)^3} \approx N_0 \int \mathrm{d}\xi_{\boldsymbol{p}} \int \frac{\mathrm{d}\Omega_{\boldsymbol{p}}}{4\pi}, \tag{B.22}$$

where N_0 is the density of states at the Fermi level, $\xi_{\boldsymbol{p}} = \frac{\boldsymbol{p}^2}{2m}$, and $\Omega_{\boldsymbol{p}}$ is the solid angle in momentum space. Next we assume that $|v(\boldsymbol{q}-\boldsymbol{p})|$ depends weakly on $\xi_{\boldsymbol{p}}$ so that we can write

$$\begin{aligned}\hat{\sigma}(X,p) &\approx n_i \int \frac{\mathrm{d}\Omega_{\boldsymbol{p}}}{4\pi} |v(\boldsymbol{p}-\boldsymbol{q}_F)|^2 \int \mathrm{d}\xi_{\boldsymbol{p}} G(X,q) \\ &= \frac{n_i \pi}{i} \int \frac{\mathrm{d}\Omega_{\boldsymbol{p}}}{4\pi} |v(\boldsymbol{p}-\boldsymbol{q}_F)|^2 \check{g}(X,E,\check{g}_F)\end{aligned} \tag{B.23}$$

Here we follow the notation often used in the literature by writing σ instead of Σ to indicate that we are expressing the self-energy in terms of the quasiclassical Green function.

Diffusive limit

For the quasiclassical self-energy we approximate that the main contribution comes from the s-wave Green function $\check{g}_s$. Using Equation (B.23) the relaxation-time τ can be defined

$$\frac{1}{\tau} = 2\pi n_i N_0 \int \frac{\mathrm{d}\Omega_{\boldsymbol{p}}}{4\pi} |v(\boldsymbol{q}-\boldsymbol{p})|^2, \tag{B.24}$$

such that the self-energy can be written

$$\sigma(\boldsymbol{R},T,\boldsymbol{p}_F,E) \approx -\frac{i}{2\tau}\check{g}_s. \tag{B.25}$$

Appendix C

Spin-Orbit Coupling Boundary Condition

*This derivation is copied from the specialization project and only a few changes have been made. The derivation follows [30] closely.

To derive the boundary condition, the first step is setting up the Hamiltonian consisting of interactions between the electrons on the left side of the barrier, the interactions between the electrons at the right side, and the tunneling term where the electrons on the right side interact with the electrons at the left side. We set up the Hamiltonian in momentum space as follows

$$\begin{aligned} H &= H_L + H_R + H_T \\ H_L &= \sum_{\boldsymbol{p}\boldsymbol{p}'\sigma\sigma'} H_{L,\sigma\sigma'}(\boldsymbol{p},\boldsymbol{p}') a^\dagger_{\boldsymbol{p}\sigma} a_{\boldsymbol{p}',\sigma'} \\ H_R &= \sum_{\boldsymbol{p}\boldsymbol{p}'\sigma\sigma'} H_{R,\sigma\sigma'}(\boldsymbol{p},\boldsymbol{p}') b^\dagger_{\boldsymbol{p}\sigma} b_{\boldsymbol{p}',\sigma'} \\ H_T &= \sum_{\boldsymbol{p}\boldsymbol{p}'\sigma\sigma'} [T_{\sigma\sigma'}(\boldsymbol{p},\boldsymbol{p}') a^\dagger_{\boldsymbol{p}\sigma} b_{\boldsymbol{p}'\sigma'} + T^*_{\sigma\sigma'}(\boldsymbol{p},\boldsymbol{p}') b^\dagger_{\boldsymbol{p}'\sigma'} a_{\boldsymbol{p}\sigma}]. \end{aligned} \tag{C.1}$$

Here $a^\dagger, a$ are the creation and annihilation operator of electrons at the left side of the interface, and $b^\dagger, b$ are the creation and annihilation operators of electrons at the right side of the interface.

We could include more terms to the left side and right side Hamiltonian H_L and H_R, like the BCS interaction terms. However these terms will not contribute to the tunneling current, therefore we leave them out. The tunneling Hamiltonian is here written in a general manner, and we will keep it like this for the first part of the derivation. Later on we will introduce the specific tunneling term that corresponds to Rashba spin-orbit coupling.

Equation of motion for creation and annihilation operators

The equation of motion for the field operators can be derived using the Heisenberg equation $i\partial_t a = [H, a]$

$$\begin{aligned} i\partial_t a_{\boldsymbol{p}\sigma} &= \sum_{\boldsymbol{p}'\sigma'} \left[H_{L,\sigma\sigma'}(\boldsymbol{p},\boldsymbol{p}') a_{\sigma'\boldsymbol{p}'} + T_{\sigma\sigma'}(\boldsymbol{p},\boldsymbol{p}') b_{\boldsymbol{p}'\sigma'} \right], \\ -i\partial_t a^\dagger_{-\boldsymbol{p}\sigma} &= \sum_{\boldsymbol{p}'\sigma'} \left[H_{L,\sigma\sigma'}(-\boldsymbol{p},-\boldsymbol{p}') a^\dagger_{-\boldsymbol{p}'\sigma'} + T^*_{\sigma\sigma'}(-\boldsymbol{p},-\boldsymbol{p}') b^\dagger_{-\boldsymbol{p}'\sigma'} \right], \\ i\partial_t b_{\boldsymbol{p}\sigma} &= \sum_{\boldsymbol{p}'\sigma'} \left[H_{R,\sigma\sigma'}(\boldsymbol{p},\boldsymbol{p}') + T^*_{\sigma'\sigma}(\boldsymbol{p}',\boldsymbol{p}) a_{\boldsymbol{p}'\sigma'} \right], \\ -i\partial_t b_{-\boldsymbol{p}\sigma} &= \sum_{\boldsymbol{p}'\sigma'} \left[H_{R,\sigma\sigma'}(-\boldsymbol{p},-\boldsymbol{p}') b^\dagger_{-\boldsymbol{p}'\sigma'} + T_{\sigma'\sigma}(-\boldsymbol{p}',-\boldsymbol{p}) a_{-\boldsymbol{p}'\sigma'} \right]. \end{aligned} \tag{C.2}$$

Continuing in the same way as earlier, we switch to the spin $\otimes$ Nambu space notation where

$$A_{\boldsymbol{p}} = \begin{pmatrix} a_{\boldsymbol{p}\uparrow} \\ a_{\boldsymbol{p}\downarrow} \\ a^\dagger_{-\boldsymbol{p}\uparrow} \\ a^\dagger_{-\boldsymbol{p}\downarrow} \end{pmatrix}, \tag{C.3}$$

and equivalently for $B_{\boldsymbol{p}}$. We write down the equation of motion in this spin $\otimes$ Nambu notation

$$i\hat{\rho}_3 \partial_t A_{\boldsymbol{p}} = \sum_{\boldsymbol{p}} \left[\hat{H}_L(\boldsymbol{p},\boldsymbol{p}') A_{\boldsymbol{p}'} + \hat{T}(\boldsymbol{p},\boldsymbol{p}') B_{\boldsymbol{p}'} \right], \tag{C.4}$$

$$i\hat{\rho}_3 \partial_t B_{\boldsymbol{p}} = \sum_{\boldsymbol{p}} \left[\hat{H}_R(\boldsymbol{p},\boldsymbol{p}') B_{\boldsymbol{p}'} + \hat{\bar{T}}(\boldsymbol{p},\boldsymbol{p}') A_{\boldsymbol{p}'} \right], \tag{C.5}$$

where

$$\hat{H}_{L(R)}(\boldsymbol{p},\boldsymbol{p}') = \begin{pmatrix} \underline{H}_{L(R)}(\boldsymbol{p},\boldsymbol{p}') & 0 \\ 0 & \underline{H}_{L(R)}(-\boldsymbol{p},-\boldsymbol{p}') \end{pmatrix}, \tag{C.6}$$

$$\hat{T}(\boldsymbol{p},\boldsymbol{p}') = \begin{pmatrix} \bar{T}(\boldsymbol{p},\boldsymbol{p}') & 0 \\ 0 & \bar{T}^*(\boldsymbol{p},\boldsymbol{p}') \end{pmatrix}. \tag{C.7}$$

Defining more Green functions

To proceed we need to define some more Green functions. We will now introduce greater, lesser and time-ordered Green functions. In addition we introduce the concept of connected Green functions. These connected Green functions will be correlation functions of one electron operator from the left side and one from the right side and they will be called C instead of G, so it should be paid attention to the difference between C and G in the calculation that follows. In addition we add a subscript R or L, for "right" and "left" which indicated which electron operator type we are using, or the order they are in. The lesser Green functions are defined as

$$\begin{aligned} \hat{C}^<_L(\boldsymbol{p},t;\boldsymbol{p}',t') &= i\left\langle [[A^\dagger_{\boldsymbol{p}'}(t')]^T [B_{\boldsymbol{p}}(t)]^T]^T \right\rangle, \\ \hat{C}^<_R(\boldsymbol{p},t;\boldsymbol{p}',t') &= i\left\langle [[B^\dagger_{\boldsymbol{p}'}(t')]^T [A_{\boldsymbol{p}}(t)]^T]^T \right\rangle, \\ \hat{G}^<_L(\boldsymbol{p},t;\boldsymbol{p}',t') &= i\left\langle [[A^\dagger_{\boldsymbol{p}'}(t')]^T [A_{\boldsymbol{p}}(t)]^T]^T \right\rangle, \\ \hat{G}^<_R(\boldsymbol{p},t;\boldsymbol{p}',t') &= i\left\langle [[B^\dagger_{\boldsymbol{p}'}(t')]^T [B_{\boldsymbol{p}}(t)]^T]^T \right\rangle. \end{aligned} \tag{C.8}$$

In the same manner we define the greater Green functions

$$\begin{aligned}
\hat{C}_L^{>}(\boldsymbol{p},t;\boldsymbol{p}',t') &= i\left\langle B_{\boldsymbol{p}}(t)A_{\boldsymbol{p}'}^{\dagger}(t')\right\rangle, \\
\hat{C}_R^{>}(\boldsymbol{p},t;\boldsymbol{p}',t') &= i\left\langle A_{\boldsymbol{p}}(t)B_{\boldsymbol{p}'}^{\dagger}(t')\right\rangle, \\
\hat{G}_L^{>}(\boldsymbol{p},t;\boldsymbol{p}',t') &= i\left\langle A_{\boldsymbol{p}}(t)A_{\boldsymbol{p}'}^{\dagger}(t')\right\rangle, \\
\hat{G}_R^{>}(\boldsymbol{p},t;\boldsymbol{p}',t') &= i\left\langle B_{\boldsymbol{p}}(t)B_{\boldsymbol{p}'}^{\dagger}(t')\right\rangle.
\end{aligned} \tag{C.9}$$

We also define the Keldysh Green functions in the same manner

$$\hat{C}_L^{K}(\boldsymbol{p},t;\boldsymbol{p}',t) = -i\hat{\rho}_3\left\langle [B_{\boldsymbol{p}}(t),A_{\boldsymbol{p}'}^{\dagger}(t')]\right\rangle, \tag{C.10}$$

also for the right side Green function and for the connected Green functions. Lastly, we also define the time-ordered Green functions

$$\begin{aligned}
\hat{C}_L(\boldsymbol{p},t;\boldsymbol{p}',t') &= -i\hat{\rho}_3\left\langle \mathcal{T}B_{\boldsymbol{p}}(t)A_{\boldsymbol{p}'}^{\dagger}(t')\right\rangle \\
&= -i\hat{\rho}_3\Theta(t-t')\left\langle B_{\boldsymbol{p}}(t)A_{\boldsymbol{p}'}^{\dagger}(t')\right\rangle + i\hat{\rho}_3\left\langle [[A_{\boldsymbol{p}'}^{\dagger}(t')]^T[B_{\boldsymbol{p}}(t)]^T]^T\right\rangle.
\end{aligned} \tag{C.11}$$

One should pay attention to that the lesser and greater Green functions are defined without a $\hat{\rho}_3$ whereas the Keldysh Green functions and the time-ordered Green function are defined with.

Tunneling current

To find the tunneling current we use $J = e\partial_t N_L = -e\partial_t N_R$, where N_L and N_R is the number operator of the left and right side respectively. Notice that we have defined that the direction of the current is from the left side toward the right side.

The number operator of left-side electrons reads

$$N_L = \sum_{\boldsymbol{p}s} a_{\boldsymbol{p}s}^{\dagger}a_{\boldsymbol{p}s}. \tag{C.12}$$

We use our equations of motion and we see that we can write it in terms of a trace over the lesser connected Green function

$$\langle\partial_t N_L\rangle = -\sum_{\boldsymbol{p}\boldsymbol{p}'}\mathrm{Tr}[\hat{T}(\boldsymbol{p},\boldsymbol{p}')\hat{C}_L^{<}(\boldsymbol{p}',t;\boldsymbol{p},t)]. \tag{C.13}$$

To evaluate this we will also need the time derivative of the connected time-ordered Green function, which can be found to be

$$i\hat{\rho}_3\partial_t\hat{C}_L(\boldsymbol{p},t;\boldsymbol{p}',t) = \sum_{\boldsymbol{q}}[\hat{H}^R(\boldsymbol{p},\boldsymbol{q})\hat{C}_L(\boldsymbol{q},t;\boldsymbol{p}',t') + \hat{\tilde{T}}(\boldsymbol{p},\boldsymbol{q})\hat{G}_L]. \tag{C.14}$$

This can be written as

$$\sum_{\boldsymbol{q}}[i\hat{\rho}_3\partial_t\delta_{\boldsymbol{q}\boldsymbol{p}} - \hat{H}^R(\boldsymbol{p},\boldsymbol{q})] = \sum_{\boldsymbol{q}}\hat{\tilde{T}}(\boldsymbol{p},\boldsymbol{q})\hat{G}_L(\boldsymbol{q},r;\boldsymbol{q}',t'), \tag{C.15}$$

to which we can write the solution

$$\hat{C}(\boldsymbol{p},t,\boldsymbol{p}',t') = \int \mathrm{d}t_1\sum_{\boldsymbol{q}\boldsymbol{q}'}\hat{G}_{0,R}(\boldsymbol{p},t;\boldsymbol{q},t_1)\hat{\tilde{T}}(\boldsymbol{q},\boldsymbol{q}')\hat{G}_L(\boldsymbol{q}',t_1;\boldsymbol{p}',t'). \tag{C.16}$$

Here $\hat{G}_{0,R}$ refer to the solution of the system where H_T is not included, that satisfies

$$\sum_{\boldsymbol{q}}[i\hat{\rho}_3\partial_t\delta_{\boldsymbol{pq}} - \hat{H}^R(\boldsymbol{p},\boldsymbol{q})]\hat{G}_{0,R}(\boldsymbol{q},t;\boldsymbol{p}',t') = \delta(t-t')\delta_{\boldsymbol{pp}'}. \tag{C.17}$$

If we first deform this integral to the Keldysh contour we can use Langreth rules on Equation (C.16). These rules are explained in the book by Haug and Jauho [63] and state that if one have $C = \int_C AB$, where A, B and C are time-ordered Green functions and the subscript C on the integral means it is over the Keldysh contour, one also have $C^< = \int_t[A^RB< + A^<BA]$, where the integral is over the real time axis. One also has the equivalent for the greater Green function. By these rules we get

$$\begin{aligned}
\hat{\rho}_3\hat{C}^<(\boldsymbol{p},t;\boldsymbol{p}',t) = \int \mathrm{d}t_1 \sum_{\boldsymbol{qq}'}[&\hat{G}^R_{0,R}(\boldsymbol{p},t;\boldsymbol{q},t_1)\hat{\tilde{T}}(\boldsymbol{q},\boldsymbol{q}')\hat{\rho}_3\hat{G}^<_L(\boldsymbol{q}',t_1;\boldsymbol{p}',t') \\
&+ \hat{\rho}_3\hat{G}^<_{0,R}(\boldsymbol{p},t;\boldsymbol{q},t_1)\hat{\tilde{T}}(\boldsymbol{q},\boldsymbol{q}')\hat{G}^A_L(\boldsymbol{q}',t_1;\boldsymbol{p}',t')], \\
\hat{\rho}_3\hat{C}^>(\boldsymbol{p},t;\boldsymbol{p}',t) = \int \mathrm{d}t_1 \sum_{\boldsymbol{qq}'}[&\hat{G}^R_{0,R}(\boldsymbol{p},t;\boldsymbol{q},t_1)\hat{\tilde{T}}(\boldsymbol{q},\boldsymbol{q}')\hat{\rho}_3\hat{G}^>_L(\boldsymbol{q}',t_1;\boldsymbol{p}',t') \\
&+ \hat{\rho}_3\hat{G}^>_{0,R}(\boldsymbol{p},t;\boldsymbol{q},t_1)\hat{\tilde{T}}(\boldsymbol{q},\boldsymbol{q}')\hat{G}^A_L(\boldsymbol{q}',t_1;\boldsymbol{p}',t')].
\end{aligned} \tag{C.18}$$

Now we use the relation between the Keldysh, greater and lesser Green function

$$\hat{G}^K = \hat{\rho}_3(\hat{G}^< + \hat{G}^>), \tag{C.19}$$

and that for equal time we have $\hat{G}^< = \hat{G}^>$ we can write Equation (C.13) as follows

$$\begin{aligned}
&\langle\partial_t N_L\rangle \\
&\quad = -\frac{1}{2}\sum_{\boldsymbol{pp}'\boldsymbol{qq}'}\int \mathrm{d}t_1 \mathrm{Tr}\left[\hat{\rho}_3\left(\hat{T}(\boldsymbol{p},\boldsymbol{p}')\check{G}_{0,R}(\boldsymbol{p}',t;\boldsymbol{q},t_1)\hat{\tilde{T}}(\boldsymbol{q},\boldsymbol{q}')\check{G}_L(\boldsymbol{q}',t_1;\boldsymbol{p},t)\right)^K\right].
\end{aligned} \tag{C.20}$$

In the same manner we can calculate $\langle\partial_t N_R\rangle = \langle\partial_t \sum_{\boldsymbol{ps}} b^\dagger_{\boldsymbol{ps}} b_{\boldsymbol{ps}}\rangle$ by using the Green functions defined on the right side of the barrier C_R, G_R. We get

$$\langle\partial_t N_R\rangle = -\frac{1}{2}\sum_{\boldsymbol{pp}'\boldsymbol{qq}'}\int \mathrm{d}t_1 \mathrm{Tr}\left\{\hat{\rho}_3\left(\check{G}_{0,L}(\boldsymbol{p}',t;q,t)\hat{\tilde{T}}(\boldsymbol{q},\boldsymbol{q}')\check{G}_R(\boldsymbol{q}',t;\boldsymbol{p},t)T(\boldsymbol{p},p')\right)^K\right\}. \tag{C.21}$$

We use the average of the two expressions we found above in the expression for the tunneling current

$$\langle\partial_t N\rangle = \tfrac{1}{2}\left(\langle\partial_t N_L\rangle - \langle\partial_t N_R\rangle\right). \tag{C.22}$$

We Fourier transform the expression and assume that the flow is stationary so that we can evaluate the expression at $t = 0$

$$\begin{aligned}
\langle\partial_t N\rangle = &\frac{1}{4}\sum_{\boldsymbol{pp}'\boldsymbol{qq}'}\int\frac{\mathrm{d}E}{2\pi}\mathrm{Tr}[\hat{\rho}_3\left(\check{G}_{0,L}(\boldsymbol{p},\boldsymbol{q};E)\hat{T}(\boldsymbol{q},\boldsymbol{q}')\check{G}_R(\boldsymbol{q}',\boldsymbol{p}';E)\hat{\tilde{T}}(\boldsymbol{p}',\boldsymbol{p})\right]^K] \\
&-\frac{1}{4}\sum_{\boldsymbol{pp}'\boldsymbol{qq}'}\int\frac{\mathrm{d}E}{2\pi}\mathrm{Tr}[\hat{\rho}_3\left(\hat{\tilde{T}}(\boldsymbol{p}',\boldsymbol{p})\check{G}_{0,R}(\boldsymbol{p},\boldsymbol{q};E)\hat{\tilde{T}}(\boldsymbol{q},\boldsymbol{q}')\check{G}_L(\boldsymbol{q}',\boldsymbol{p}';E)\right)^K].
\end{aligned} \tag{C.23}$$

From the current expression we have

$$J \sim \int \mathrm{d}E \mathrm{Tr}(\hat{\rho}_3 \check{I}^K), \tag{C.24}$$

where $\hat{I} = \check{G}\nabla\check{G}$ is the current matrix. Next, we approximate $\check{G}_0 \approx \check{G}$, so that we can write

$$\check{I} \sim \sum_{\boldsymbol{p}\boldsymbol{p}'\boldsymbol{q}\boldsymbol{q}'} [\check{G}_L, \hat{T}\check{G}_R\hat{\tilde{T}}] + \text{Traceless terms} \tag{C.25}$$

where the traceless terms means terms where the Keldysh component of the 8×8 matrix multiplied with the $\hat{\rho}_3$ matrix, is traceless.

Rashba spin orbit coupling.

Until now we have not specified what the tunneling terms look like. One can use different tunneling terms where the simplest is just to let the $\hat{T} = \mathrm{diag}(T, T, T, T)$. This would give quite simple boundary conditions for the Green function namely the Kuprianov-Lukiichev boundary conditions. Here we use a more complicated tunneling Hamiltonian where Rashba spin-orbit coupling is present.

Following Linder and Amundsen we choose a tunneling term with a symmetrized Rashba spin-orbit coupling term to ensure hermiticity. We define the tunneling Hamiltonian in real space as

$$H_T = \sum_{\sigma\sigma'} \int \mathrm{d}\boldsymbol{r} \left[a^\dagger_\sigma T_{\sigma\sigma'}(\boldsymbol{r}) b_{\sigma'}(\boldsymbol{r}) + \text{h.c.} \right], \tag{C.26}$$

with

$$T(\boldsymbol{r}) = T_0(\boldsymbol{r}_\parallel) = T_0\delta(\boldsymbol{r}_\perp - R_0) - i\{T_{ij}(\boldsymbol{r}_\parallel)\delta(\boldsymbol{r}_\perp - R_0)\tau_j, \partial_i\}. \tag{C.27}$$

Here $\boldsymbol{r}_\parallel$ is the part of $\boldsymbol{r}$ that is parallel with the interface, and $\boldsymbol{r}_\perp$ is the component of $\boldsymbol{r}$ that is orthogonal to the interface. We have here used that the tunneling term only appears at $\boldsymbol{r}_\perp = R_0$, meaning that we assume an infinitesimally thin layer of spin-orbit coupling material between the superconductor and the other material.

We rewrite this tunneling Hamiltonian in terms of the Fourier-transformed fermionic operator

$$\begin{aligned} H_T &= \sum_{\sigma\sigma'} \int \mathrm{d}\boldsymbol{r} \sum_{\boldsymbol{p}\boldsymbol{p}'} a^\dagger_{s\boldsymbol{p}} e^{-i\boldsymbol{p}\cdot\boldsymbol{r}} T_{\sigma\sigma'}(\boldsymbol{r}) e^{i\boldsymbol{p}'\cdot\boldsymbol{r}} b_{\sigma'\boldsymbol{p}'} \\ &= \sum_{\sigma\sigma'} a^\dagger_{\sigma\boldsymbol{p}} T_{\sigma\sigma'}(\boldsymbol{p}, \boldsymbol{p}') b_{\sigma'\boldsymbol{p}'} \quad \text{where} \\ T_{\sigma\sigma'}(\boldsymbol{p}, \boldsymbol{p}') &= \int \mathrm{d}\boldsymbol{r} e^{-i\boldsymbol{p}\cdot\boldsymbol{r}} T_{\sigma\sigma'}(\boldsymbol{r}) e^{i\boldsymbol{p}'\cdot\boldsymbol{r}} \\ &= \int \mathrm{d}\boldsymbol{r}_\parallel [T_0(\boldsymbol{r}_\parallel) + T_{ij}(\boldsymbol{r}_\parallel)(p_i + p'_i)\tau_{\sigma\sigma',j}] e^{-(\boldsymbol{p}-\boldsymbol{p}')\cdot\boldsymbol{r}_\parallel}. \end{aligned} \tag{C.28}$$

In the last line the T from above is inserted. Further, we approximate the interface to be only one point.

$$\begin{aligned} T_0(\boldsymbol{r}_\parallel) &= \delta(\boldsymbol{r}_\parallel) T_0 \\ T_{ij}(\boldsymbol{r}_\parallel) &= \delta(\boldsymbol{r}_\parallel) T_{ij} \end{aligned} \tag{C.29}$$

where T_0 and T_{ij} are constants. This gives

$$T_{\sigma\sigma'}(\boldsymbol{p}, \boldsymbol{p}') = T_0 + T_{ij}(p_i + p'_i)\tau_{\sigma\sigma',j} = \tilde{T}_{\sigma\sigma'}(\boldsymbol{p}, \boldsymbol{p}'). \tag{C.30}$$

Tunneling terms in the case of Rashba SOC

We now find the tunneling current terms by going to the continuum limit so that the sum in Equation (C.25) can be expressed by integrals, and we perform the integration. First, we write the T-term in a convenient notation

$$\begin{aligned}\hat{T}(\boldsymbol{p},\boldsymbol{p}') &= T_0 + (p_i - p_i')T_{ij}\hat{\rho}_3\hat{\sigma}_j = T_0 + (p_i - p_i')\hat{t}_i,\\ \hat{t}_i &= T_{ij}\hat{\rho}_3\hat{\tau}_j.\end{aligned} \tag{C.31}$$

Also here will use the quasiclassical approximation and write the integral in terms of the quasiclassical Green function

$$\check{g}_{R/L}(\boldsymbol{p}_F, \boldsymbol{R}=0) = \frac{1}{2\pi}\int \mathrm{d}\boldsymbol{q}\int \mathrm{d}\xi_{\boldsymbol{p}}\check{G}_{R/L}(\boldsymbol{p},\boldsymbol{q}). \tag{C.32}$$

We start by looking at the integral

$$\int \mathrm{d}\boldsymbol{p}\int \mathrm{d}\boldsymbol{p'}\int \mathrm{d}\boldsymbol{q}\int \mathrm{d}\boldsymbol{q'}\hat{T}(\boldsymbol{p}',\boldsymbol{p})\check{G}_R(\boldsymbol{p},\boldsymbol{q})\hat{\tilde{T}}(\boldsymbol{q}\boldsymbol{q}')\check{G}_L(\boldsymbol{q}',\boldsymbol{p}'). \tag{C.33}$$

Using the dirty limit approximation writing $\check{g} = \check{g}_s + \boldsymbol{p}_F\cdot\check{\boldsymbol{g}}_p$ with $\check{\boldsymbol{g}}_p = -\tau v_F\check{g}_s\nabla\check{g}_s$ as we got from the Usadel equation. Making use of the identity $\int\frac{\mathrm{d}\Omega}{4\pi}p_{F,i}p_{F,j}/p_F^2 = \frac{1}{3}\delta_{ij}$ we can write Equation (C.33)

$$\begin{aligned}&T_0^2\check{g}_{R,s}\check{g}_{L,s} - mDT_0\check{g}_{R,s}\partial_i\check{g}_{R,s}\hat{t}_i\check{g}_{L,s} - mDT_0\check{g}_{R,s}\hat{t}_i\check{g}_{L,s}\partial_i\check{g}_{L,s}\\ &\quad - mDT_0\hat{t}_i\check{g}_{R,s}\partial_i\check{g}_{R,s}\check{g}_{L,s} - mDT_0\hat{t}_i\check{g}_{R,s}\check{g}_{L,s}\partial_i\check{g}_{L,s} + \tfrac{2}{3}\boldsymbol{p}_F^2\hat{t}_i\check{g}_{R,s}\hat{t}_i\check{g}_{L,s},\end{aligned} \tag{C.34}$$

where $D = \frac{v_F^2\tau}{3}$. Here the a factor 1/3 was missing from the last term in the paper by Linder and Amundsen [30]. For Rashba spin-orbit coupling we have $T_{ij} = T_1 n_k\varepsilon_{kji}$. We can write the whole tunneling term from Equation (C.25) by writing the commutator of the terms that include $\check{g}_{L,s}$,

$$\begin{aligned}D\check{g}_{L,s}\partial_z\check{g}_{L,s} = {}& T_0^2[\check{g}_{L,s},\check{g}_{R,s}] + \tfrac{2}{3}T_1^2p_F^2[\check{g}_{L,s},\boldsymbol{\tau}_\parallel\check{g}_{R,s}\boldsymbol{\tau}_\parallel]\\ &- mDT_1T_0[\check{g}_{L,s},\{\boldsymbol{\tau}_\parallel,(\check{g}_{R,s}\nabla\check{g}_{R,s})\times\boldsymbol{e}_z\}]\\ &- mDT_1T_0[(\check{g}_{L,s}\nabla\check{g}_{L,s})\times\boldsymbol{e}_z,\{\boldsymbol{\tau}_\parallel,\check{g}_{R,s}\}]\\ &+ \text{Traceless terms},\end{aligned} \tag{C.35}$$

where $\boldsymbol{e}_z$ is the unit vector in z-direction.

We do also want an expression $D\check{g}_{R,s}\partial_z\check{g}_{R,s}$, expressed by the opposite side Green function. This can be found by noting in Equation (C.23) that $\hat{\tilde{T}}$ and $\hat{\rho}_3$ commute, so we can also write the expression in Equation (C.25) as

$$\check{I} \sim \sum_{\boldsymbol{p}\boldsymbol{p}'\boldsymbol{q}\boldsymbol{q}'}[\hat{\tilde{T}}\check{G}_L\hat{T},\check{G}_R] = -\sum_{\boldsymbol{p}\boldsymbol{p}'\boldsymbol{q}\boldsymbol{q}'}[\check{G}_R,\hat{\tilde{T}}\check{G}_L\hat{T}]. \tag{C.36}$$

Since $\hat{\tilde{T}} = \hat{T}$ we see that the only difference is that we have switched $\check{G}_L$ with $\check{G}_R$ and gotten a minus sign. From this we conclude that we can write

$$\begin{aligned}D\check{g}_{R,s}\partial_z\check{g}_{R,s} = {}& T_0^2[\check{g}_{L,s},\check{g}_{R,s}] - \tfrac{2}{3}T_1^2p_F^2[\check{g}_{R,s},\boldsymbol{\tau}_\parallel\check{g}_{L,s}\boldsymbol{\tau}_\parallel]\\ &+ mDT_1T_0[\check{g}_{R,s},\{\boldsymbol{\tau}_\parallel,(\check{g}_{L,s}\nabla\check{g}_{L,s})\times\boldsymbol{e}_z\}]\\ &+ mDT_1T_0[(\check{g}_{R,s}\nabla\check{g}_{R,s})\times\boldsymbol{e}_z,\{\boldsymbol{\tau}_\parallel,\check{g}_{L,s}\}]\\ &+ \text{Traceless terms}.\end{aligned} \tag{C.37}$$

Moving forward, the s-subscript will be dropped.

Terms from reflection at interface

In addition to the terms we already found we could also have some traceless terms in our $\check{I}$, and we will find them now by looking at terms that originate from reflection at the interface surface. This is found by integrating the Usadel equation over the interface, so we start by reminding ourselves that the Usadel equation in normal metal reads

$$D\bar{\nabla}(\check{g}\bar{\nabla}\check{g}) + i[E\hat{\rho}_3, \check{g}]. \tag{C.38}$$

The spin orbit coupling is included in the $\bar{\nabla}... = \nabla... - i[\hat{\boldsymbol{A}}, ...]$. Here we have included the $\hat{\rho}_3$ and e in the $\hat{\boldsymbol{A}}$ so that

$$\hat{\boldsymbol{A}} = e\begin{pmatrix} \underline{\boldsymbol{A}} & 0 \\ 0 & -\underline{\boldsymbol{A}}^* \end{pmatrix}, \tag{C.39}$$

where $\underline{\boldsymbol{A}}$ is upgraded to a matrix.

A broader discussion about the origin of the Rashba spin-orbit coupling and the relevance it has in modern research can be found in the paper by Manchon et al. [64]. It can be shown that a Rashba Hamiltonian that breaks the inversion symmetry in z-direction, as the interface in consideration here, can be written

$$H_{SOC} = -\frac{\alpha}{m}(\boldsymbol{k} \times \hat{\boldsymbol{\tau}}) \cdot \boldsymbol{z}, \tag{C.40}$$

which be obtained by setting

$$\underline{\boldsymbol{A}} = e\alpha(-\tau_y, \tau_x, 0). \tag{C.41}$$

It should be noted here that in the derivation of the quasiclassical theory the Rashba spin-orbit coupling by this argument could be introduced from the start, by upgrading the $\boldsymbol{A}$ to a matrix as it is used here.

We integrate Equation (C.38) from $z = -d$ to $z = d$. The spin-orbit coupling material is assumed to be thin so that we can neglect spatial variations of $\check{g}$ in this region, therefore the right side of the Usadel equation integrates to zero, and we get

$$\begin{aligned}(\check{g}\partial_z\check{g})|_d - (\check{g}\partial_z\check{g})|_{-d} - id\nabla\check{g}[\hat{\boldsymbol{A}}, \check{g}]|_d - i\check{g}[\hat{\boldsymbol{A}}, \nabla\check{g}] \\ - id[\hat{\boldsymbol{A}}, \check{g}\nabla\check{g}]|_d - d[\hat{\boldsymbol{A}}, \check{g}[\hat{\boldsymbol{A}}, \check{g}]]|_d \\ = 0,\end{aligned} \tag{C.42}$$

where we have also approximated the derivatives with their value at $z = d$. If we did not have any spin-orbit coupling the $(\check{g}\partial_z\check{g})|_d$ would be equal to the tunneling current, thus we can identify $(\check{g}\partial_z\check{g})|_{-d}$ as the contribution from the tunneling current $\check{I}_T$. We can now write

$$\begin{aligned}(\check{g}\partial_z\check{g})|_d = \hat{I}_T + id\nabla\check{g}[\hat{\boldsymbol{A}}, \check{g}]|_d - 2id\check{g}\nabla\check{g}\hat{\boldsymbol{A}}|_d \\ + id\check{g}\hat{\boldsymbol{A}}\nabla\check{g}|_d + id\hat{\boldsymbol{A}}\check{g}\nabla\check{g}|_d + d[\hat{\boldsymbol{A}}, \check{g}\hat{\boldsymbol{A}}\check{g}]|_d.\end{aligned} \tag{C.43}$$

Now putting in our $\hat{\boldsymbol{A}}$, and writing $\check{g}|_{-d} = \check{g}_L$ gives us

$$\check{g}_R\partial_z\check{g}_R = \hat{I}_T + id\alpha\partial_y[\hat{\rho}_x, \check{g}_R] - 2id\alpha\check{g}_R\partial_y\check{g}_R\hat{\rho}_x + id\alpha\check{g}_R\hat{\rho}_x\partial_y\check{g}_R \tag{C.44}$$

$$+ id\alpha\hat{\rho}_x\check{g}_R\partial_y\check{g}_R + d\alpha^2[\hat{\rho}_x, \check{g}_R\hat{\rho}_x\check{g}_R] + d\alpha^2[\hat{\rho}_y, \check{g}_R\hat{\rho}_y\check{g}_R], \tag{C.45}$$

where we have defined $\hat{\rho}_x = \hat{\rho}_3\hat{\tau}_x$, $\hat{\rho}_y = \hat{\rho}_3\hat{\tau}_y$. Deriving the expression for $\check{g}_L\nabla\check{g}_L$ is similar, we just write the other terms evaluated at $z = -d$. In the paper by Linder and Amundsen, the equation above had an extra constant term that should not be there.

Final form of the boundary conditions

We conclude this section by writing out all the terms in the boundary condition including the tunneling and the reflection terms

$$\begin{aligned} D\check{g}_L\partial_z\check{g}_L = {} & T_0^2[\check{g}_L,\check{g}_R] + \tfrac{2}{3}T_1^2p_F^2[\check{g}_L,\hat{\boldsymbol{\tau}}_\parallel\check{g}_R\hat{\boldsymbol{\tau}}_\parallel] - mDT_1T_0[\check{g}_L,\{\hat{\tau}_{\parallel,x},\check{g}_R\partial_y\check{g}_R\}] \\ & - mDT_1T_0[\check{g}_L\partial_y\check{g}_L,\{\hat{\tau}_{\parallel,x},\check{g}_R\}] - iDd\alpha\partial_y[\hat{\rho}_x,\check{g}_L] \\ & + 2iDd\alpha\check{g}_L\partial_y\check{g}_L\hat{\rho}_x - iDd\alpha\check{g}_L\hat{\rho}_x\partial_y\check{g}_L - iDd\alpha\hat{\rho}_x\check{g}_L\partial_y\check{g}_L \\ & - Dd\alpha^2[\hat{\rho}_x,\check{g}_L\hat{\rho}_x\check{g}_L] - Dd\alpha^2[\hat{\rho}_y,\check{g}_L\hat{\rho}_y\check{g}_L], \end{aligned} \tag{C.46}$$

$$\begin{aligned} D\check{g}_R\partial_z\check{g}_R = {} & T_0^2[\check{g}_L,\check{g}_R] - \tfrac{2}{3}T_1^2p_F^2[\check{g}_R,\hat{\boldsymbol{\tau}}_\parallel\check{g}_L\hat{\boldsymbol{\tau}}_\parallel] + mDT_1T_0[\check{g}_R,\{\hat{\tau}_{\parallel,x},\check{g}_L\partial_y\check{g}_L\}] \\ & + mDT_1T_0[\check{g}_R\partial_y\check{g}_R,\{\hat{\tau}_{\parallel,x},\check{g}_L\}] + iDd\alpha\partial_y[\hat{\rho}_x,\check{g}_R] \\ & - 2iDd\alpha\check{g}_R\partial_y\check{g}_R\hat{\rho}_x + iDd\alpha\check{g}_R\hat{\rho}_x\partial_y\check{g}_R + iDd\alpha\hat{\rho}_x\check{g}_R\partial_y\check{g}_R \\ & + Dd\alpha^2[\hat{\rho}_x,\check{g}_R\hat{\rho}_x\check{g}_R] + Dd\alpha^2[\hat{\rho}_y,\check{g}_R\hat{\rho}_y\check{g}_R]. \end{aligned} \tag{C.47}$$

Bibliography

[1] H. Kamerlingh Onnes, "Further experiments with liquid helium. B. On the change in the resistance of pure metals at very low temperature, etc. III. The resistance of platinum at helium temperatures," in *KNAW, Proceedings*, vol. 13, Amsterdam, 1911, pp. 1107–1113.

[2] H. Kamerlingh Onnes, "Further experiments with liquid helium. C. On the change of electric resistance of pure metals at very low temperature etc. IV. The resistance of pure mercury at helium temperatures," in *KNAW, Proceedings*, vol. 13, Amsterdam, 1911, pp. 1274–1276.

[3] H. Kamerlingh Onnes, "Further experiments with liquid helium. D. On the change of the electrical resistance of pure metals at very low temperature, etc. V. The disappearance of the resistance of mercury," in *KNAW, Proceedings*, vol. 14, Amsterdam, 1911, pp. 113–115.

[4] J. Bardeen, L. N. Cooper, and J. R. Schrieffer, "Theory of superconductivity," *Physical Review*, vol. 108, no. 5, pp. 1175–1204, 1957. DOI: 10.1103/PhysRev.108.1175.

[5] W. Meissner and R. Ochsenfeld, "Ein neuer Effekt bei Eintritt der Supraleitfähigkeit," *Naturwissenschaften*, vol. 21, no. 44, pp. 787–788, 1933. DOI: 10.1007/BF01504252.

[6] F. S. Bergeret, A. F. Volkov, and K. B. Efetov, "Long-range proximity effects in superconductor-ferromagnet structures," *Physical Review Letters*, vol. 86, no. 18, pp. 4096–4099, 2001. DOI: 10.1103/PhysRevLett.86.4096.

[7] F. S. Bergeret, A. F. Volkov, and K. B. Efetov, "Odd triplet superconductivity and related phenomena in superconductor-ferromagnet structures," *Reviews of Modern Physics*, vol. 77, no. 4, pp. 1321–1373, 2005. DOI: 10.1103/RevModPhys.77.1321.

[8] M. Eschrig, J. Kopu, J. C. Cuevas, and G. Schön, "Theory of half-metal/superconductor heterostructures," *Physical Review Letters*, vol. 90, no. 13, p. 137 003, 2003. DOI: 10.1103/PhysRevLett.90.137003.

[9] A. I. Buzdin, "Proximity effects in superconductor-ferromagnet heterostructures," *Reviews of Modern Physics*, vol. 77, no. 3, pp. 935–976, 2005. DOI: 10.1103/RevModPhys.77.935.

[10] J. W. A. Robinson, J. D. S. Witt, and M. G. Blamire, "Controlled injection of spin-triplet supercurrents into a strong ferromagnet," *Science*, vol. 329, no. 5987, pp. 59–61, 2010. DOI: 10.1126/science.1189246.

[11] H. G. Giil and J. Linder, "Effective quasiclassical models for odd-frequency superconductivity: Energy-inversion symmetry, preserved spectral weight, and Meissner response," *Physical Review B*, vol. 106, no. 22, p. 224 506, 2022. DOI: 10.1103/PhysRevB.106.224506.

[12] M. Eschrig, "Spin-polarized supercurrents for spintronics," *Physics Today*, vol. 64, no. 1, pp. 43–49, 2011. DOI: 10.1063/1.3541944.

[13] M. Eschrig, "Spin-polarized supercurrents for spintronics: A review of current progress," *Reports on Progress in Physics*, vol. 78, no. 10, p. 104 501, 2015. DOI: 10.1088/0034-4885/78/10/104501.

[14] R. S. Keizer, S. T. B. Goennenwein, T. M. Klapwijk, G. Miao, G. Xiao, and A. Gupta, "A spin triplet supercurrent through the half-metallic ferromagnet CrO_2," *Nature*, vol. 439, no. 7078, pp. 825–827, 2006. DOI: 10.1038/nature04499.

[15] Y. Kalcheim, O. Millo, M. Egilmez, J. W. A. Robinson, and M. G. Blamire, "Evidence for anisotropic triplet superconductor order parameter in half-metallic ferromagnetic $La_{0.7}Ca_{0.3}Mn_3O$ proximity coupled to superconducting $Pr_{1.85}Ce_{0.15}CuO_4$," *Physical Review B*, vol. 85, no. 10, p. 104 504, 2012. DOI: 10.1103/PhysRevB.85.104504.

[16] Y. Kalcheim, O. Millo, A. Di Bernardo, A. Pal, and J. W. A. Robinson, "Inverse proximity effect at superconductor-ferromagnet interfaces: Evidence for induced triplet pairing in the superconductor," *Physical Review B*, vol. 92, no. 6, p. 060 501, 2015. DOI: 10.1103/PhysRevB.92.060501.

[17] N. Satchell and N. O. Birge, "Supercurrent in ferromagnetic Josephson junctions with heavy metal interlayers," *Physical Review B*, vol. 97, no. 21, p. 214 509, 2018. DOI: 10.1103/PhysRevB.97.214509.

[18] C. González-Ruano *et al.*, "Superconductivity-induced change in magnetic anisotropy in epitaxial ferromagnet-superconductor hybrids with spin-orbit interaction," *Physical Review B*, vol. 102, no. 2, p. 020 405, 2020. DOI: 10.1103/PhysRevB.102.020405.

[19] C. R. Reeg and D. L. Maslov, "Proximity-induced triplet superconductivity in Rashba materials," *Physical Review B*, vol. 92, no. 13, p. 134 512, 2015. DOI: 10.1103/PhysRevB.92.134512.

[20] P. Högl, A. Matos-Abiague, I. Žutić, and J. Fabian, "Magnetoanisotropic Andreev reflection in ferromagnet-superconductor junctions," *Physical Review Letters*, vol. 115, no. 11, p. 116 601, 2015. DOI: 10.1103/PhysRevLett.115.116601.

[21] A. Costa and J. Fabian, "Superconducting triplet pairings and anisotropic magnetoresistance effects in ferromagnet/superconductor/ferromagnet double-barrier junctions," *Physical Review B*, vol. 104, no. 17, p. 174 504, 2021. DOI: 10.1103/PhysRevB.104.174504.

[22] M. G. Blamire and J. W. A. Robinson, "The interface between superconductivity and magnetism: Understanding and device prospects," *Journal of Physics: Condensed Matter*, vol. 26, no. 45, p. 453 201, 2014. DOI: 10.1088/0953-8984/26/45/453201.

[23] V. L. Berezinskii, "New model of the anisotropic phase of superfluid He^3," *JETP Letters*, vol. 20, no. 9, pp. 287–289, 1974.

[24] J. Linder and A. V. Balatsky, "Odd-frequency superconductivity," *Reviews of Modern Physics*, vol. 91, no. 4, p. 045 005, 2019. DOI: 10.1103/RevModPhys.91.045005.

[25] J. Linder, A. Sudbø, T. Yokoyama, R. Grein, and M. Eschrig, "Signature of odd-frequency pairing correlations induced by a magnetic interface," *Physical Review B*, vol. 81, no. 21, p. 214 504, 2010. DOI: 10.1103/PhysRevB.81.214504.

[26] J. Linder and J. W. A. Robinson, "Superconducting spintronics," *Nature Physics*, vol. 11, no. 4, pp. 307–315, 2015. DOI: 10.1038/nphys3242.

[27] G. Eilenberger, "Transformation of Gorkov's equation for type II superconductors into transport-like equations," *Zeitschrift für Physik*, vol. 214, no. 2, pp. 195–213, 1968. DOI: 10.1007/BF01379803.

[28] V. Chandrasekhar, "Proximity-coupled systems: Quasiclassical theory of superconductivity," in *The Physics of Superconductors, Vol. II. Superconductivity in Nanostructures, High-Tc and Novel Superconductors, Organic Superconductors*, K. H. Bennemann and J. B. Ketterson, Eds. Heidelberg: Springer Berlin, 2004, pp. 55–110. DOI: 10.1007/978-3-642-18914-2_3.

[29] K. D. Usadel, "Generalized diffusion equation for superconducting alloys," *Physical Review Letters*, vol. 25, no. 8, pp. 507–509, 1970. DOI: 10.1103/PhysRevLett.25.507.

[30] J. Linder and M. Amundsen, "Quasiclassical boundary conditions for spin-orbit coupled interfaces with spin-charge conversion," *Physical Review B*, vol. 105, no. 6, p. 064 506, 2022. DOI: 10.1103/PhysRevB.105.064506.

[31] J. A. Ouassou, A. Pal, M. Blamire, M. Eschrig, and J. Linder, "Triplet Cooper pairs induced in diffusive s-wave superconductors interfaced with strongly spin-polarized magnetic insulators or half-metallic ferromagnets," *Scientific Reports*, vol. 7, no. 1, p. 1932, 2017. DOI: 10.1038/s41598-017-01330-1.

[32] J. A. Ouassou, S. H. Jacobsen, and J. Linder, "Conservation of spin supercurrents in superconductors," *Physical Review B*, vol. 96, no. 9, p. 094 505, 2017. DOI: 10.1103/PhysRevB.96.094505.

[33] I. Gomperud and J. Linder, "Spin supercurrent and phase-tunable triplet Cooper pairs via magnetic insulators," *Physical Review B*, vol. 92, no. 3, p. 035 416, 2015. DOI: 10.1103/PhysRevB.92.035416.

[34] W. Belzig, F. K. Wilhelm, C. Bruder, G. Schön, and A. D. Zaikin, "Quasiclassical Green's function approach to mesoscopic superconductivity," *Superlattices and Microstructures*, vol. 25, no. 5, pp. 1251–1288, 1999. DOI: 10.1006/spmi.1999.0710.

[35] A. I. Larkin and Y. N. Ovchinnikov, "Quasiclassical method in the theory of superconductivity," *Soviet Physics JETP*, vol. 28, no. 6, pp. 1200–1205, 1969.

[36] J. P. Morten, "Spin and charge transport in dirty superconductors," M.Sc. thesis, NTNU, Trondheim, 2005.

[37] E. H. Fyhn, "Exotic Vortex Structures in Diffusive Superconducting Systems," M.Sc. thesis, NTNU, Trondheim, 2019.

[38] M. Amundsen, "Quasiclassical Theory Beyond 1D: Supercurrents and Topological Excitations," M.Sc. thesis, NTNU, Trondheim, 2016.

[39] A. Kamenev, *Field Theory of Non-Equilibrium Systems*. Cambridge: Cambridge University Press, 2011. DOI: 10.1017/CBO9781139003667.

[40] T. Kita, *Statistical Mechanics of Superconductivity*. Tokyo: Springer, 2015. DOI: 10.1007/978-4-431-55405-9.

[41] L. P. Gor'kov, "Theory of superconducting alloys," in *Superconductivity, Conventional and Unconventional Superconductors*, K. H. Bennemann and J. B. Ketterson, Eds. Heidelberg: Springer Berlin, 2008, pp. 201–224. DOI: 10.1007/978-3-540-73253-2_5.

[42] L. V. Keldysh, "Diagram technique for nonequilibrium processes," *Soviet Physics JETP*, vol. 20, no. 4, pp. 1018–1026, 1965.

[43] L. P. Gor'kov and E. I. Rashba, "Superconducting 2D system with lifted spin degeneracy: Mixed singlet-triplet state," *Physical Review Letters*, vol. 87, no. 3, p. 037 004, 2001. DOI: 10.1103/PhysRevLett.87.037004.

[44] J. W. Serene and D. Rainer, "The quasiclassical approach to superfluid ^{3}He," *Physics Reports*, vol. 101, no. 4, pp. 221–311, 1983. DOI: 10.1016/0370-1573(83)90051-0.

[45] U. Eckern and A. Schmid, "Quasiclassical Green's function in the BCS pairing theory," *Journal of Low Temperature Physics*, vol. 45, no. 1–2, pp. 137–166, 1981. DOI: 10.1007/BF00661147.

[46] J. Rammer and H. Smith, "Quantum field-theoretical methods in transport theory of metals," *Reviews of Modern Physics*, vol. 58, no. 2, pp. 323–359, 1986. DOI: 10.1103/RevModPhys.58.323.

[47] R. Balian and N. R. Werthamer, "Superconductivity with pairs in a relative p wave," *Physical Review*, vol. 131, no. 4, pp. 1553–1564, 1963. DOI: 10.1103/PhysRev.131.1553.

[48] A. P. Mackenzie and Y. Maeno, "The superconductivity of Sr_2RuO_4 and the physics of spin-triplet pairing," *Reviews of Modern Physics*, vol. 75, no. 2, pp. 657–712, 2003. DOI: 10.1103/RevModPhys.75.657.

[49] M. Kurpianov and V. Lukichev, "Influence of boundary transparency on the critical current of dirty SS's structures," *Soviet Physics JETP*, vol. 67, no. 6, pp. 1163–1168, 1988.

[50] A. Cottet, D. Huertas-Hernando, W. Belzig, and Y. V. Nazarov, "Spin-dependent boundary conditions for isotropic superconducting Green's functions," *Physical Review B*, vol. 80, no. 18, p. 184 511, 2009. DOI: 10.1103/PhysRevB.80.184511.

[51] M. Eschrig, A. Cottet, W. Belzig, and J. Linder, "General boundary conditions for quasiclassical theory of superconductivity in the diffusive limit: Application to strongly spin-polarized systems," *New Journal of Physics*, vol. 17, no. 8, p. 083 037, 2015. DOI: 10.1088/1367-2630/17/8/083037.

[52] T. Tokuyasu, J. A. Sauls, and D. Rainer, "Proximity effect of a ferromagnetic insulator in contact with a superconductor," *Physical Review B*, vol. 38, no. 13, pp. 8823–8833, 1988. DOI: 10.1103/PhysRevB.38.8823.

[53] N. Schopohl and K. Maki, "Quasiparticle spectrum around a vortex line in a d-wave superconductor," *Physical Review B*, vol. 52, no. 1, pp. 490–493, 1995. DOI: 10.1103/PhysRevB.52.490.

[54] S. H. Jacobsen, J. A. Ouassou, and J. Linder, "Critical temperature and tunneling spectroscopy of superconductor-ferromagnet hybrids with intrinsic Rashba-Dresselhaus spin-orbit coupling," *Physical Review B*, vol. 92, no. 2, p. 024 510, 2015. DOI: 10.1103/PhysRevB.92.024510.

[55] P. Virtanen *et al.*, "SciPy 1.0: Fundamental algorithms for scientific computing in Python," *Nature Methods*, vol. 17, no. 3, pp. 261–272, 2020. DOI: 10.1038/s41592-019-0686-2.

[56] R. C. Dynes, V. Narayanamurti, and J. P. Garno, "Direct measurement of quasiparticle-lifetime broadening in a strong-coupled superconductor," *Physical Review Letters*, vol. 41, no. 21, pp. 1509–1512, 1978. DOI: 10.1103/PhysRevLett.41.1509.

[57] B. D. Josephson, "Possible new effects in superconductive tunnelling," *Physics Letters*, vol. 1, no. 7, pp. 251–253, 1962. DOI: 10.1016/0031-9163(62)91369-0.

[58] A. Golubov, M. Kupriyanov, and E. Il'ichev, "The current-phase relation in Josephson junctions," *Reviews of Modern Physics*, vol. 76, no. 2, pp. 411–469, 2004. DOI: 10.1103/RevModPhys.76.411.

[59] S. Aunsmo. "Sigriaun/solving-usadel-nummerically." (2023), [Online]. Available: https://github.com/sigriaun/Supercurrent-induced-proximity-effects-at-spin-orbit-coupled-interfaces (visited on 06/14/2023).

[60] M. Tachiki, T. Koyama, and S. Takahashi, "Superconducting properties in layered cuprate oxides," in *Advances in Superconductivity III*, K. Kajimura and H. Hayakawa, Eds., Tokyo: Springer, 1991, pp. 45–51. DOI: 10.1007/978-4-431-68141-0_7.

[61] K. Senapati, M. G. Blamire, and Z. H. Barber, "Spin-filter Josephson junctions," *Nature Materials*, vol. 10, no. 11, pp. 849–852, 2011. DOI: 10.1038/nmat3116.

[62] D. Einzel, "Interpolation of BCS response functions," *Journal of Low Temperature Physics*, vol. 130, no. 5, pp. 493–508, 2003. DOI: 10.1023/A:1022483819173.

[63] H. Haug and A.-P. Jauho, *Quantum Kinetics in Transport and Optics of Semiconductors*. Heidelberg: Springer Berlin, 2007. DOI: 10.1007/978-3-540-73564-9.

[64] A. Manchon, H. C. Koo, J. Nitta, S. M. Frolov, and R. A. Duine, "New perspectives for Rashba spin–orbit coupling," *Nature Materials*, vol. 14, no. 9, pp. 871–882, 2015. DOI: 10.1038/nmat4360.

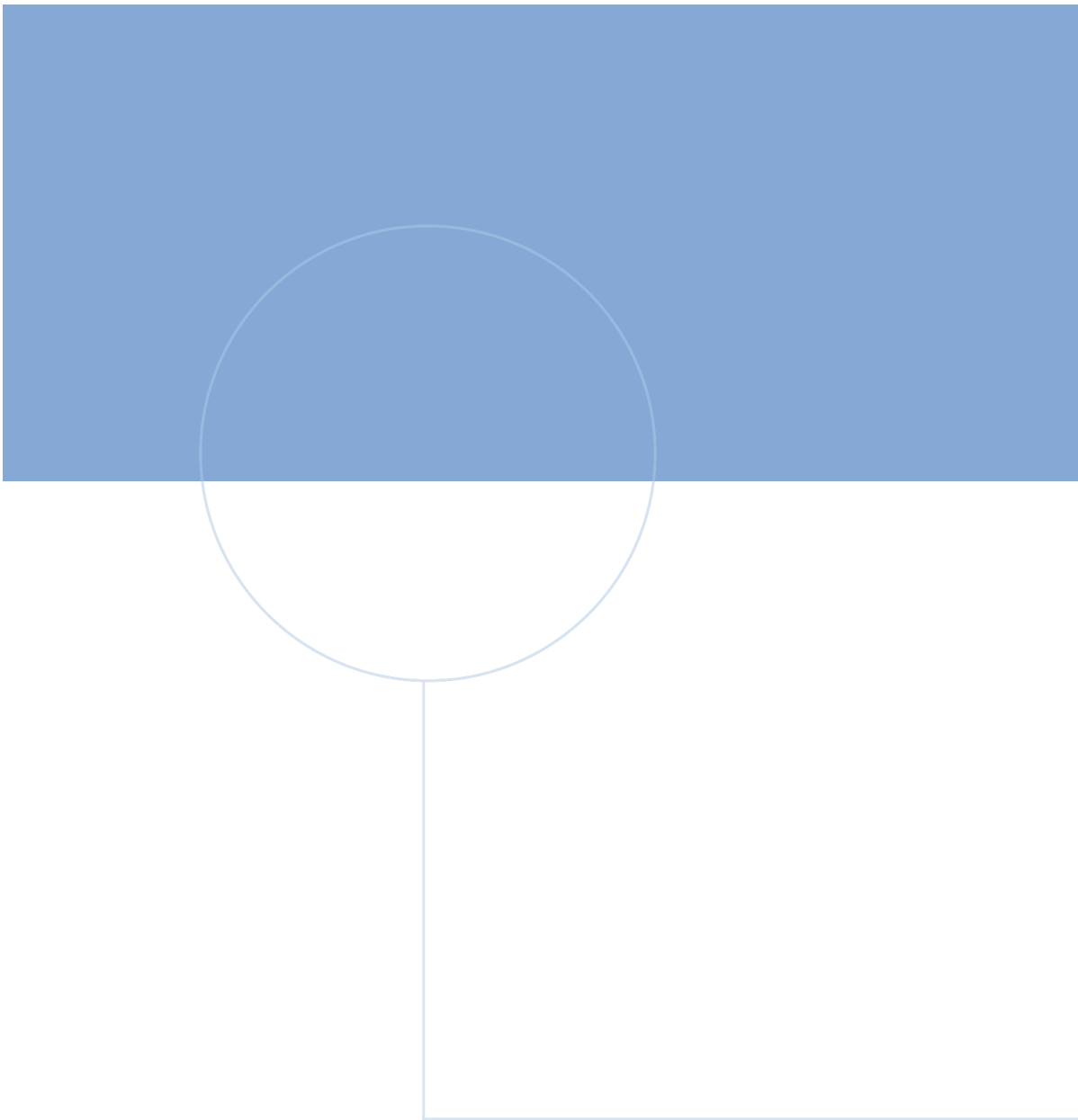

NTNU
Norwegian University of
Science and Technology

QuSpin